UNIVERSITÀ
DEGLI STUDI
FIRENZE

DOTTORATO DI RICERCA IN SCIENZE CHIMICHE

CICLO XXXIV

COORDINATORE Prof. PIERO BAGLIONI

"Green" Poly(vinyl alcohol)/Starch based cryogels for the cleaning of works of art: Application, characterization, and investigation of the Amylose/Amylopectin structural role

(Criogeli "Green" a base di Poli(vinilalcol) e Amido per la pulitura di manufatti artistici: Applicazione, caratterizzazione e studio del ruolo strutturale di Amilosio e Amilopectina)

SSD CHIM/12

Dottorando
Dott. Vanessa Rosciardi

_____
(firma)

Tutore
Prof. Piero Baglioni

_____
(firma)

Coordinatore
Prof. Piero Baglioni

_____
(firma)

Anni 2018/2021

“Green” Poly(vinyl alcohol)/Starch based cryogels for the cleaning of works of art: Application, characterization, and investigation of the Amylose/Amylopectin structural role

Table of contents

Abstract

Cultural Heritage assets are crucial to mankind, as they are drivers of welfare and economic improvement. If properly preserved, this patrimony can boost job creation, social inclusion, and cultural identity. Unfortunately, degradation processes inevitably threaten works of art.

Colloids and material science have been providing effective solutions to preserve works of art in the last decades. In the specific case of cleaning of painted artworks, excellent results have been obtained using highly performing gels based on synthetic polymers like poly (vinyl pyrrolidone) (PVP) and poly (hydroxyethyl methacrylate) (pHEMA).

However, there is still large room for the formulation of polymer networks that retain optimal cleaning ability but have higher eco-compatibility. In this perspective, we have developed and studied different biocomposite hydrogels based on poly(vinyl alcohol) (PVA) and rice starch (RS) obtained via freeze-thawing, with water as the only used solvent.

The PVA/RS hydrogels have been extensively characterized from a morphological, rheological, and structural point of view and have been tested as cleaning tools on painted mock-ups with excellent outcomes, showing performances comparable with their state-of-the-art synthetic counterparts. Furthermore, the introduction of a biopolymer in the synthetic path improved the sustainability of the art cleaning formulations, while maintaining optimal and tunable mechanical behavior.

Besides, the reduction of usage and disposal of materials based on synthetic polymers is an urgent and transversal need, and biocomposite PVA/starch-based systems could meet the requirements that different applications demand., being broadly tunable by simply varying the PVA:starch ratio in their formulation.

Nevertheless, starch as a raw product comes with a high variety of features, especially regarding the composition of its polymeric portion (i.e., the amylose to amylopectin ratio), which is cardinal in determining the properties of the biocomposite systems.

The investigation of the fundamental interactions between PVA, amylose, and amylopectin has therefore been deemed necessary to set a reliable base from which to start developing state-of-the-art materials, drastically reducing the usage of synthetic reagents without compromises in terms of performances.

Said mutual interactions and their consequences have been investigated by means of direct laser imaging of fluorescently labeled systems, thermal analysis and Small-Angle X-ray Scattering, coupling the results with rheological measurements and gel fraction trends to provide a preliminary theoretical framework, the aim of which is to support future developments of highly performing eco-sustainable materials.

List of abbreviations

CLSM = Confocal Laser Scanning Microscopy

DSC = Differential Scanning Calorimetry

F/T = freeze/thawing

FT-IR = Fourier Transform Infra-Red spectroscopy

GA = glutaraldehyde

HVPDs = highly viscous polymeric dispersions

μFT-IR = Fourier Transform Infra-red microscopy

pHEMA = poly (2-hydroxyethyl methacrylate)

pMMA = poly (methyl methacrylate)

P/s = poly (vinyl alcohol)/starch

PVA = poly (vinyl alcohol)

PVP = poly (vinyl pyrrolidone)

SAXS = Small-Angle X-ray Scattering

SEM = Scanning Electron Microscopy

tel-PVA = telechelic PVA

TEPA = tetraethylenepentamine

Introduction

The complex network of interactions that links Society and Cultural Heritage is extended to the point that the two concepts can be described only through their mutual relationships.

The Merriam-Webster dictionary defines society as "a community, nation, or broad grouping of people having common traditions, institutions, and collective activities and interests"[1], where said common traditions and collective activities are nothing but the backbone of what we intend as culture. According to Gonzalez-Perez and Parcero-Oubiña, "cultural value is assigned by people to things" through interpretive processes that have a meaning only with the consensus of a given community[2].

It is therefore clear that, while the creation of a cultural patrimony requires a context of shared values (i.e., a society), the existence of such contexts relies on culture itself. In other words, society is simultaneously the cause and the effect of the Cultural Heritage (tangible and intangible) that it produces.

Furthermore, Cultural Heritage actively contributes to strengthening the overall resilience of societies, thanks to some of its intrinsic values, such as a sense of place and belonging, that are crucial in supporting people's collective identity and self-esteem[3]. Another crucial role of Cultural Heritage is to preserve historical memory and transfer it to communities across generations, acting as a witness of "how people in the past have proven to be resilient and been capable of absorbing adversity in various ways"[3] being therefore able to inspire people today to face changes through adaptation.

To do so, the tangible Cultural Heritage must be accessible to the community, in the double meaning of being materially reachable

(physically and economically) and clearly "readable". The former feature depends mostly on socioeconomic parameters, while the latter relies on the state of conservation of the artifacts, being readability definable as the ability of the object to deliver its meaning through its appearance.

Given these premises, the importance of preserving Cultural Heritage from losses and damages naturally arises. This task is far from being simple. Indeed, our tangible cultural patrimony is broadly heterogeneous, consisting of artifacts, works of art, and monuments, which correspond to a wide range of employed materials and techniques. Furthermore, any target to be preserved can display different conservation issues, adding complexity to an already delicate process.

Research and development of increasingly sophisticated materials to be used throughout the entire conservation process have lately flourished. Materials Science, in particular, has been fundamental in finding new solutions to face the challenges of preserving Cultural Heritage, producing state-of-the-art materials specifically developed to match the requirements of different target materials and conservation steps, from consolidation to cleaning.

Cleaning of artworks is one of the most delicate processes faced in conservation practice, owing to its irreversibility[4]. Its aim is to remove soil, dirt, grime (greasy material, dust, etc.), and natural or synthetic polymers from the surface of coated artifacts to restore, as far as possible, their aesthetic appearance, which is in turn tightly connected with their ethical and social meaning.

The main challenge faced in cleaning operations relies on gaining selected removal of unwanted layers without altering the original components of the artifact, a task made difficult by the complex interplay between surface layers[5]. Selectivity can be granted through the choice of the appropriate cleaning fluid, which has evolved from being

based on simple solubility considerations to relying on more specific interactions[6].

However, selectivity alone is not enough, and controllability of the process is mandatory too, especially when facing the treatment of delicate, water-sensitive surfaces. To grant a higher control, the direct use of free cleaning fluids on the artifacts has been progressively abandoned. Instead, cleaning solutions have been confined into increasingly sophisticated and tunable materials, which development has been possible thanks to the flourishing collaboration between material scientists and conservators.

In the specific case of cleaning of painted artworks, state-of-the-art retentive matrixes are today represented by gels based on polymers like poly (vinyl alcohol) (PVA)[7], poly (2-hydroxyethyl methacrylate) (pHEMA)[8], poly (vinyl pyrrolidone) (PVP)[9], and poly (methyl methacrylate) (pMMA), some of which were successfully applied on masterpieces of artists of exceptional importance, such as Pablo Picasso, Jackson Pollock, and Roy Lichtenstein.

Nonetheless, these systems are still far from being the "perfect solution" to conservation issues, since they do not sufficiently respond to ecological requirements that are indeed becoming growingly important in every "polymer-related" production field.

Moreover, the preservation of cultural heritage without the contemporary safeguard of environmental patrimony would result in a dangerous contradiction. Hence, the latest challenge in material science applied to conservation is represented by the development of high-performing yet eco-sustainable materials.

In this perspective, the goal of our research was to prepare, characterize and apply novel green systems for artworks conservation. In particular, we focused on the specific case of cleaning of painted artworks, an operation that is mostly carried through the use of gel matrices.

Previous works have revealed that the efficiency of the cleaning process strongly relies on the porosity of the applied gel, its viscoelastic behavior, and high water content, while the safety of the operation is ensured by a good cohesion of the system, which grants a residue-free interaction with the treated surface.

Therefore, our target material to be synthesized was represented by a strong gel displaying the aforementioned features and obtained starting from "green" materials and through eco-compatible preparation methods. Besides, materials prepared with these premises could be applied in fields that go far beyond the conservation of cultural heritage, since they have to fulfill some important general requirements such as non-toxicity and biodegradability or, even better, bio compostability.

To pursue our aim, we started from a synthetic base, represented by PVA, which is one of the world's most-produced water-soluble polymers[10]. One of its main advantages is represented by its ability to form strong gels by simply freeze-thawing its aqueous solutions, with no other reactants nor solvents needed. This feature mainly arises from its abundance in hydroxyl groups, which ensure the formation of a number of hydrogen interactions high enough to promote the formation of crystalline domains that act as tie-points in the newly formed gel network[11].

PVA is reported to be biodegradable, although its biodegradation occurs efficiently exclusively in specific conditions and/or in the presence of certain microorganisms[12]. Hence, since our goal is to go greener, we started from a standard formulation of a pure PVA gel, and then we progressively substituted the synthetic polymer with a natural compound, here represented by starch.

Starch is a natural, cheap, and abundant material. It is mainly constituted by two polymers, amylose, and amylopectin, in a ratio between 15:85 and 25:75[13]. The two polymers are chemically identical, being both formed by α-D-glucose units, but differ in the branching degree, since amylose is mostly linear, while amylopectin is characterized by an

important number of ramifications. Amylose and amylopectin both display available hydroxyl functionalities, therefore hydrogen interactions with PVA chains are reasonably expected.

Indeed, PVA and starch have been already coupled to obtain biocomposite materials, and several works are reported. However, the majority of the research is focused on the formulation of films[14–16], while few works regard the preparation of PVA/starch-based cryogels[17,18]. Moreover, in said cases, the research is mainly centered on their application, and little characterization of the material is reported.

Hence, the first part of this work mainly focuses on the development and systematic characterization of different PVA/starch (P/s) hydrogels obtained via freeze-thawing. Tunability of their macroscopic properties was achieved by varying the PVA to starch ratio and relating the effect of the composition to their structure at the nano and micro-scale. Several techniques were employed for this purpose, including Small-Angle X-ray Scattering (SAXS), Confocal Laser Scanning Microscopy (CLSM), Scanning Electron Microscopy (SEM), Fourier Transform Infra-Red spectroscopy (FT-IR), oscillatory rheological measurements, and Differential Scanning Calorimetry (DSC).

Once fully characterized, the systems deemed as suitable for cleaning purposes were applied on artificially soiled painted mock-ups displaying different conservation issues: a water-sensitive, poorly bounded tempera, and an alkyd painted surface characterized by a highly irregular texture. The outcomes of the cleaning operations were assessed through Fourier Transform Infra-red microscopy (μFT-IR) and compared with the ones obtained after the application of two state-of-the-art synthetic materials recently accepted in restoration practice[19,20] and commercially known under the name of HWR® and Peggy6® Nanorestore. Our P/s biocomposite systems, beyond representing an improvement in terms of eco-sustainability, resulted to be as effective as their synthetic counterparts.

Furthermore, the characterization of the P/s cryogels highlighted that polymer-polymer interactions strongly depend on the relative amount of each component in the blend and are crucial in determining the final properties of the systems, which are broadly tunable and can therefore meet a considerable number of applicative needs. Nevertheless, starch as a raw product comes with variable features, especially regarding the composition of its polymeric portion, i.e., the amylose to amylopectin ratio.

It is therefore clear that the characterization of generic P/s biocomposites is meaningful only limited to specific contexts, while a better knowledge of the role of each polymer (i.e., PVA, amylose, and amylopectin) could set a theoretical basis for predicting the composition/properties relations of P/s networks. Especially in the perspective of a realistically affordable and scalable production of biocomposite products, a step back into the fundamental interactions between the main involved components is necessary to set a reliable base from which to start developing state-of-the-art materials, drastically reducing the usage of synthetic reagents without compromises in terms of performances.

Consequently, the second part of this work focused on the interactions between PVA, amylose, and amylopectin. We conveniently simplified the complete P/s system as bi- and tri- component formulations (tri- and quadri-, counting water) constituted by PVA, amylose, amylopectin, or both, in variable ratios. Direct CLSM imaging of fluorescently labeled polymers, thermal analysis, and SAXS profiles of the samples have been coupled with rheological measurements and gel fraction trends to provide a preliminary theoretical framework. The obtained information aims to support future developments of highly performing eco-sustainable materials, whose application can go far beyond the conservation of Cultural Heritage.

For the sake of completeness, given the complex theoretical base on which the SAXS experiments rely, an additional chapter about the technique is provided at the end of this work.

Part 1.

PVA/starch biocomposite cryogels

1.1 General Background

1.1.1 PVA cryogels: The freeze-thawing process

Poly(vinyl alcohol) (PVA) is a water-soluble synthetic polymer with the formula $[CH_2CH(OH)]_n$. Unlike other polymers, PVA is not synthesized from its monomeric units due to the high instability of vinyl alcohol. Instead, the production of PVA relies on the polymerization of vinyl acetate to poly (vinyl acetate) (PVAc), followed by the hydrolysis of PVAc to PVA. The hydrolysis reaction is characterized by a yield lower than 100%, meaning that PVA chains carry residual acetate functionalities whose number significantly affects some important polymer properties such as the solubility in water and the ability to crystallize[21,22]. PVA is employed in the production of materials in numerous fields, from pharmaceutics to the textile industry.

Regardless of its destiny, before processing PVA is crosslinked through one of the following methods:

1. "Traditional" chemical crosslinking, through the employment of crosslinking agents such as glutaraldehyde and acetaldehyde in the presence of sulfuric acid, acetic acid, or methanol[23].
2. Irradiation-induced chemical crosslinking, where the formation of crosslinks is observed after exposing PVA to electron beams or γ-rays[24].

3. "Physical" crosslinking, based on the formation of PVA crystallites induced by thermal treatments[25,26].

Of the three strategies, the last is the one that suits the most the premises of eco-sustainability that are the base of this work, as it does not require the use of additional reactants nor solvents besides water.

Indeed, PVA aqueous solutions can undergo physical crosslinking either through solvent evaporation or freeze-thawing processes. In both events, the structure of the final system is a polymeric network whose tie points are PVA crystallites instead of chemical covalent bonds. Regarding the case of solvent evaporation, drying the system leads to a progressive increase in the PVA concentration that favors the interchain hydrogen interactions and promotes the consequent formation of crystalline domains[27].

Overall, crystallization of PVA obtained via freeze-thawing also relies on the increment of concentration of the polymer, but here this event is triggered by a phase separation mechanism[25].

Briefly, when a PVA solution is subjected to sub-zero temperatures, free water molecules freeze first and act as nucleation points for growing ice crystals. As crystallization proceeds, water molecules are subtracted from the continuous solution and progressively "concentrate" PVA chains in a separating polymer-rich phase.

As the PVA concentration increases and the chains come into closer contact, also pushed by the pressure generated by ice volume expansion, hydrogen bonding and crystallite formation occur.

After thawing, these hydrogen interactions remain intact while the ice melts, and water is retained in the newly formed non-degradable three-dimensional hydrogel whose network is held together by PVA crystalline domains. The overall mechanism is graphically illustrated in figure 1.

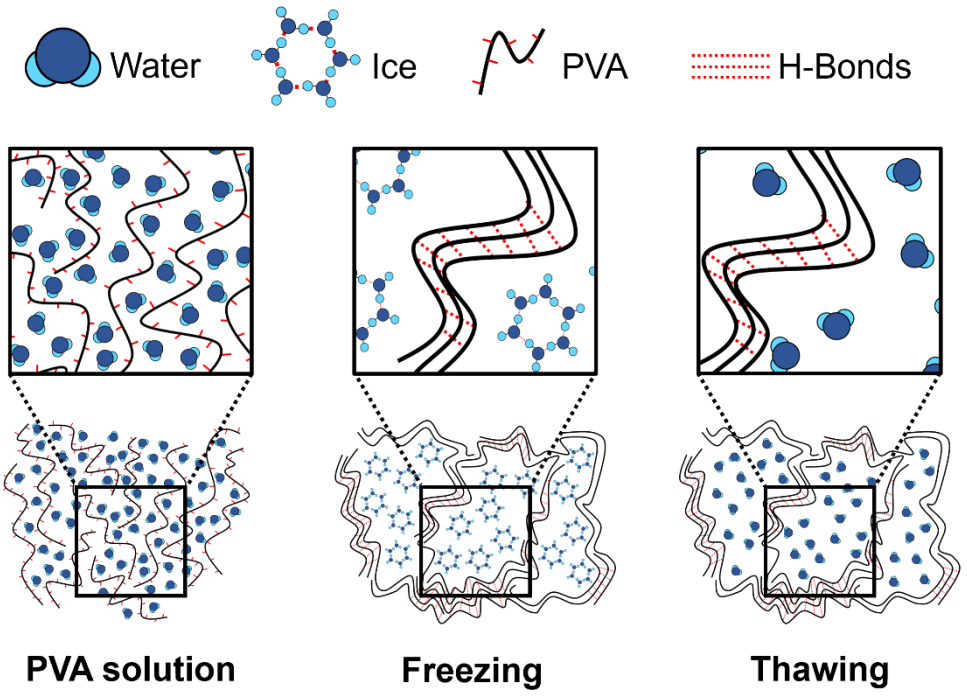

Figure 1. Schematical representation of the main steps characterizing the evolution of a PVA solution to a PVA physically crosslinked hydrogels. Inter- and intra-chain hydrogen bonding is promoted by water freezing and phase separation, leading to the formation of locally ordered crystalline structures. The crystallites act as tie-points of a three-dimensional gel network and do remain in the structure after thawing.

Freeze-thawed PVA hydrogels were first reported in 1975 by Peppas[28]. In its pioneering work, PVA crystallites were characterized through turbidimetric measurements of freeze-thawed samples, and their formation resulted related to the concentration of PVA in solution, the freezing time, and the tawing time. Since then, significant research has been performed on analyzing the impact that various processing parameters have on hydrogel properties and gelation.

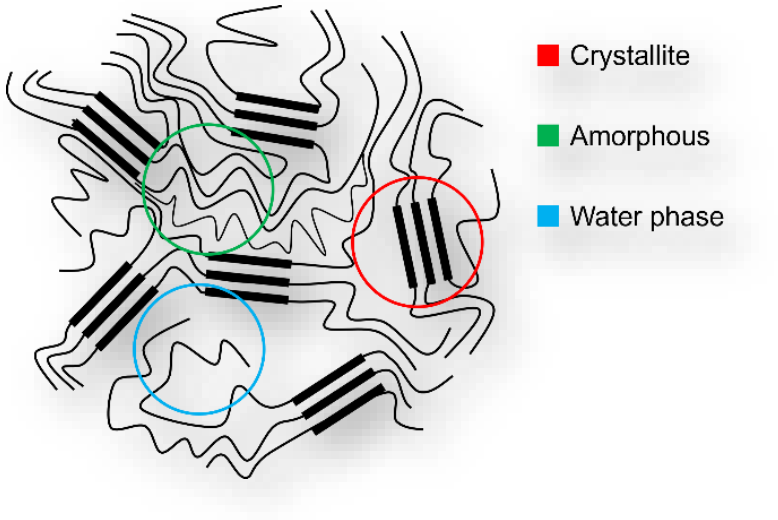

Figure 2. Schematic representation of the structural organization of a freeze-thawed PVA hydrogel. The gel consists of three main phases: a water phase with a low PVA concentration, an amorphous phase in which polymeric chains are partially mobile, and a crystalline phase in which the chains are densely packed.

The main findings resulting from the rich work on freeze-thawed PVA (F/T PVA) hydrogels can be summarized as follows:

- The structure of F/T PVA hydrogels consists of three phases: a water phase of low PVA concentration, an amorphous phase, and a crystalline phase that partially hinders the motion of the amorphous chains[29] (see figure 2).
- Crystalline structures in F/T PVA have a layered organization: a double layer of chains packed together and interacting through hydrogen bonds, with van der Waals forces operating between different bilayers[11].
- PVA crystalline melting range is between 200 and 240°C, with melting temperatures depending on the size of the crystal[23].

- The dimensions of PVA crystals can be determined by scattering experiments. Crystallites have an average size ranging from 50 to 70 Å and are separated by a distance of 150 to 200 Å[30,31].
- The molecular weight of PVA influences the size of crystallites, with longer chains leading to the formation of bigger crystals[25].
- The crystallinity of the F/T PVA systems is positively correlated to freezing time, PVA solution concentration, and PVA hydrolysis degree (i.e., the longer the freezing time and the higher the PVA concentration and degree of hydrolysis, the higher the crystallinity of the gel)[25].
- An increase in the number of freeze-thawing cycles corresponds to an increase in the elastic modulus and a decrease in the adhesive properties, which are maximized at two freeze-thawing cycles[32].

Freeze-thawed PVA gels have been widely applied in transversal fields. Their non-toxic character, tunable viscoelastic response, high water content, and good diffusive properties have made these materials particularly appropriate for medical and biological applications[33,34]. Nonetheless, the same features happen to be very appealing also for their application as retentive matrixes for the cleaning of painted surfaces with historical and artistic value.

1.1.2 PVA-based systems for cleaning art

PVA has excellent potential for developing tailored systems for the cleaning of Cultural Heritage. It can be processed in several ways to obtain materials characterized by broadly different features, especially concerning mechanical resistance, viscoelastic behavior, and water retention. PVA viscous solutions and hydrogels have been synthesized, characterized, and applied on various artistic surfaces by several research groups. What follows is a summary of the PVA-based systems developed for the cleaning of artifacts over the last decade.

1.1.2.1 PVA/borax high viscosity dispersions

PVA-based highly viscous polymeric dispersions (HVPDs) can be obtained through a mild crosslinking of polymeric chains in water in presence of borax ($Na_2B_4O_7 \cdot 10H_2O$)[35,36]. From a rheological point of view, PVA/borax HVPDs cannot be considered real gels since they exhibit frequency-dependent mechanical behavior and finite relaxation time[37]. However, these systems show a certain versatility in terms of viscoelastic properties and their elasticity can be increased by changing the PVA to borax ratio or their total concentration[38]. Interestingly, PVA/borax HVPDs show some adaptability also regarding the loadable solvents.

For instance, Carretti et Al. have reported the preparation of thermodynamically stable aqueous PVA/borax dispersions containing acetone or propanol as cosolvents[39]. When it comes to cleaning artistic surfaces, the possibility to load the systems with organic solvents is particularly advantageous, given the frequent presence on the artifacts of non-water-soluble coatings and varnishes[40]. Indeed, in the same

work, a PVA/borax HVPD loaded with acetone was used to remove an oxidized shellac-based varnish from a 15th-century egg tempera painting.

However, PVA/borax systems are not free from important drawbacks. Even if, as mentioned above, their elastic response can be enhanced by tuning the polymer to crosslinker ratio, they are still viscous solutions. While their flowability facilitates the application on irregular surfaces, their consistency causes unprecise removal from the treated artifacts and unwanted residues can be left behind.

Despite representing a step forward compared to the use of free cleaning fluids, PVA/borax HVPDs have been rapidly abandoned due to their limitations and substituted with more performing materials.

1.1.2.2 PVA-based peelable films

In addition to the synthesis method described in the previous paragraph, PVA-based highly viscous polymeric dispersions (HVPDs) can be obtained by preparing PVA solutions with a high polymer concentration. As seen before, systems of this sort do not have sufficient inner cohesion. However, starting from an HVPD and exploiting the PVA film-forming ability, a more suitable material can be obtained.

Indeed, PVA HVPDs can be applied on surfaces as such, and let dry until a film with appropriate viscoelastic features is formed. Additionally, the film-formation time can be shortened by introducing organic cosolvents in the system[41]. After the evaporation of the liquid fraction, the film can be safely "peeled-off" in one piece using tweezers. Furthermore, to improve the mechanical behavior of the obtained film, plasticizers can be added to the formulation[42].

These PVA-based peelable systems have proven particularly useful as cleaning tools for metal artifacts since they are often characterized by highly three-dimensional and non-horizontal surfaces on which the application of a highly viscous system guarantees optimal coverage. Moreover, PVA HVPDs with appropriate formulations can be loaded with solutions of chelating agents and therefore be applied on metals for the removal of corrosion products.

Guaragnone et Al. have recently applied PVA-based peelable systems loaded with tetraethylenepentamine (TEPA) for the selective removal of copper corrosion products from bronze artifacts[42]. In addition to the obtained excellent results, they found that loading the TEPA in the polymer matrix reduces the time needed for film formation since it induces alkaline hydrolysis of acetyl groups in PVA chains, promoting the association of the chains into more ordered structures.

However, the removal of the dry PVA film from the treated artifacts exerts a mechanical action on the involved surface. These kinds of systems, while being suitable to be applied on coherent layers, are therefore too harsh for powdery, poorly bound surfaces such as the ones encountered on archaeological objects. In such cases, the use of a gel instead of an HVPD is preferred. The next sections will discuss the properties of the main PVA-based gels employed for the cleaning of Cultural Heritage.

1.1.2.3 Chemically cross-linked PVA

Poly(vinyl alcohol) has a strong hydrophilic character, which is key for its solubility in water. However, moisture sensitivity and the high water absorption rate of PVA can cause a reduction in mechanical properties and hence limits its applicability[43]. Nevertheless, the water absorption

of a PVA-based system can be reduced by introducing crosslinking points.

In addition to physical methods, PVA can be chemically crosslinked with several moieties such as, for example, dialdehydes, dicarboxylic acids, tricarboxylic acids, diisocyanates, and boric acid[44]. Despite leading to the formation of retentive hydrogel matrixes with good mechanical features, this approach has the disadvantage of requiring the use of toxic and hard-to-remove reagents.

To overcome this drawback, a valid alternative to classical crosslinking agents was investigated by Paradossi et Al. in 1996[45] and recently repurposed by Mazzuca et Al. with an application on Cultural Heritage[46].

The approach proposed by Paradossi's group was to use PVA as *both* the polymeric chain *and* the crosslinker, exploiting the instability of the few head-to-head associated monomers in the chains. Indeed, PVA is prevalently formed by 1,3-glycol repeating units, but a detectable percentage of 1,2- glycol units is usually present. As schematically depicted in figure 3, the 1,2-glycol units can be split using sodium periodate ($NaIO_4$), leading to the formation of PVA chain segments carrying aldehyde groups at both ends, called telechelic PVA (tel-PVA).

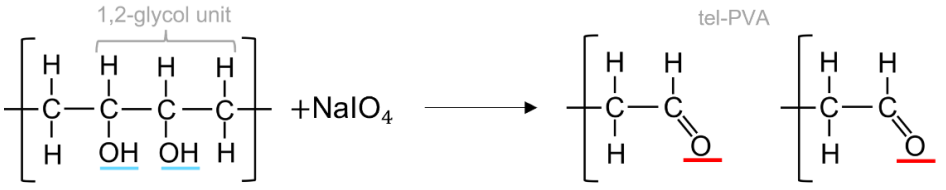

Figure 3. Formation of telechelic PVA by splitting 1,2-glycol units in PVA chains. The reaction is conducted exploiting the instability of the head-to-head monomers in presence of $NaIO_4$.

A chemically crosslinked PVA/tel-PVA gel is then obtained adding aqueous chloridric acid (HCl) to a solution of the two polymers and leaving the mixture to evolve overnight.

Being totally free from hazardous reactants, these systems have found many applications, especially in the biomedical field[47]. Furthermore, their water retentivity and mechanical properties have been deemed suitable by Mazzuca et al. for applications on water-sensitive artifacts[46].

They prepared PVA/tel-PVA gels with variable composition and applied them to extract soluble degradation products from naturally aged paper samples dating back to the XVIII century, obtaining promising results. However, chemically crosslinked PVA gels display pores of small dimensions that can be enough for the removal of soluble products from a paper surface but could be less effective on particulate soil and dust, where broader pores have been deemed as necessary for efficient cleaning[7]. Moreover, the chemical crosslinking produces rather rigid gels that are mechanically resistant but show poor adaptability on more textured surfaces. As discussed in the next section, PVA-based gels prepared via freeze-thawing can overcome these issues.

1.1.2.4 Freeze-thawed PVA/PVA

As summarized in section 1.1.1, crystallinity, elastic response, and adhesiveness of pure freeze-thawed PVA (F/T PVA) hydrogels can be tuned through the modification of the processing parameters (i.e., PVA concentration and molecular weight, freezing time, and freeze-thawing cycles). However, subjecting a PVA solution to freeze-thawing leads to the formation of a gel with a defined organization, whose peculiar morphology cannot be modified unless by introducing other components in the system. Indeed, F/T PVA hydrogels are always characterized by domains that reflect the anisotropy of the dendritic

growth of ice crystals and in which the polymer walls define a system of tight, elongated pores. The pores sections have an elliptical shape and maximum diameters of around 4 μm[7].

While this arrangement does not hinder the diffusion of solutions and small molecules inside the gel network[48], it can hamper the incorporation of larger objects, like particulate soil and dust, into the pores, and their movement inside the hydrogel. To boost the cleaning performances of F/T PVA gels without renouncing the "green" character of their formulation, a strategy is to induce phase-separation events in the pre-gel solutions, to trigger structural modifications of the final systems.

Mastrangelo et Al. have recently reported the formulation of an F/T PVA-based hydrogel with a sponge-like structure obtained by the above method[7].

Briefly, they first explored the phase behavior of aqueous solutions containing two PVA with different molecular weights and hydrolysis degrees and determined the conditions in which the polymers were not mutually miscible. Exploiting this immiscibility, they prepared a biphasic mixture with an appropriate PVA/PVA ratio in water and subjected it to a freeze-thawing cycle. As a result, and after washing, the gel porosity changed from the typical PVA packed structure of elongated channels into a nonordered pattern of interconnected and broader pores.

Moreover, the induced morphological changes were proven to affect the viscoelastic response of the gel, making it more mechanically compliant. Altogether, these new features resulted in higher cleaning efficacy than pure PVA networks, also representing an improvement in comparison with more rigid chemically cross-linked networks.

The phase-separation route, induced by the introduction of other polymers in the pre-gel solution, is a promising strategy for the synthesis of hydrogels with tailorable properties that match the specific needs that cleaning different artistic surfaces can require. Indeed, the PVA-based

hydrogels presented in this work have been developed on these premises, exploring the effects that polymers different from PVA can have on the formation of an F/T PVA network.

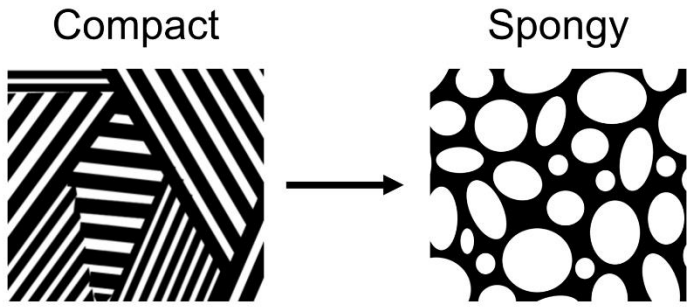

Figure 4. Schematic representation of the structural changes induced by phase separation in pre-gel PVA solutions. On the left, the typical organization of a freeze-thawed PVA gel is depicted. This morphology can be drastically modified by the introduction of a second non-miscible polymer in the PVA solution, resulting in the formation of spongy porous systems (right image).

1.1.3 PVA/starch-based materials

1.1.3.1 PVA/starch films

Starch is the major form of stored carbohydrate in plants such as corn, wheat, rice, and potatoes, and is mainly composed of a mixture of amylose and amylopectin (in a ratio comprised between 15:85 and 25:75[13]. Amylose is a linear α-glucan with an average molecular weight ranging from 10^5 to 10^6, containing almost exclusively (1→4)-α-linkages, with a small presence of (1→6)-α- linkages (usually less than

0,1%[49]). Amylopectin is a highly branched macromolecule with a larger molecular weight than amylose, usually comprised between 10^7 and 10^9, displaying 95% (1→4)-α- and 5% (1→6)-α- linkages[49]. Both amylose and amylopectin show great variability in molecular size, structure, and polydispersity depending on their botanical origin.

Starch, either natural or chemically modified, can be used to produce bio compostable films by simply casting its aqueous solutions[50]. Although, these films have been reported to show poor moisture barrier and mechanical properties, and these disadvantages represent a big limitation to their application[51]. Moreover, natural starch is characterized by low thermal stability, which limits its large-scale processability.

Indeed, natural starch does not have a thermoplastic behavior. However, in the presence of plasticizing agents (e.g., water, glycerol, sorbitol, urea, and formamide) and at high temperatures and shear rates, a thermoplastic mixture can be obtained, enabling the use of starch in injection, extrusion, and blowing equipment, similarly to synthetic plastics[52]. Still, thermoplastic starch cannot be used in many applications owing to its sensitivity to humidity and inferior mechanical properties.

To overcome these limitations without compromising its eco-sustainable character, starch can be blended with other biodegradable, renewable, or synthetic polymers, such as poly (vinyl alcohol) (PVA)., to obtain "green" materials with high performances.

Since 1980, many attempts have been made to obtain PVA/starch-based films with features that could allow their extensive production and application[51]. If, in general, blending starch with PVA improves the mechanical properties of starch-based materials, the overall performances of the obtained biocomposite systems are not quite appropriate for them to replace their totally synthetic counterparts.

One of the mechanical issues displayed by films composed of PVA and starch is represented by their poor tensile strength. A conventional approach used to overcome this limitation consists of the addition of plasticizers in the blend. The most used plasticizer for PVA/starch composites is a mixture of glycerol and water[53], but other chemicals have been successfully employed over the years.

Amongst the others, citric acid has been reported to double the elongation at break and drastically lower the water absorbance of PVA/starch films. This behavior is ascribed to the ability of citric acid to form hydrogen bonds with the other components increasing the inter- and intramolecular interactions between starch and PVA[54].

In a study from 2008, Shi et al. confirmed that, compared to the hydroxyl groups on glycerol, the carboxyl groups on citric acid can form stronger hydrogen bonds between the latter and the other molecules, also increasing the thermal stability of PVA/starch blends. Moreover, they reported the occurrence of an esterification reaction between citric acid and starch in films processed at 140°C, which enhanced further their mechanical properties and resistance to solubilization[55].

The effects of glycerol can be improved by using it in a mixture with urea to form complex plasticizers. By adding this mixture to PVA/starch blends, Zhou et al. obtained films whose polymer matrix was proven to be formed by a continuous phase and whose rheological properties were improved, if compared to analogous films containing glycerol alone. The effect was again related to an increase in hydrogen interactions between the blend's components, favored by the presence of urea as a co-plasticizer[56].

Another important issue displayed by PVA/starch films is their poor water resistance, due to the hydrophilic nature of the polymers themselves. To decrease their hydrophilic character, several treatments have been developed, including chemical modifications of the primary

components, cross-linking reactions, acid treatments[57], and surface modification of the films[51].

To cite a few, the use of poly (ethylene-co-acrylic acid) as the crosslinker in PVA/starch films is proven to increase the elongation at break and the overall tensile strength[58], and similar results can be obtained using glutaraldehyde[59], which also improves the water resistance of the blends. A lowering in the films' hydrophilicity is also observed when using hexamethoxymethylmelamine as the crosslinking agent, which also gives films with good mechanical properties, even without the presence of a plasticizing agent [60].

What arises from this brief overview is the strong correlation between mechanical and water resistance with the "unavailability" of -OH residues. In other words, the more the hydroxyl groups of PVA and starch are involved in bonds, the more the PVA/starch biocomposites show improved mechanical response and insoluble character. It is important to notice that, aside from "forcing" -OH groups to form bonds through the addition of external components or crosslinking agents, the freeze-thawing strategy represents an important "green" alternative approach to favor strong interactions between hydroxyl functionalities. This aspect will be discussed later in this work.

1.1.3.2 PVA/starch hydrogels

Whereas films have been developed and studied for decades, PVA/starch-based hydrogels have received some attention only in more recent times. Their versatility and interesting multiple applications, however, have pushed this field of research to grow fast in the last ten years. To summarize, we can broadly divide PVA/starch hydrogels into two main categories: chemically-crosslinked and physically-crosslinked gels.

Chemically cross-linked PVA/Starch hydrogels

Beyond its green character, starch is a versatile reagent, thanks to its abundance in available hydroxyl groups. Indeed, starch can be covalently cross-linked with PVA exploiting the reactivity of its -OH functionalities towards bi- or multifunctional compounds such as glutaraldehyde (GA)[61], and bi- or tricarboxylic acids. Generally speaking, the effect of introducing chemical crosslinks in the system translates into the formation of matrixes with low porosity, higher rigidity, and decreased swelling ability[62]. In order to modulate these effects, Onofre and Wang, incorporated carboxymethyl and aminoethyl groups substituents on starch chains after crosslinking with epichlorohydrin, obtaining hydrogels with improved swelling power [63].

Another approach for improving and tailoring PVA/starch gels is to chemically modify starch prior to its use in the synthesis. Functionalization of starch with monophosphate and subsequent crosslinking with succinic acid, adipic acid, glutaric acid, maleic acid, or citric acid yields a strong improvement of swelling power, and an increase in the long-term network stability[64]. Resistance of the network towards harsh pH conditions can be achieved by functionalization of starch with hydroxypropyl groups prior to crosslinking with sodium trimetaphosphate or sodium tripolyphosphate[65]. To increase the porosity of the cross-linked networks, third components can be added as pore-forming agents, which is the strategy that Thakur et Al. recently applied on the synthesis of PVA/starch gels crosslinked with GA for water/oil separation purposes[66].

As already mentioned for PVA chemical gels, all these systems have in common the drawback of using hazardous solvents and reactants, which is to be avoided in "green" approaches.

Physically cross-linked PVA/Starch hydrogels

A suitable approach for preparing biocomposite networks without the necessity of adding toxic reagents nor organic solvents is to freeze-thaw PVA/starch aqueous solutions. Despite the rather easy preparation method, literature on physically cross-linked PVA/Starch hydrogels is less vast than one could expect. The advantage of their biocompatible non-toxic character has quickly gathered the attention of researchers belonging to the bio-medical field, almost skipping the involvement of material scientists. As a consequence, even though their application for drug delivery and wound dressing is widely and successfully reported[67–69], insights into their structure, formation mechanism, and, in general, composition/properties relationships are far less known. Indeed, as far as we know, most of the characterization of PVA/starch F/T hydrogels does not go much further than microscopical observations and FT-IR measurements, and even PVA/starch compatibility in such systems is still a matter of debate. Up to date, there are two main points on which researchers agree: first, that the addition of starch in PVA cryogenic networks causes the appearance of a broad porosity[18], and second, that PVA/starch interactions may occur through hydrogen bonding[70]. Since widely porous hydrogels have been proved to be particularly effective for cleaning artistic surfaces, PVA/starch FT gels can represent a valid and greener alternative to the synthetic systems currently used in the conservation field. Moreover, lacking extended characterization, an in-depth analysis of their structure and properties is necessary to fill an important gap of knowledge. In the next experimental section, both these aspects will be faced.

Submitted Paper I

1.2 "Green" Biocomposite PVA/starch Cryogels as new advanced tools for the Cleaning of Artifacts

1.2.1 Overview

1.2.1.1 Context

The cleaning of painted surfaces with historical value is a particularly delicate task and the challenges that it poses vary from case to case[4]. Modern and contemporary paintings may present textured and irregular surfaces, while older works of art have issues regarding the stability and cohesion of the painted layers, and both can be constituted of water-sensitive materials.

To match the variety that connotes these artifacts, the need for different and ad-hoc cleaning tools arises. Lately, hydrogels with different features have been successfully applied for the cleaning of Cultural Heritage, from rigid water-retentive and chemically cross-linked matrixes to compliant physically entangled networks[7-9]. Aside from the variety of synthesis methods, the optimal features that gels designed for this purpose should have are rather precise.

To be effective as cleaning tools, hydrogels have to be characterized by a good inner cohesion, to not to leave residues on the treated surfaces, a broad and interconnected porosity, to boost dirt capture and removal, and high water content but good water retention, to ensure efficient yet safe performances when applied on sensitive materials.

Moreover, coping with the transversal need of abandoning the production and use of synthetic polymers, these features should be ideally displayed by materials prepared through green synthetic routes starting from eco-sustainable materials.

Regarding the synthetic strategy, poly(vinyl alcohol) (PVA) is the perfect candidate as starting material, since strong hydrogels can be obtained by its solutions via freeze-thawing, with no crosslinkers nor organic solvents required[11].

However, PVA is a synthetic polymer, and both its production and disposal are not free from environmental drawbacks. To improve the eco-compatibility of PVA-based freeze-thawed gels (F/T PVA), a possible strategy is to partially substitute the synthetic polymer with natural ones.

In this work, we chose to employ rice starch, a raw natural polymer-containing product, rather than a pure polymer that requires the processing of the primary source. Beyond reducing the amount of needed synthetic polymer for the preparation of hydrogels, the presence of polymeric chains different from PVA can trigger phase separation events in the pre gel solutions, with consequences on the structure and morphology of the final network.

As recently reported, F/T PVA can be switched from a more compact to a porous sponge-like gel, by introducing a second polymer in the starting solution, and this new feature has been deemed as responsible for the enhancement of the gel's dirt-capture ability[7].

Besides, starch contains two different polymers (amylose and amylopectin), and their behavior in a PVA solution is still largely unexplored. It is reasonable, however, to expect the arising of different equilibria, depending on the relative amount of the three polymers in the system. This translates into the possibility to obtain, without varying the components nor the synthesis technique, a broad variety of different hydrogels, that can match the requirements of different artistic surfaces.

Furthermore, despite having been prepared and applied by a few research groups, there is a vast gap of knowledge on freeze-thawed hydrogels based on PVA and native starch, and the characterization of these systems is scarce and barely reported.

1.2.1.2 Aim

This work develops around two different yet connected objectives: the synthesis and extended physicochemical characterization of biocomposite PVA/starch cryogels, and their application as cleaning tools on painted surfaces.

The main aim of the gels' characterization is to obtain the information for building a theoretical framework about composition/structure relationships. The effects that different structural arrangements have on the final properties of the systems have been also explored. This knowledge can allow the formulation of materials with tailorable features that can be tuned to match the requirements of diverse applicative purposes.

In our case, the goal is to use the acquired information to develop hydrogels to be safely and effectively used as cleaning tools on painted surfaces displaying different issues.

1.2.1.3 Findings

Regardless of the mixing ratio, introducing starch in PVA solutions triggers phase separation phenomena with the consequent formation of broad porous sponge-like structures.

Moreover, the presence of starch in the network causes a progressive increase in the gels' compliance, without compromising their elastic

behavior. Indeed, from a rheological point of view, all the investigated systems (starch content up to 66% of the total polymeric fraction) behave as chemical-like strong gels, despite the tendency of starch alone to form soft physical gels.

As regards the interactions intercurring between PVA and starch, in the systems characterized by a 1:1 ratio of the components we observed the formation of properly mixed networks, held together by hybrid tie points in which both PVA and starch are present.

The PVA/starch interactions are not limited to this specific composition. In all the systems, a decrease of PVA relative crystallinity was detected, suggesting that interactions with starch's polymer hinder PVA-PVA hydrogen bonding. Said interactions are more likely to occur between PVA and linear amylose, while branched amylopectin is believed to segregate in a separate phase acting as a porogen.

By varying the PVA/starch ratio, we tuned some hydrogels' fundamental features such as viscoelastic behavior, porosity, and water-retentive ability. This allowed us to obtain tailored gels to be used as cleaning tools on two artificially soiled painted surfaces.

For the application on a highly-textured, irregular alkyd paint, a gel with high compliance and broad pores was synthesized. For the treatment of a flat, water-sensitive tempera, we prepared a gel with a higher elastic modulus, broad porosity, and excellent water-retentive ability. The outcomes of both the cleaning operations were excellent and comparable to the ones obtained after the application, on the same painted surfaces, of state-of-the-art synthetic gels specifically developed for Cultural Heritage.

Furthermore, given their biocompatibility and environmentally friendly character, PVA/starch cryogels are easily transferable to transversal fields where "green" and biocompatible confining networks are needed.

“Green” Biocomposite Poly(vinylalcohol)/starch cryogels as new advanced tools for the Cleaning of Artifacts

Vanessa Rosciardi, David Chelazzi, and Piero Baglioni

(Submitted Manuscript)

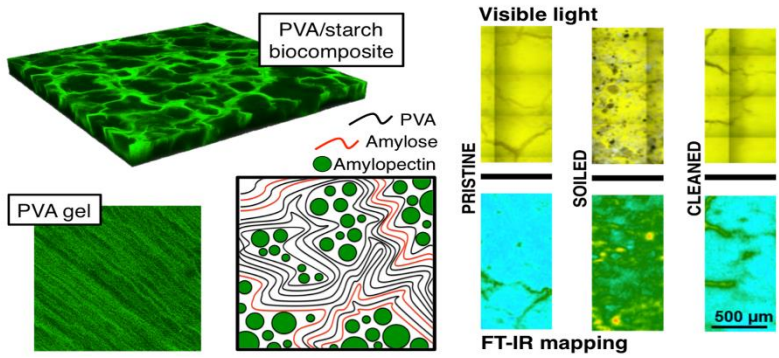

Abstract: The formulation of gels from synthetic polymers has improved the cleaning of works of art, but there is still large room for the formulation of materials with optimal efficacy and higher eco-compatibility. Here, Poly (vinyl alcohol) (PVA) and rice starch (RS) were used to obtain biocomposite hydrogels through a robust and “green” route based on freeze-thawing. The composites behave as strong gels whose structure and viscoelastic response are controlled tuning the PVA/RS ratio. X-ray scattering and thermal analysis suggested the formation of hybrid PVA-RS links. Starch amylopectin likely acts as a porogen, while amylose forms hydrogen bonds with PVA. The gels adhere to rough paint layers and remove soil effectively without residues, as assessed by micro-Fourier transform Infrared spectroscopy (µFTIR) imaging. Overall, the PVA/RS composites are as effective as

their fully synthetic counterparts but provide a significant step forward in terms of eco-sustainability.

Introduction

Cultural Heritage assets are crucial to mankind, as they are drivers of welfare and economic improvement. If properly preserved, this patrimony can boost job creation, social inclusion, and cultural identity, in a word, increase the resiliency of our socio-economic system.

Unfortunately, works of art are inevitably threatened by degradation processes, which must be addressed and counteracted to grant accessibility to the works and their transfer to future generations [1]. One of the most delicate topics involves the cleaning of the artifacts, where soil or detrimental coatings need to be removed from the surface of the objects [2].

The main challenge relies on gaining selective removal of unwanted layers [3] without altering the original components of the artifacts, a task made difficult by the high number of interactions at play between surface layers [4]. In the specific case of painted artworks, one of the most iconic forms of artistic production, several approaches have been proposed over the years, pointing towards higher levels of cleaning control and specificity towards the target materials that need to be removed [5] [6] [7].

Besides, cleaning tools must cope with the fundamental requirements of the Green Deal, i.e., the constituents of the cleaning systems must be environmentally friendly and possibly based on green chemistry [8] [9]. Several cleaning fluids have been employed to clean artworks, including organic solvents [10], aqueous solutions (of chelating agents, enzymes, and surfactants [11]), and microemulsions [12] [13] [14].

To improve control of the cleaning action, the fluids have been confined [15] into increasingly sophisticated and tunable materials, from more

"traditional" media (e.g., viscous dispersions of cellulose ethers and polyacrylic acid) to state-of-the-art retentive systems. Excellent results have been obtained using gels based on polymers like Poly (vinyl alcohol) (PVA) [11] [16], Poly (2-hydroxyethyl methacrylate) (pHEMA) [17], Poly (vinyl pyrrolidone) (PVP) and Poly (methyl methacrylate) (pMMA), that represent the most advanced cleaning systems in the field.

Among these, PVA displays some fundamental advantages. Firstly, it is the world's most produced water-soluble polymer [18] (on the order of several hundred kton/yr) and its synthesis is often integrated in the production cycles of petrochemical industries. Besides, its solubility in water accounts for the possibility to obtain strong hydrogels by simply freezing and thawing PVA aqueous solutions (without using synthetic crosslinkers, toxic solvents or additives) and is also key to its biodegradability [19], which makes it more eco-sustainable.

In the field of art conservation, the latest improvement regards the formulation of networks where PVA is blended with other synthetic polymers, such as PVP or PVA chains with different hydrolysis degree ("twin-chain" hydrogels); blending in these polymers changed the pore structure and mechanical behavior of the PVA networks, boosting soil capture and enhancing the feasibility of the cleaning intervention [20]. However, despite these crucial advantages, there is still large room for the formulation of polymer networks that retain optimal cleaning performances but have higher eco-compatibility.

Concerningly, PVA industrial practice, inflated by the good properties of the polymer, is increasingly causing sustainability issues, owing to the ecological impact of waste release in water [21]. Therefore, coping with the global need to formulate alternative and sustainable materials, we propose here composite polymer networks in which PVA is partially substituted by starch, a widely available and compostable biomaterial.

Starch is a natural mixture of amylose and amylopectin (in a ratio comprised between 15:85 and 25:75 [22]). Amylose is a linear α-glucan

with an average molecular weight ranging from 10^5 to 10^6, containing almost exclusively (1→4)-α-linkages, with a small presence of (1→6)-α-linkages (usually less than 0,1% [23]). Amylopectin is a highly branched macromolecule with larger molecular weight than amylose, usually comprised between 10^7 and 10^9, displaying 95% (1→4)-α- and 5% (1→6)-α- linkages [24]. Both amylose and amylopectin show great variability in molecular size, structure, and polydispersity depending on their botanical origin.

Compared to the other starches, rice starch displays many advantages due to its hypoallergenicity, small size of granules, and great freeze-thaw stability of its pastes [25]. Rice starch is largely available since rice is one of the most consumed and cultivated food in the world (accounting for 80% of the caloric daily income in Asian countries, with production rates of 60 million tons per year [26]).

We combined the advantages of PVA and rice starch with the aim of obtaining greener yet highly performing biocomposite hydrogels. Composite PVA/starch films and gels have been previously explored. Xiao and Yang, for instance, synthesized a PVA/starch hydrogel grafting Polyvinyl acetate (PVAc) onto starch via radical copolymerization [27], Zhai et al. have obtained analogous systems employing gamma radiation [28]. Kenawi et al. have used hydroxyethyl starch, a synthetic derivative obtained reacting amylopectin and ethylene oxide [29]. Despite having interesting features, these systems all share the disadvantage of being obtained through chemical processes starting from monomeric precursors, rather than raw "ready to use" materials.

This limitation can be conveniently overcome by switching from a purely chemical to a physicochemical approach, recurring to liquid-liquid phase separation process by freeze-thawing PVA-starch solution to obtain the biocomposite systems. Nevertheless, there is a vast gap of knowledge on freeze-thawed hydrogels based on PVA and native starch, and the characterization of these systems is scarce and barely reported [30] [31] [32].

To fill this gap, in this contribution we prepared and characterized different biocomposite hydrogels starting from water, PVA and rice starch. To the best of our knowledge, such a complete characterization of PVA/starch biocomposite cryogels is unprecedented. The aim of our study was to systematically control the structure and physico-chemical behavior of the composites by tuning the starch content, through a green and sustainable synthetic route.

The obtained systems behave as strong (chemical-like) gels, with excellent elastic properties and high adaptability towards rough surfaces. Considering the potential applications of these materials, even beyond Cultural Heritage preservation, and the current lack of knowledge about their features, we provided here an extended characterization of the hydrogels from a morphological, structural, rheological and thermal point of view, formulating hypothesis on the gels' formation mechanism.

Then, we applied for the first time the biocomposite hydrogels to remove soil from painting mock-ups. We addressed two different paint surfaces representative of the most recurring and problematic issues in real conservation practice: a water-based tempera, poorly bound and highly water-sensitive, and an alkyd paint layer whose roughness and irregularities mimic the challenging, hard to clean, surfaces typically encountered in modern and contemporary art.

Results and Discussion

Morphological and structural features

Confocal Laser Scanning Microscopy (CLSM) revealed the micrometric organization of the hydrogels in their swollen state (Figure 1a and 1b): the PVA gel obtained after 2 freeze-thawing cycles (sample A) exhibits a typical semi-oriented structure with tight elongated pores [15], a pattern that is also partially found in sample C (PVA/starch ratio 1:1), although interrupted by the presence of large irregular cavities (up to 100 μm). On the contrary, samples B and D (1:2 and 2:1 PVA to starch ratio, respectively) show spongy structures, with wide pore size distributions. However, despite their similarity, sample D appears to be "denser" than sample B, which seemingly displays wider pores.

The different porosity patterns found in samples B-D suggest that, in the pre-gel solution, at least one of the starch's constituents segregates in a separate phase and thus acts as porogen. Said component is then washed away during the cryogel storage in water, leaving hollow spaces behind it. In the case of sample C, such behavior is less pronounced, indicating better miscibility of the PVA with starch polymers.

Scanning Electron Microscopy (SEM) provided a more detailed view of the samples, allowing the acquisition of well-resolved images at higher magnifications while supporting the CLSM observations. It must be noticed, however, that SEM experiments required the freeze-drying of the samples and the structures observed with the two imaging techniques can appear slightly different due to the diverse hydration state of the gels.

As reported in Figure 2, at lower magnification sample A appears rather compact, with channel-like pores oriented along a main direction in a

subparallel pattern, while the starch-containing samples show an overall broader porosity, in agreement with CLSM observations.

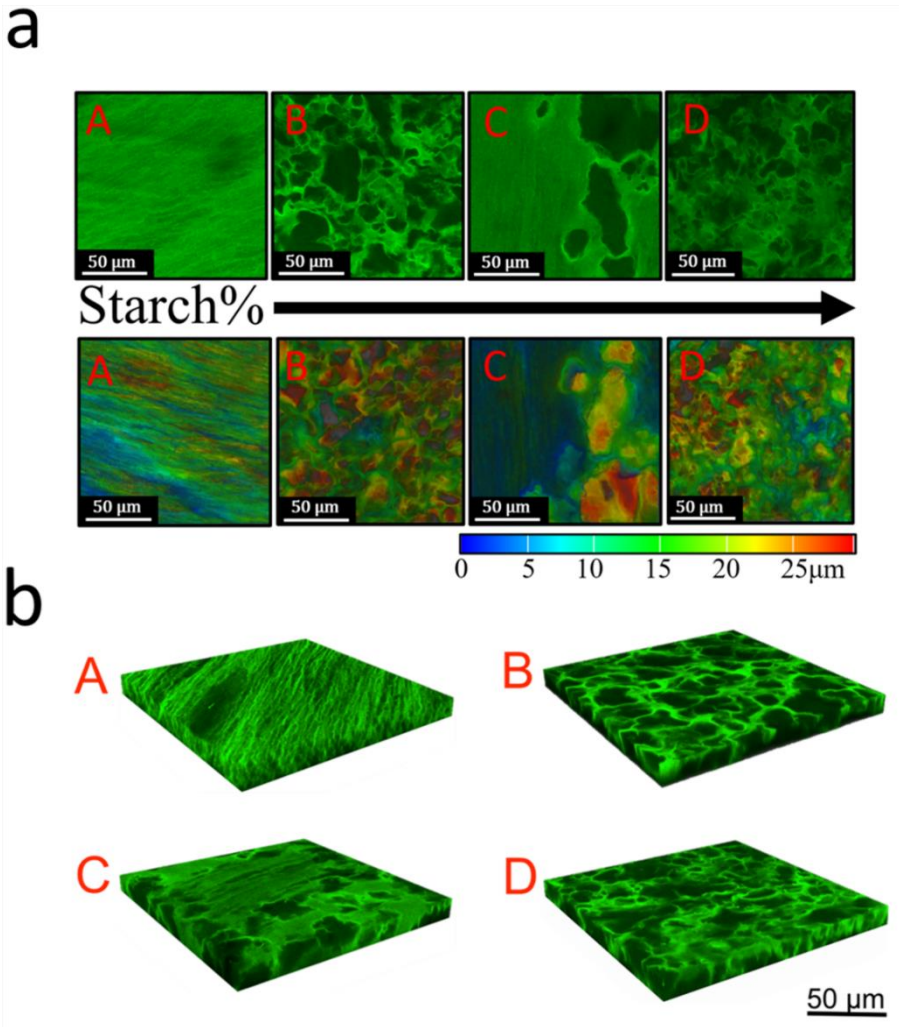

Figure 1. a) Morphological details of the hydrogel samples in the micrometric scale, obtained by CLSM imaging (**A**:PVA gel, **B**:PVA/starch 2/1, **C**:PVA/starch 1/1, **D**:PVA/starch 1/2). The upper row shows 2D sections of the samples collected at 20µm depth from the outer surface. The lower row displays 30µm thick slices represented in 2D using false-colours to show the depth of cavities along the z-axis. **b)** 3D view of 20µm thick slices of the samples.

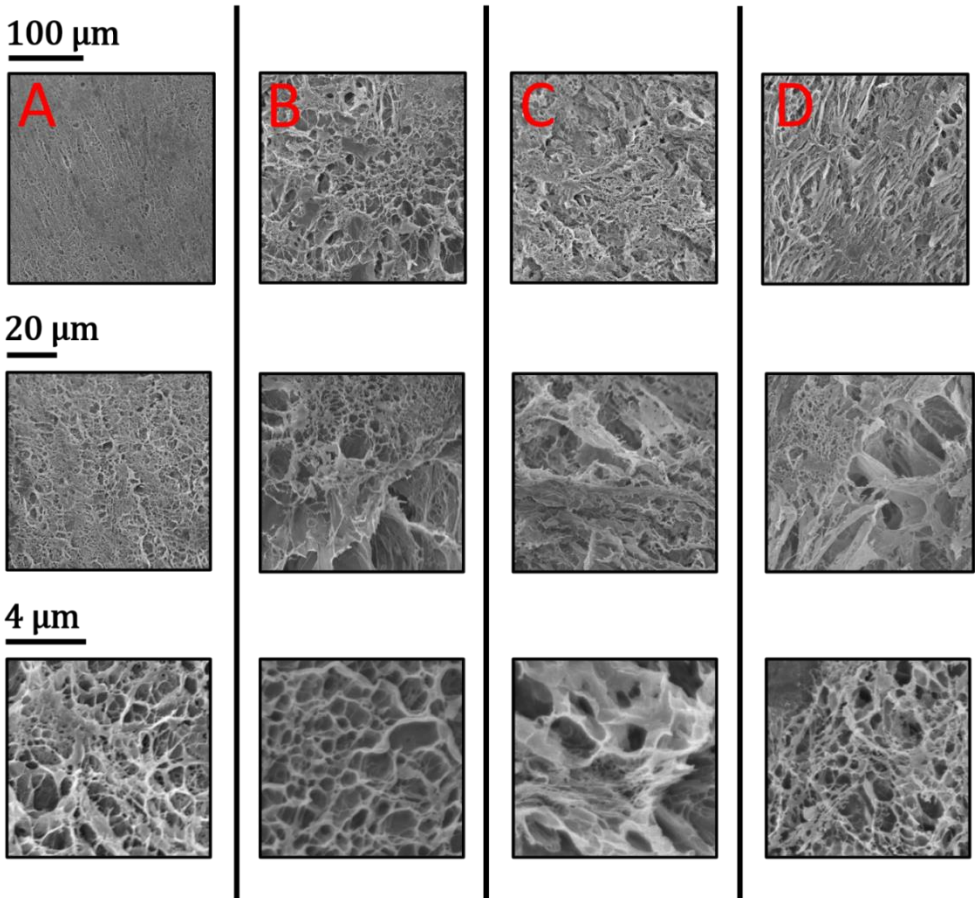

Figure 2. SEM imaging of the xerogel samples (**A**:PVA gel, **B**:PVA/starch 2/1, **C**:PVA/starch 1/1, **D**:PVA/starch 1/2). Each row provides the same magnification for different samples; magnification increases along columns.

Sample B displays a quite defined fractal organization, which is observable for sample A only at higher magnifications. Sample C shows a different organization and appears to be formed by fibrous compact domains with lamellar substructures. In the compact zones, a scarcely defined micrometric porosity is also detected. Sample D, the one with the highest starch content, seems to be constituted by spongy portions, displaying micrometric pores bridged by fibrous junctions, that in turn form the thick walls of larger macropores.

The different morphology of the two domains could indicate a difference in composition, where PVA chains form the spongy regions (whose porosity resembles that of sample A), while the much larger starch polymers are able to form wider gaps and long fibrous junctions.

Chord length analysis, carried out on SEM images, was used to describe quantitatively the dimensional distribution of the voids (pore-phase) and walls (gel-phase) [33] in the samples, to support numerically the morphological observations (more information on chord length analysis is available in SI).

The collected data show typical exponential decays in log f(R) vs R (μm) plots (see Figure 3). To extrapolate the characteristic dimension, here called λ (persistence length), for the pore and the gel phases, the exponential curves were linearly fitted considering only the most frequent chord lengths (lower frequency limit set to $0.5x10^{-3}$).

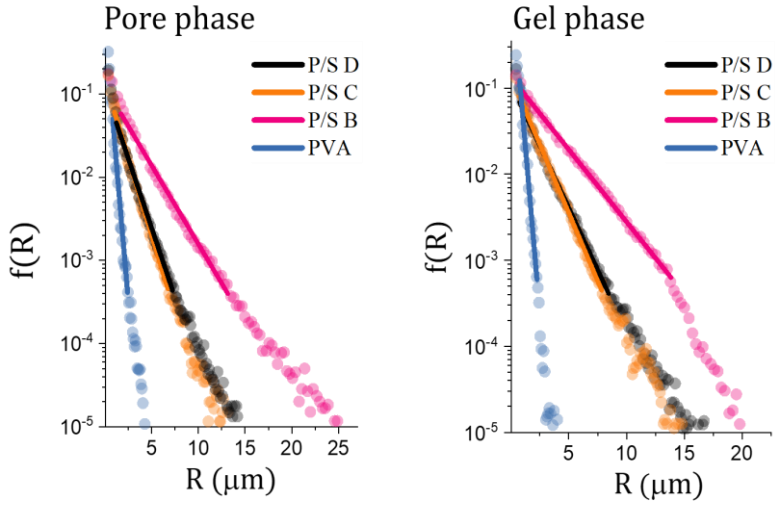

Figure 3. Chord-length analysis of xerogels (**A** = PVA gel; **P/S B** = PVA:starch 2:1; **P/S C** = PVA:starch 1:1; **P/S D** = PVA:starch 1:2). Plots of log f(R) (frequency of occurrence) vs R (μm) (chord length). Points = raw data; Lines = fitting of the exponential decays.

The fitting function is simply y = mx + q, where m corresponds to -1/λ. The obtained values are summarized in Table 1. Both pores' persistence lengths and maximum sizes follow the order A<C<D<B, with sample B showing significantly higher values than the other formulations.

Table 1. Summary of the dimensional parameters obtained through chord-length analysis performed on the SEM images of the PVA and PVA/starch xerogels. Uncertainty is ca. 0.12 μm, calculated from the minimum chord length value (set at 4 pixels).

Sample[a]	λ Pores[b] (μm)	Maximum pore size (μm)	λ Walls[c] (μm)	Maximum wall size (μm)
A	0.76	4.55	0.65	3.79
B	5.55	24.98	5.88	20.06
C	2.69	12.57	3.13	14.98
D	2.99	14.96	3.44	17.32

[a] **A** = PVA gel; **B** = PVA:starch 2:1; **C** = PVA:starch 1:1; **D** = PVA:starch 1:2. [b] Pore phase characteristic length scale. [c] Wall phase characteristic length scale.

All the starch-containing samples show a clearly augmented porosity compared to the PVA gel (sample A), evidencing the porogen role of at least one of starch's polymers.

It is worth noticing that, confirming what observed through microscopy imaging, amongst B, C, and D, the pores' dimension does not increase linearly with starch content, but instead shows a minimum value corresponding to sample C, which is characterized by an intermediate starch to PVA ratio (1:1), highlighting again that in this system the phase separation events in the pre-gel solution are less pronounced.

A similar non-linear relation between gels' structure and starch content was also detected at the nanometric scale by Small Angle X-Ray Scattering (SAXS) experiments. The SAXS curves for each sample were fitted using a shape-independent model specifically developed for gel networks [34], (SAXS curves are reported in SI, Figure S1).

The applied fitting equation accounts for two contributions to the scattered intensity, one due to fixed polymer junctions (i.e., the tie points of the network) and the other due to polymer chains in a liquid-like environment.

For such systems, the scattered intensity I(q), is described by Equation (1),

Equation (1)

$$I_{(q)} = I_L(0)\frac{1}{\left[1+\frac{D^f+1}{3}\left(q^2\xi^2\right)\right]^{\frac{D^f}{2}}} + I_G(0)\,exp\left(-\frac{q^2R^2}{3}\right) + B$$

where $I_L(0)$ and $I_G(0)$ are, respectively, the Lorentz and Guinier parameters, D^f is the fractal exponent, ξ is the correlation length, and R is the radius of gyration of larger objects. The obtained values for ξ, D^f and R are summarized in Table 2, while the complete fitting parameters are available in SI, Table S3.

For classical chemical gels, ξ and R are usually considered as the dimensions of the mesh and the tie points of the polymeric network. In the case of PVA-based cryogels, this approach is not strictly applicable, owing to the peculiar structure of the gels. In such systems, the network is made of polymeric chains densely packed in crystalline domains, and

amorphous regions in which the chains are more disordered and in a liquid-like environment.

Hence, in our case, R refers to the radius of gyration of the denser objects, while ξ can be assumed as the mean distance between the chains in the amorphous portion of the samples (Figure 4).

Table 2. SAXS curves fitting parameters

Sample[a]	ξ[b] (nm)	D[f] [c]	R[d] (nm)
A	3.6±0.1	3.10±0.01	4.9±0.1
B	4.6±0.1	2.94±0.01	4.6±0.1
C	4.7±0.1	2.96±0.01	5.2±0.1
D	4.5±0.1	3.13±0.01	4.5±0.1

[a] **A** = PVA gel; **B** = PVA:starch 2:1; **C** = PVA:starch 1:1; **D** = PVA:starch 1:2. [b] Correlation length. [c] Fractal dimension [R] Gyration radius of the denser scattering objects (i.e., network's tie points).

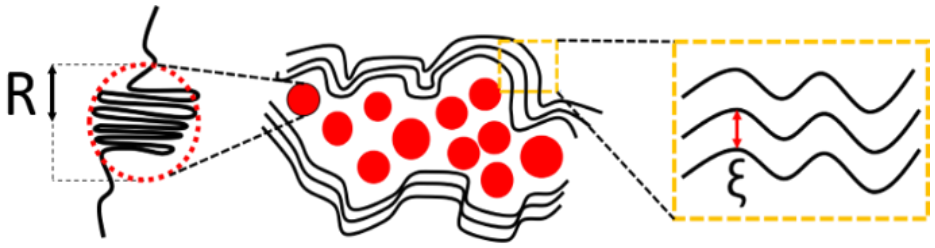

Figure 4. Schematic representation of the dimensional meaning of radius of gyration (R) and correlation length (ξ) in PVA-based cryogels, where the classical concept of crosslinked network is not applicable. Red spheres: denser scattering objects; Black lines: amorphous domains displaying PVA chains in a liquid-like environment.

As reported in Table 2, R values are not linearly dependent on the starch content. Instead, compared to a pure PVA gel (sample A), R decreases at 33% starch content (sample B), then shows a maximum for sample C (PVA:starch 1:1) and decreases again for sample D (PVA:starch 1:2). It

is worth noticing that sample C is characterised by the absolute highest value of R in the set (even higher than sample A).

Because studies on PVA-based cryogels have related the radius of gyration to the dimension of PVA crystallites, one could assume that in sample C their dimension is the highest amongst the samples' set.

Nevertheless, Differential Scanning Calorimetry (DSC) measurements confuted this hypothesis. The DSC curves exhibit melting peaks only in the 190-210°C span (see SI, Figure S2), excluding the presence of crystalline amylose and amylopectin, which melt at much lower temperatures (60-120°C) [35].

Thus, the melting events have been associated to PVA only: the melting temperature of PVA, which is directly associated to the size of the polymer crystalline domains [36][37], is highest for the pure PVA network (sample A) and decreases when starch is added (see Table 3).

The maximum value of R detected in SAXS experiments for sample C is therefore more likely to represent a hybrid tie point in the hydrogel network, composed of PVA crystalline domains in tight connection with starch chains, reasonably showing both crystalline and dense amorphous portions.

The occurrence of large hybrid tie points for sample C could be explained considering that, at 1:1 PVA:starch ratio, the PVA-starch heteropolymeric interactions are statistically maximized, helping the formation of composite aggregates during freeze-thawing, with pressure forces, generated by ice crystals, neighbouring chains together.

The fractal exponent (D^f) of samples B and C is comprised between 1 and 3, which corresponds to a mass fractal dimension typical of complex morphologies such as the branched networks encountered in hydrogels [38]; the higher value of sample C indicates the formation of a more complex network structure [39]. In samples A and D, a D^f value between 3 and 4 indicates a surface fractal dimension.

According to Kolb and Hermann [40], surface fractals are formed when the local concentration of colloidal aggregates approaches unity, a condition enhanced in the case of tightly interacting homopolymer chains. The freeze-thawing process further favors local crowding by means of pressure, promoting non-classical nucleation driven by local density fluctuations [41] [42]. Moreover, a surface fractal dimension close to 3, as found for both A and D, suggests the presence of a rough interface between more and less crowded domains [38].

The correlation lengths (ξ) for all the starch-containing samples (B, C and D) are larger than that of sample A (PVA gel), and their value increases with starch content, as reasonably expected when large polymers (amylose and amylopectin) act as spacers between PVA chains.

Table 3. Summary of values derived from melting events as detected by DSC and as recalculated in respect to PVA content, along with gel fraction percentages.

Sample[a]	T_m[b] (°C)	ΔH_m[c] ($J*g^{-1}$)	$\Delta H_m(w)$[d] ($J*g^{-1}$)	X_C[e] (%)	$X_C(w)$[f] (%)	G%[g]
A	206.4 ±0.6	37.4 ±1.9	37.4 ±1.9	23.2 ±1.4	23.2 ±1.4	88.3 ±2.4
B	196.4 ±1.4	19.5 ±0.3	29.5 ±0.5	12.1 ±0.2	18.3 ±0.3	60.7 ±2.8
C	200.7 ±1.1	10.7 ±0.5	21.4 ±1.1	6.6 ±0.4	13.3 ±0.7	51.1 ±1.1
D	192.0 ±3.7	6.1 ±0.5	18.5 ±1.4	3.8 ±0.3	11.49 ±0.9	47.4 ±2.6

[a] **A** = PVA gel; **B** = PVA:starch 2:1; **C** = PVA:starch 1:1; **D** = PVA:starch 1:2. [b] Melting temperature (at peak and as detected by DSC). [c] Melting enthalpy as detected by DSC. [d] Melting enthalpy as recalculated with respect to PVA content. [e] Crystalline fraction of the entire sample. [f] Crystalline fraction of PVA. [g] Gel fraction obtained through gravimetric methods.

The DSC and gel fraction data provided further insight into the PVA-starch interaction. Figure 5 shows the melting enthalpies (ΔH_m) and gel fraction values (G%) plotted versus increasing starch content. ΔH_m decreases through the A-D series, suggesting the role of starch in hindering the crystallization of PVA, owing to augmented interactions between the different polymers at the expense of PVA-PVA H-bonds[43].

When ΔH_m is weighted by the relative PVA content, it is also evident that the steepest decrease occurs in the 33-50% starch content range. Because ΔH_m and G% decrease in a similar way, one might assume that PVA crystallites are the main responsible for the network formation. To test this hypothesis, we recalculated G% considering only the PVA content of the gel dry mass (pre-washing). The weighed G% curve (see Figure 5) grows steeply for starch content >33%, reaching values higher than 100%, which has no physical meaning.

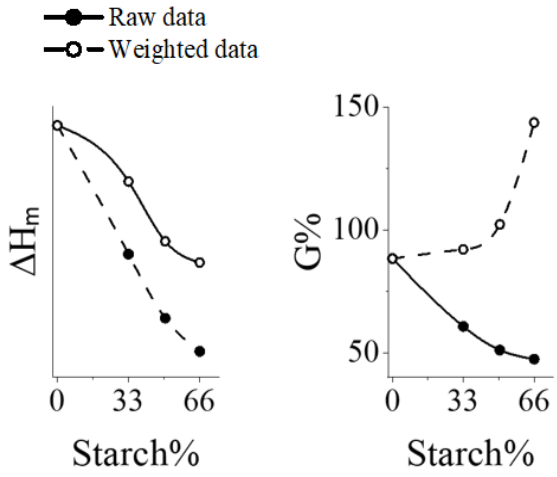

Figure 5. Trends of the melting enthalpies (ΔH_m) and gel fractions (G%) vs. starch content for the PVA and PVA/starch gels. Full points represent raw data, hollow points correspond to data recalculated with respect to PVA content.

This indicates that starch remains in large quantities inside the gel network even after washing, and thus is likely to have a significant structural role: even if starch polymers do not recrystallize during the hydrogels' formation and reduce PVA crystallinity, they participate with PVA in the construction of the gel network.

Overall, a possible picture emerged to describe the different gel formation mechanisms as PVA is blended with starch.

In cryogels derived from mixing PVA and starch in a 1:2 ratio, the microstructure that typically arises in pure PVA gels is heavily disrupted, although polyvinyl alcohol crystallites are still responsible for holding the long-range gel structure.Starch is likely partially washed away and partially present as non-interconnected amorphous domains.

When PVA and starch are in a ratio of 1:1, they can form a composite network, with most of the junctions made of a hybrid mixture of crystalline PVA and amorphous starch polymers, most likely interacting through hydrogen bonds.

Increasing the starch content up to 66% of the overall solid components (i.e., PVA/starch 1:2 w/w) leads to the formation of a network held by starch polymers, with local and scarcely interconnected PVA domains that, nonetheless, exhibits a rheological behavior typical of chemical-gels.

Starch is known to form gel-like systems from cooling solutions with a concentration of 6% w/w or more [44], which is the case of sample D. The proposed evolution of the biocomposite hydrogels at the nanoscale is schematically depicted in Figure 6.

This indicates that starch remains in large quantities inside the gel network even after washing, and thus is likely to have a significant structural role: even if starch polymers do not recrystallize during the hydrogels' formation and reduce PVA crystallinity, they participate with PVA in the construction of the gel network.

The analysis of the FTIR spectra of the different gels (see SI, Figures S3-S8) revealed that sample A (PVA gel) has the narrowest O-H stretching (OH_v) band (centered on 3308 cm^{-1}), as expected from its higher crystallinity. Instead, band broadening is observed in samples B-D and in a starch reference, i.e., a starch dispersion that underwent the same thermal treatment as the other samples.

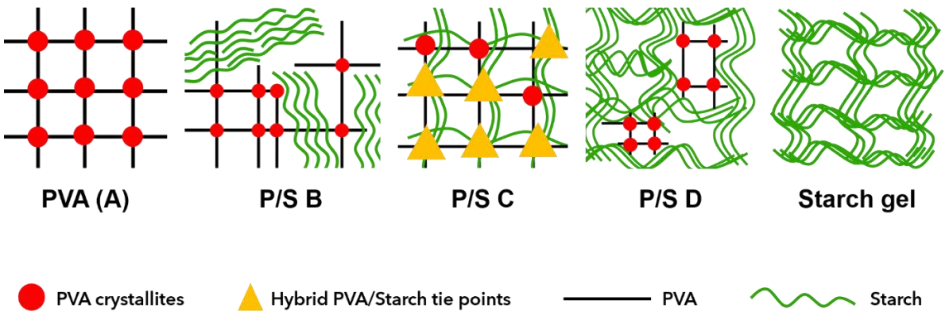

Figure 6. Schematic representation of the hypothesized evolution of the hydrogels at the nanoscale, depending on the PVA:starch ratio and according to SAXS and DSC data. (**A** = PVA gel; **P/S B** = PVA:starch 2:1; **P/S C** = PVA:starch 1:1; **P/S D** = PVA:starch 1:2).

All the PVA-starch gels show shifts in the band frequency as compared to pure systems, indicating that interaction between the two components is taking place through hydrogen bonds, as expected [45]. Indeed, hydrogen bonding between -OH groups of starch and PVA promote localized stability and miscibility of the polymers [46], fundamental requirements for the formation of a composite gel network.

Examples of possible H-bonding configurations are showed in Figure 7, where energetically favored double hydrogen bonds are depicted between hydroxyls in PVA and a model glucose unit: the two bonding sites on PVA are separated by a non-bonding monomer, and show

alternated donor-acceptor character, binding respectively to the -OH on C2 and C6 of the glucose ring.

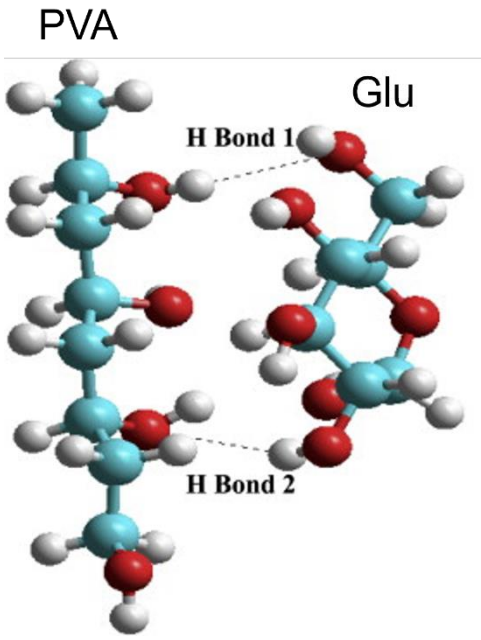

Figure 7. Geometrically optimized structures of double hydrogen bonds between a 4-monomer PVA chain and a model glucose unit (Glu), as calculated with computational simulations. The two bonding sites on PVA are separated by a non-bonding monomer, and show alternated donor-acceptor character, binding respectively to the -OH on C2 and C6 of the glucose ring. Reproduced with permission from "Computational modelling and experimental infrared spectroscopy of hydrogen bonding interactions in polyvinyl alcohol-starch blends", Lee Tin Sin et al., 2010, Elsevier.

Interestingly, C and D show the most marked shift of the OH_v band (20-30 cm^{-1}), suggesting increased PVA-starch interactions. This behavior agrees with computational studies where the highest and most stable mutual interaction is predicted at 1:1 w/w ratio [46]. Besides, it fits

nicely with the formation of hybrid tie points in the gel network when the starch content increases, which is strongly supported by our experimental data on sample C, and cannot in principle be excluded for sample D.

Hypothesis on the formation mechanism of the PVA/starch biocomposite gels

PVA and starch are both known to form gels after being dissolved in water, but the conditions for sol/gel transition are different, since PVA solutions can gel after freeze-thawing, while starch solutions undergo gelation at ambient temperature.

PVA gelation occurs through phase separation at sub-zero temperatures [47], as free water freezes expelling the polymer and progressively concentrating PVA chains in the remaining liquid phase. In such conditions, chains are pushed together close enough to give intra- and intermolecular hydrogen bonds [48], and pseudo-crystalline domains can be stably formed [49], acting as crosslinking points in the three-dimensional network.

The starch gelation is not yet completely understood [50]. Amylose and amylopectin are thought to play distinct roles both in the gelatinization and retrogradation (gelation) processes [51]. During gelatinization, starch's intermolecular bonds are broken by water and heating. At sufficiently high temperatures [52], water penetrates the amorphous domains of starch, formed by linear amylose that is the first to leach out the granules, and progressively swells crystalline domains made by tightly packed amylopectin molecules. At this stage, the system appears as a viscous solution.

If starch concentration is sufficiently high (≥6% w/w), cooling the system leads to the formation of an elastic gel through retrogradation [44]. The initial stages of gelation are dominated by a phase separation into polymer-rich and polymer-deficient phases, followed by formation of hydrogen bonds between the amylose helixes [53]. The role of amylopectin in network formation is not clear: some authors suggest that it might form separate clusters, possibly linked through amylose chains, while others proposed a structural role played by long branched amylopectin types [54].

Both gelation processes consist thus in phase separations, although taking place at different temperatures. Taking this into account, we hypothesized the following mechanism for the formation of the composite PVA/starch network at the mesoscale:

1) Solubilization of PVA and dissolution of starch granules in water at high temperatures (98°C), until a homogeneous solution is formed. Amylose is dissolved from starch granules and is predicted to be highly miscible with PVA [45]. At this stage, the system reasonably consists in a PVA/amylose solution in which amylopectin crystalline domains are still being swollen by water. Once amylopectin is solubilized, being highly branched, we can hypothesize that it will interact poorly with PVA and amylose.

2) Gelation onset at ambient temperature: upon cooling from 98°C to 25°C, amylose undergoes retrogradation, giving a first organization to the system through hydrogen bonding between helixes. Homopolymeric interactions are partially hindered by PVA chains and are not sufficiently strong to form a gel. At this stage we can imagine a primitive supramolecular arrangement that will partially guide the formation of the final structure.

3) Gelation: at subzero temperatures: water freezes forming ice crystals and concentrating the polymer-rich domains. PVA forms homopolymeric crystallites, but also interacts with amylose in non-

organized microstructures. Amylopectin reasonably segregates in separate micrometric clusters.

Finally, during thawing, ice melts leaving pores of few microns. When the gels are washed, most of the amylopectin likely abandons the structure, leaving behind significantly larger micrometric pores.

The described mechanism accounts for the microscopic gel structure observed with confocal and electron microscopy, and is also consistent with the DSC data, since no amylose crystals were detected by thermal analysis, while PVA crystallinity decreased with increasing starch content.

Viscoelastic properties of the hydrogels

Rheology tests revealed that all the hydrogels exhibit chemical-like behavior, despite being held by purely physically crosslinked networks. All the systems are classifiable as strong gels, as they show higher values of the storage (G') than the loss modulus (G") over a large span of applied stresses [55], as measured in both amplitude and frequency sweep tests (see Figure S9 in SI, and Figure 8).

Sample B shows a markedly high value of G', even higher than sample A, which contains PVA only. This could be ascribed to stronger phase separation in the pre-gel solution, which forces the polymer chains of each component into more compact domains.

Flow transition indexes have been obtained from amplitude sweep tests as the ratio between the flow point (τ_f) and the yield point (τ_y), where τ_f corresponds to the shear stress (τ) value at the crossover (i.e., when G'= G"), while τ_y corresponds to the threshold value of τ starting from which G' shows a 5% deviation from linearity.

The indexes values for the hydrogels are reported in Table 4, underlining a particularly high value for sample D (66% starch content). Higher values correspond to an increased tendency to undergo ductile fracture, rather than brittle, under external forces [56]. Indeed, sample D is macroscopically more able to stretch plastically before complete failure, retaining the plasticity of a non-crystalline starch network, with the added advantage of behaving as a strong gel.

Such mechanical properties are key to granting homogenous adhesion to rough and irregular paint surfaces, and removal in one piece without leaving polymer residues.

Table 4. Rheological data of PVA and PVA/starch gels, as obtained from amplitude sweep tests.

Sample[a]	G'[b] (Pa)	τ_y [c] (%strain)	τ_f [d] (%strain)	τ_f/τ_y[e]
A	1755.8 ±72.3	0.83 ±0.11	2.72 ±0.24	3.26 ±0.14
B	4096.9 ±156.2	1.53 ±0.13	3.80 ±0.29	2.49 ±0.22
C	905.0 ±53.1	1.08 ±0.21	2.89 ±0.16	2.68 ±0.17
D	898.8 ±36.9	1.07 ±0.18	4.67 ±0.27	4.37 ±0.25

[a] **A** = PVA gel; **B** = PVA:starch 2:1; **C** = PVA:starch 1:1; **D** = PVA:starch 1:2. [b] Mean storage modulus in the Linear Viscoelastic Region (LVR). [c] Yield point. [d] Flow point. [e] Flow transition index.

Frequency sweeps tested the time-dependent behavior of the samples in the non-destructive deformation range, with high applied frequencies simulating fast motion on short timescales, and low frequencies slow motion on long timescales. Figure 8 summarizes the behavior of G' and G" for the gels, as well as the starch content-dependency of Tanδ, numerically calculated as the ratio G"/G', which corresponds to the tangent of the phase angle between the imposed deformation and the sample response. For ideal solids (pure elastic behavior) Tanδ = 0, while for real materials its value is below 1 when the elastic behavior prevails, above 1 when the viscous response is predominant [57].

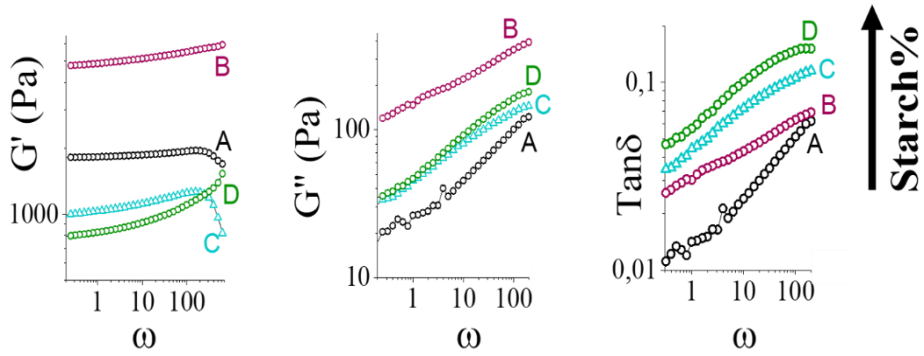

Figure 8. Rheological data obtained from frequency sweep tests on PVA and PVA/starch gels. Storage modulus (G'), loss modulus (G") and phase lag angle (Tanδ) are plotted against angular frequencies (ω, rad/sec). Error bars not shown for sake of clarity (errors do not affect the hierarchy of the displayed parameters). Tanδ values are proportionally related to the starch content of the hydrogels. (**A** = PVA gel; **B** = PVA:starch 2:1; **C** = PVA:starch 1:1; **D** = PVA:starch 1:2).

In our case, no clear trends could be observed between the values of the moduli and the samples' composition. Instead, Tanδ increases with starch content, indicating an incremented fluid-like behavior, and thus suggesting that the presence of starch confers higher flowability and compliance. This is an important feature being key in cleaning irregular surfaces with extended interfaces.

Water content and release

By definition, a hydrogel is characterized by its ability to accommodate high amounts of water in its three-dimensional structure [58]. In cleaning applications, high amounts of free water are helpful to ensure the removal of unwanted materials from the treated surfaces [59].

On the other hand, fluids uploaded in the gels must be released at a controlled rate to avoid excessive wetting, which is one of the main problems experienced by conservators when using free solvents or poorly confining systems [17]. The water content (WC%) and free water index (FWI) of the hydrogels increase with starch content (see Table 5). As previously shown in Figures 1 and 2, the addition of starch causes the formation of spongy structures, capable of loading higher amounts of water than their pure PVA compact counterpart. Besides, the hydrophilicity of starch concurs in favoring water upload.

Because WC%, FWI and Tanδ all increase along the series A-D, we can assume that starch might act as a plasticizer thanks to its ability to retain water, in addition to introducing less ordered domains in the PVA network. The plasticizing role of starch was also confirmed by the depression of the glass transition temperature of PVA around 60°C as detected by means of DSC (see SI, Table S4).

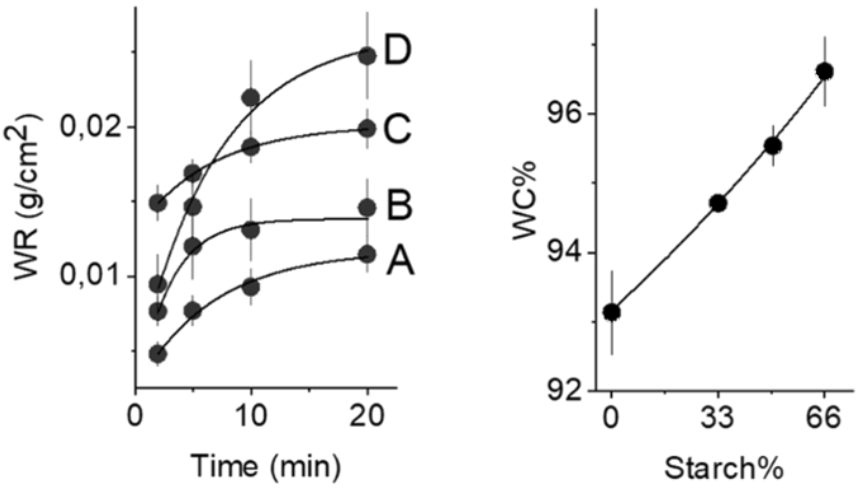

Figure 9. Left: water release (WR) from cubic hydrogels on Whatman® paper after 2, 5, 10 and 20 minutes. (**A**: PVA gel, **B**: PVA/Starch 2/1, **C**: PVA/Starch 1/1, **D**: PVA/Starch 1/2). Right: total water content (WC%).

The total water release after 20 minutes follows the order D>C>B>A. However, it is interesting to notice that the release kinetics differ among the systems (see Figure 9). In particular, sample C is characterized by fast water loss in the first 2 minutes, followed by a much slower release. Sample D, instead, shows a more gradual and lower loss than C in the first five minutes.

When used to clean artifacts, hydrogels are usually put in contact with the surface for limited amounts of time (usually 2-5 minutes per cleaning session). Controlled release of fluids and good water retention are necessary for safe applications on delicate artistic surfaces and represent the main goals that confining networks should pursue to overcome the risks of direct application of cleaning solutions. Therefore, we deemed B and D as the most suitable PVA/starch candidates for cleaning purposes.

Table 5. Water content, water release, and Free Water Index of PVA and PVA/starch gels.

Sample[a]	WC%[b]	FWI[c]	WR [d] (g/cm^2)
A	93.13 ±0.61	87.05 ±0.54	0.011 ±0.001
B	94.71 ±0.09	91.22 ±0.32	0.014 ±0.002
C	95.54 ±0.34	93.74 ±0.48	0.020 ±0.001
D	96.61 ±0.52	96.21 ±0.62	0.025 ±0.003

[a] **A** = PVA gel; **B** = PVA:starch 2:1; **C** = PVA:starch 1:1; **D** = PVA:starch 1:2. [b] Water content. [c] Free Water Index. [d] Water release on Whatmann Paper after 20 minutes of contact.

Cleaning tests

The PVA/starch gels were assessed on different soiled paint mock-ups representative of typical issues in art cleaning, namely a tempera and an alkyd paint treated with artificial particulate dirt. In addition, an alkyd mock-up soiled with artificial sebum (mimicking grease contamination from handling art objects) was also addressed (details reported in SI).

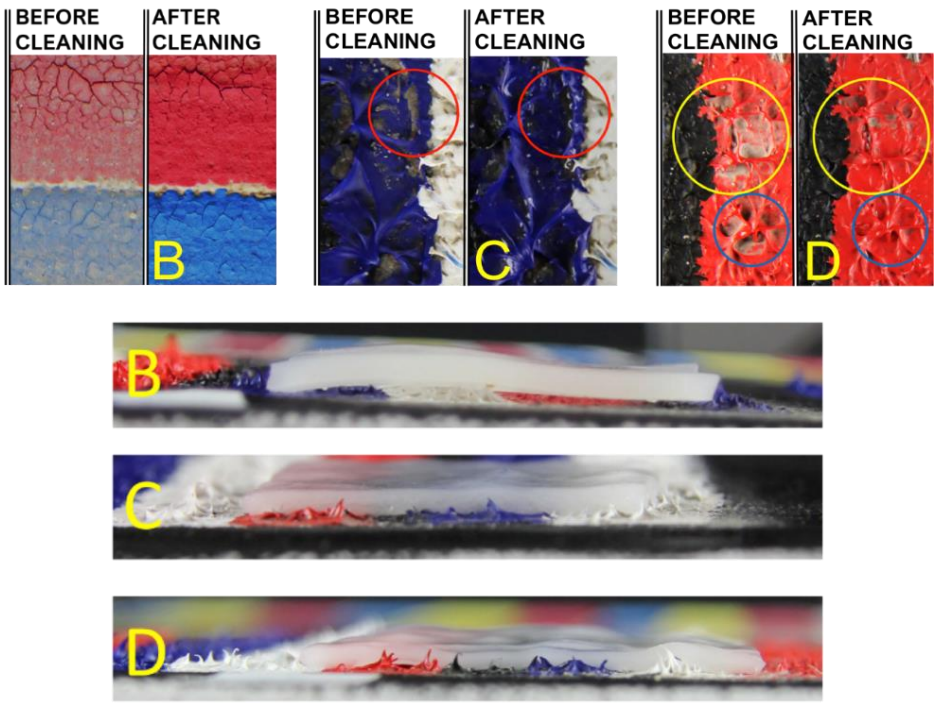

Figure 10. Cleaning of artificially soiled paint mock-ups using PVA/starch gels (**B**: PVA/Starch 2:1, **C**: PVA/Starch 1:1, **D**: PVA/Starch 1:2). Each gel was applied three times on the same spot; each application lasted 5 minutes. (Top) Soil removal from a tempera paint using gel B (left), and from alkyd paint using gel C (center) and D (right). (Bottom) Detail of the gels lying on the rough alkyd paint: adaptability increases with starch content.

In the case of the tempera, the highly water-sensitive surface requires the use of retentive gels to clean the paint without swelling or leaching it. Thus, the PVA/starch B gel was selected for dirt removal, using three short applications (5 minutes each). As shown in Figure 10, effective soil removal was achieved, preserving the texture and original craquelure of the tempera paint, with no undesired alteration or displacement of the pigments.

This confirmed that the high retentiveness of gel B is key in the treatment of water-sensitive surfaces. However, as expected from its rheological behavior, this system is not suited to clean the rough, irregular surface displayed by the alkyd paint mock-up, which is representative of modern/contemporary paintings where dirt is entrapped in cavities and holes hardly accessible by rigid gels.

Gels C and D displayed excellent adaptability to the rough surface, but their application led to different results ascribable to diversities in their microstructure and porosity. Sample C gave poor soil removal (see Figure 10), which can be explained considering that the gel's network is made by an alternation of denser domains and hollow spaces, rather than a fully interconnected porosity; the latter is essential to favor the transport of matter inside the gel and boost dirt removal [15].

Besides, gel C left the paint surface visibly wet, as expected from its water release kinetics. On the other hand, the application on the same irregular surface of gel D (which shows an interconnected, sponge-like porosity) led to excellent dirt removal, even in areas with high three-dimensionality and hidden cavities, without excessive wetting. This formulation also proved optimal for the removal of sebum soil from the alkyd paint (see SI, Figures S10 and S11), simply by loading the gel with a water solution of TAC and MPD surfactant (7% and 3% w/w, respectively).

The performance of the PVA/starch gels was also compared with that of innovative gels accepted in restoration practice, and with gellan gum, a traditional tool commonly adopted by restorers.

For the tempera mock-up, gel B was compared to a highly water-retentive chemical gel based on pHEMA and PVP, commercially available under the trademark HWR Nanorestore gel®[12]. Cleaning efficacy was assessed through high-resolution macro photography and micro-FTIR 2D imaging; the false-colour IR images map the characteristic bands (ν(O-H), 3670, 3656, 3645 cm^{-1}) of kaolinite, the main component in the artificial particulate soil. Both gel B and HWR effectively removed the soil from the tempera surface (Figures 11 and 12). All the applied systems preserved the delicate tempera surface, maintaining the original craquelure.

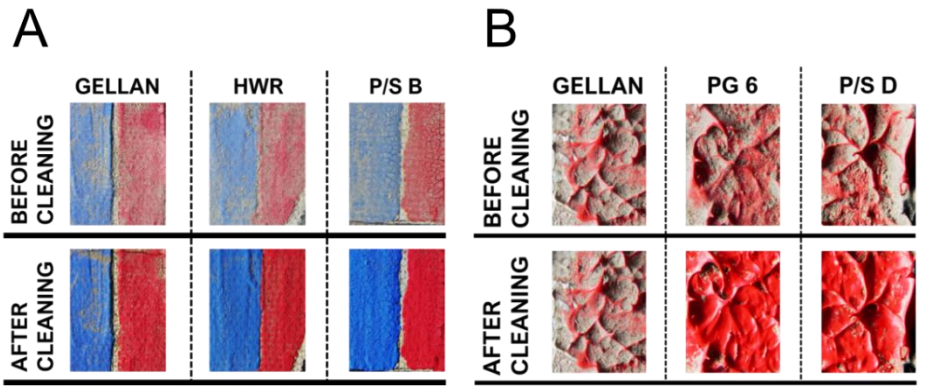

Figure 11. Macro photography images of artificially soiled tempera (A) and alkyd paints (B), treated with PVA/starch gels and commercial benchmarks. Each gel was applied three times on the same spot; each application lasted 5 minutes. **HWR**: HWR Nanorestore gel®; **P/S B**: PVA/starch 2:1; **PG 6**: PG6 Nanorestore gel®; **P/S D**: PVA/starch 1:2.

However, soil removal obtained with gellan gel was scarce: small clean areas are alternated to spots where dirt seems to concentrate (see Figure 12), suggesting that soil was mostly displaced along the surface, rather than removed by the gel.

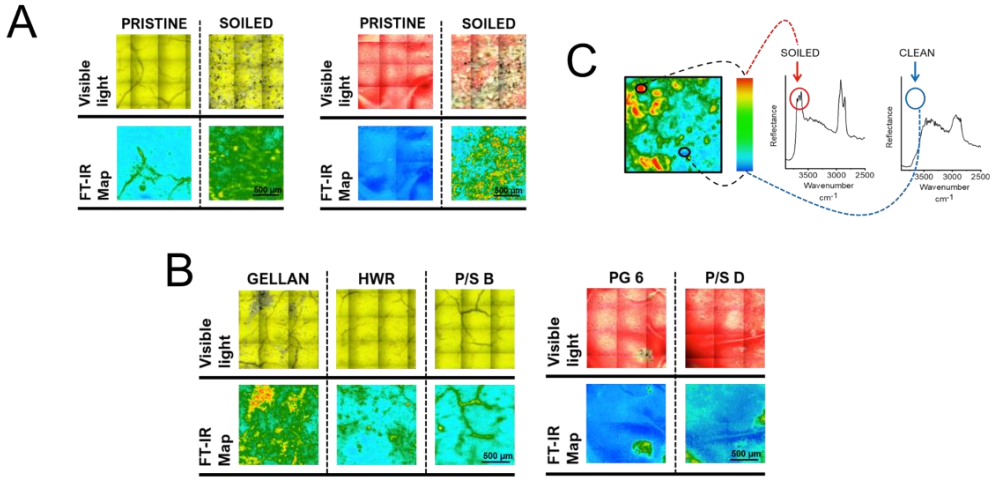

Figure 12. (**A**) Microphotography and FTIR 2D imaging of pristine and artificially soiled tempera (yellow) and alkyd (red) mock-ups. (**B**) Treatment of the mock-ups with PVA/starch gels and commercial benchmarks. Each gel was applied three times on the same spot; each application lasted 5 minutes. **GELLAN**: gellan gum sheet; **HWR**: HWR Nanorestore gel®; **P/S B**: PVA/starch 2:1; **PG 6**: PG6 Nanorestore gel®; **P/S D**: PVA/starch 1:2. (The rigid gellan sheet was completely ineffective on the rough alkyd paint, and the images are identical to those of the soiled mock-up). (**C**) Representative spectra of red (soiled) pixels and pristine/clean (blue) pixels, showing the presence or absence of the ν(O-H) peaks (3670, 3656, 3645 cm^{-1}) of kaolinite in artificial soil.

On the alkyd mock-up, PVA/Starch D was compared to PG6 Nanorestore gel®, a PVA-based hydrogel developed to remove dirt from highly irregular painted surfaces, which was recently used to clean

masterpieces by Pablo Picasso, Jackson Pollock, and Roy Lichtenstein [20] [60] [61].

Both gels showed very good adaptability to the rough paint surface, and their use led to equally optimal dirt removal (see Figure 11 and 12). It must be noticed that such performances surpassed those of the pure PVA network [20]. On such rough surfaces, the rigid gellan sheet was completely ineffective.

Besides, the PVA/starch gels did not leave detectable polymer residues on the treated paints, as assessed by FTIR imaging (see SI, Figure S12), down to the detection limit of the FPA detector (0.02 pg/µm2 [20]). This is another fundamental feature shared with the HWR and PG6 Nanorestore gel® benchmarks [20].

We can therefore conclude that the PVA/starch gels grant safe and highly effective cleaning performances, comparably to widely assessed state-of-the-art benchmarks, with the significant advantage of introducing a renewable biopolymer in the gel production process.

Conclusion

We characterized for the first time the effects of a freeze-thawing synthetic route on the gelation of PVA and native starch blends, tuning the starch content from 33 to 66% (w/w), and studying the gels' structures and structure-related properties.

Starch acts as a porogen and hinders PVA crystallization but participates in the formation of networks that can be classified as strong gels (i.e., chemical-like gels) based on their rheological behavior. The biocomposites show in general larger pores than the pure PVA gel, a

feature that allows enhanced dirt pick-up and matter transport, essential in the cleaning of surfaces.

Besides, the presence of starch makes the gels more mechanically compliant: at 1:1 and 1:2 PVA-starch ratios, the effect is such that the gels homogeneously adapt to rough, three-dimensional surfaces such as those frequently met in modern/contemporary paintings.

As starch is added, structural modifications occur at the nano and meso-scale: at 1:1 PVA-starch ratio, the two components form hybrid tie points in the network following freeze-thawing. SAXS measurements evidenced the presence of a mass fractal in the 1:1 and 2:1 formulations. Instead, for the pure PVA gel, or the 1:2 biocomposite, surface fractals are observed. At the mesoscopic scale, the biocomposite gels' formation likely relies on phase separations, with strong PVA-amylose interactions, while amylopectin mainly acts as a porogen.

The biocomposite PVA/starch gels gave excellent results when applied to remove dirt from paint surfaces. The 2:1 formulation is the most water-retentive and rigid, and proved optimal for the cleaning (with water) of highly water-sensitive tempera paints. The 1:2 formulation, being more compliant, granted homogeneous dirt removal from highly three-dimensional paints.

Overall, the performances of the new PVA-starch gels matched those of the most effective state-of-the-art cleaning tools in terms of efficacy and cleaning control, surpassing either their pure PVA analogue or the traditional gellan gum.

In conclusion, this paper reports on a "green", robust route to control the physical properties of PVA/starch composite gels with high effectiveness as confining systems to clean water sensitive and irregular artistic surfaces.

By introducing starch in the synthetic path, the sustainability of art cleaning formulations is improved, while maintaining and improving optimal mechanical behaviour and cleaning performances. These

features candidate the biocomposites as innovative tools in art conservation and many other applicative fields.

Besides, given their biocompatibility and environmentally friendly character, these systems are easily transferable to transversal fields where "green" and biocompatible confining networks are needed, such as drug delivery, tissue engineering, topical treatments, cosmetics, and many others.

Author Contributions

Vanessa Rosciardi: conceptualization, experimental analysis, data curation, writing of the original draft. **David Chelazzi**: data curation, writing of the original draft. **Piero Baglioni**: conceptualization, project administration, supervision, validation.

References for Paper I

[1] S. Lorusso, *Conservation Science in Cultural Heritage* **2018**, *18* (1), 177-199.

[2] J. H. Stoner in *Conservation of Easel Paintings*, (Eds.: R. Rushfield), Routledge, **2013**, pp 42-58.

[3] P. Baglioni, D. Chelazzi, *Chem. Eur. J.* **2021**, *27*, 10798.

[4] G. Hedley in *Measured opinions: collected papers on the conservation of paintings,* (Eds.: C. Villers), United Kingdom Institute for Conservation, **1993**; pp 112–122.

[5] P. Baglioni; D. Chelazzi, R. Giorgi, G. Poggi, *Langmuir* **2013**, 29, 5110-5122.

[6] P. Baglioni, E. Carretti, D Chelazzi, *Nat. Nanotechnol.* **2015**, *10* (4), 287-290.

[7] M. Baglioni, J. A. L. Domingues, E. Carretti, E. Fratini, D. Chelazzi, R. Giorgi, P. Baglioni, *ACS Appl. Mater. Interfaces* **2018**, *10* (22), 19162-19172.

[8] R. Wolbers in *Cleaning Painted Surfaces: Aqueous Methods*; Archetype Publications, **2000**, pp 36-54.

[9] C. Samorì, P. Galletti, L. Giorgini, R. Mazzeo, L. Mazzocchetti, S. Prati, G. Sciutto, F. Volpi, E. Tagliavini, *ChemistrySelect* **2016***, 1,* 4502.

[10] R. Mastrangelo, C. Montis, N. Bonelli, P. Tempesti, *Phys. Chem. Chem. Phys.* **2017**, *19*, 23762-23772.

[11] M. Baglioni, C. Montis, D. Chelazzi, R. Giorgi, D. Berti, P. Baglioni, *Angew. Chem. Int. Ed.* **2018**, *57*, 7355.

[12] N. Bonelli, C. Montis, A. Mirabile, D. Berti, P. Baglioni, *Proc. Natl. Acad. Sci. USA* **2018**, *115* (23), 5932-5937.

[13] D. Chelazzi, R. Bordes, R. Giorgi, K. Holmberg, P. Baglioni, *Curr. Opin. Colloid Interface Sci.* **2020**, *45*, 108–123.

[14] D. Chelazzi, R. Giorgi, P. Baglioni, *Angew. Chem. Int. Ed.* **2018**, *57*, 7296.

[15] E. Carretti, E. Fratini, D. Berti, L. Dei, P. Baglioni, *Angew. Chem. Int. Ed.* **2009**, *48*, 8966-8969.

[16] T. Guaragnone, A. Casini, D. Chelazzi, R. Giorgi, *Appl. Mater. Today* **2020**, *19*, 100549.

[17] J. A. L. Domingues, N. Bonelli, R. Giorgi, E. Fratini, F. Gorel, P. Baglioni, *Langmuir* **2013**, *29* (8), 2746-2755.

[18] E. Chiellini, A. Corti, S. D'Antone, R. Solaro, *Prog. Polym. Sci.* **2003**, *28* (6), 963-1014.

[19] Y. Watanabe, M. Morita, N. Hamada, Y. Tsujisaka, *Agr. Biol. Chem.* **1975**, *39* (12), 2447-2448.

[20] R. Mastrangelo, D. Chelazzi, G. Poggi, E. Fratini, L. P. Buemi, M. L. Petruzzellis, P. Baglioni, *Proc. Natl. Acad. Sci. USA* **2020**, 117 (13), 7011-7020.

[21] K. Y. Huang, C. T. Wang, W. L. Chou, C. M. Shu, *Int. J. Photoenergy* **2015**, 623492.

[22] R. F. Tester, J. Karkalas, X. Qi, *J. Cereal Sci.* **2004**, *39* (2), 151-165.

[23] A. Buléon, P. Colonna, V. Planchot, S. Ball, *J. Biol. Macromol.* **1998**, *23* (2), 85-112.

[24] J. P. Mua, D. S. Jackson, *J. Agric. Food Chem.* **1997**, *45* (10), 3840-3847.

[25] C. R. Mitchell in *Starch, 3rd ed.* (Eds.: J. BeMiller, R. Whistler) Academic Press, **2009**, pp 569-578.

[26] J. Bao, C. J. Bergman in *Starch in Food*, (Eds.: A. C. Eliasson), Woodhead, **2004**, pp 379-382.

[27] C. Xiao, M. Yang, M., *Carbohydr. Polym.* **2006**, *64* (1), 37-40.

[28] M. Zhai, F. Yoshii, T. Kume, K. Hashim, *Carbohydr. Polym.* **2002**, *50* (3), 295-303.

[29] E. R. Kenawy, E. A. Kamoun, M. S. Mohy Eldin, M. A. El-Meligy, *Arab. J. Chem.* **2014**, *7* (3), 372-380.

[30] A. M. N. Santos, A. P. D. Moreira, C. W. P. Carvalho, R. Luchese, E. Ribeiro, G. B. McGuinness, M. F. Mendes, R. N. Oliveira, *Materials (Basel)* **2019**, *12* (4), 559.

[31] S. Ceylan, D. Göktürk, D. Demir, M. Damla Özdemir, N. Bölgen, *Int. J. Polym. Mater.* **2018**, *67* (14), 855-864.

[32] L. P. Bagri, J. Bajpai, A. K. Bajpai, *J. Macromol. Sci. A* **2009**, *46* (11).

[33] P. Levitz, *Cem. Concr. Res.* **2007**, *37* (3), 351–359.

[34] M. Shibayama, T. Tanaka, C. C. Han, *J. Chem. Phys.* **1992**, *97* (9), 6829–6841.

[35] Å. Rindlav-Westling, M. Stading, P. Gatenholm, *Biomacromolecules* **2002**, *3* (1), 84-91.

[36] J. Sun, S. L. Simon, *Thermochim. Acta* **2007**, *463* (1–2), 32–40.

[37] D. Zahn, *ChemPhysChem*. **2015,** *16*, 2069-2075.

[38] Q. Jiang, C. C. Yang, J. C. Li, *Macromol. Theory Simul.* **2003**, *12* (1), 57–60.

[39] R. Besselink, T. M. Stawski, A. E. S. van Driessche, L. G. Benning, *J. Chem. Phys*. **2016**, *145* (21), 211908.

[40] F. Song, L. M. Zhang, J. F. Shi, N. N. Li, *Colloid Surface B* **2010**, *81* (2), 486-491.

[41] M. Kolb, H. J. Herrmann, *Phys. Rev. Lett*. **1987**, *59*, 454.

[42] J. F. Lutsko, G. Nicolis, *Phys. Rev. Lett*. **2006**, *96*, 046102.

[43] X. Luo, J. Li, X. Lin, *Carbohydr. Polym*. **2012**, *90* (4), 1595-1600.

[44] S. G. Ring, *Starch/Stärke* **1985**, *37* (3), 80-83.

[45] H. G. Xiong, S. W. Tang, H. L. Tang, P. Zou, *Carbohydr. Polym*. **2008**, *71* (2), 263–268.

[46] L. T. Sin, W. A. Rahman, A. R. Rahmat, A. A. Samad, *Polymer* **2010**, *51* (5), 1206–1211.

[47] J. L. Holloway, A. M. Lowman, G. R. Palmese, *Soft Matter* **2013**, *9*, 826-833.

[48] C. M. Hassan, P. Trakarnpan, N. A. Peppas in *Water-Soluble Polymers: Solution Properties and Applications*, (Eds. Z. Amjad), Springer, Boston, MA, **1998**; pp 31-40.

[49] C. M. Hassan, N. A. Peppas, *Macromolecules* **2000**, *33* (7), 2472-2479.

[50] P. K . Kumar, H. S. Joyner, J. Tang, B. A. Rasco, S. S. Sablani, *Food Bioproc. Tech.* **2020**, *13*, 1491-1504.

[51] M. J. Miles, V. J. Morris, P. D. Orford, S. G. Ring, *Carbohydr. Res.* **1985**, *135* (2), 271-281.

[52] D. L. E. Waters, R. J. Henry, R. F. Reinke, M. A. Fitzgerald, *Plant Biotechnol. J.* **2006**, *4*, 115–122.

[53] S. J. McGrane, D. E. Mainwaring, H. J. Cornell, C. J. Rix, *Starch/Stärke* **2004**, *56*, 122-131.

[54] S. Wang, C. Li, L. Copeland, Q. Niu, S. Wang, *Compr. Rev. Food Sci. Food Saf.* **2015**, *14* (5), 568-585.

[55] D. R. Picout, S. B. Ross-Murphy, *Sci. world J.* **2003**, *3*, 105-121.

[56] A. Corker, H. C. H. Ng, R. J. Poole, E. García-Tuñón, *Soft Matter* **2019**, *15*, 1444-1456.

[57] R. R. Eley, *J. Coat. Technol. Res.* **2019**, *16*, 263-305.

[58] E. M. Ahmed, *J. Adv. Res.* **2015**, *6* (2), 105-121.

[59] N. Bonelli, G. Poggi, D. Chelazzi, R. Giorgi, P. Baglioni, *J. Colloid Interf. Sci.* **2019**, *536*, 339-348.

[60] L. P. Buemi, M. L. Petruzzellis, D. Chelazzi, M. Baglioni, R. Mastrangelo, R. Giorgi, P. Baglioni, *Herit Sci.* **2020**, *8* (1), 77.

[61] A. Bartoletti, R. Barker, D. Chelazzi, N. Bonelli, P. Baglioni, J. Lee, L. V. Angelova, B. Ormsby, *Herit Sci.* **2020**, *8* (1), 9.

Supporting Information for Paper I

Supporting Information for:

"Green" Biocomposite Poly(vinylalcohol)/starch cryogels as new advanced tools for the Cleaning of Artifacts

Vanessa Rosciardi, David Chelazzi, and Piero Baglioni

Experimental Procedures

Hydrogels' preparation and storage

Hydrogels were prepared via freeze-thawing starting from aqueous solutions of PVA (99% hydrolyzed, 146000-186000 Mw, Sigma Aldrich) and commercial rice starch (used without further purification). All the pre-gel solutions contained a total amount of reagents fixed to 9 g/100 mL, with variable PVA to starch w:w ratios (1:0, 2:1, 1:1, 1:2, corresponding to hydrogel samples that will be named, from now on, A, B, C and D).

The preparation process can be resumed as follows: reagents were added in the specified proportions to water (purified by a Millipore system with resistivity > 18 MΩ/cm) in round bottomed flasks; the suspensions were then kept at 98°C for 3 hours under vigorous stirring, to obtain homogeneous viscous solutions. The solutions were poured in two types of molds (polystyrene molds to obtain "flat" hydrogels, 14 x 7 x 0.2 cm^3, and silicone molds to obtain "cubic" hydrogels, 1 x 1 x 1 cm^3) and let cool to ambient temperature. Afterwards, the solutions were kept at -20°C then thawed at 25°C. The freezing and thawing process was then repeated once, under the same conditions.

The obtained hydrogels were stored in water for 2 weeks, to allow the polymeric fraction that was not stably involved in the newly formed three-dimensional network to leave the structure. All the hydrogels were stored at room temperature, and the storage water was changed daily.

Thermal analysis

Thermogravimetric analysis (TGA) was performed with a SDT Q600 (TA Instruments) to obtain the gels' water content. Small amounts of samples (wet weights ranging from 15 to 25 mg) were heated from 25°C to 230°C, at a rate of 10°C/min. Differential Scanning Calorimetry (DSC) measurements were performed by means of a DSC Q1000 (TA Instruments) apparatus.

Three different experimental settings were used for each type of gel. Two experiments were performed on freeze-dried samples, one to detect glass transition (T_g) events (heating ramp from 25 to 150°C, heating rate 10°C/min) and another to detect melting (T_m) of crystalline domains (heating ramp from 100 to 250°C, heating rate 5°C/min).

The crystallinity degree (Xc) of the PVA in the gels was calculated as the ratio between the detected specific enthalpy of fusion of the samples and the specific enthalpy of fusion of a perfectly crystalline PVA (161 J/g). No melting peaks, other than those of PVA, were detected in the DSC curves.

Finally, the last experimental set up was used to detect the amount of free water, starting from swollen samples and letting them equilibrate at -60°C before heating up to 25°C with a rate of 5°C/min.

The free water index (FWI) of the systems was calculated as follows:

Equation (S1)

$$FWI = \frac{\Delta H_{exp}}{WC \cdot \Delta H_{theo}}$$

Where ΔH_{exp} (J/g) corresponds to the melting enthalpy of free frozen water determined by integrating the corresponding DSC peak at around 0°C, WC is the water weight fraction in the totally swollen hydrogel, and ΔH_{theo} is the theoretical value of the specific enthalpy of fusion for bulk water (333.61 J/g). Hermetically sealed steel pans were used.

All the TGA and DSC results are presented as average of 3 repeats.

Gel fraction

Cubic gel samples (pre-swelling volume = 1mL) were used to estimate the gel fraction (G%). G% expresses polymers' amount stably linked to the three-dimensional gel network, and was calculated as the ratio between the weight of the xerogel (obtained by freeze-drying the hydrogel after equilibration in water), W_d, and the weight of the initial polymer content of the same sample (considering 1 mL of the pre-gel solutions, whose concentration is known), W_0:

Equation (S2)

$$G(\%) = \frac{W_d}{W_0} \cdot 100$$

Water content and release

The total water content of hydrogels after equilibration in water for 3 weeks was calculated as follows:

Equation (S3)

$$WC = \frac{\left(W_w - W_d \right)}{W_d} \cdot 100$$

where W_w and W_d are the weights of the wet gel and the dry gels, respectively, obtained by TGA. For the evaluation of water release by the gels, completely swollen cubic gel samples were placed on Whatman® filter paper after gentle blotting to remove excess surface water. The filter paper was weighed before contact with the gels, and after 5, 10, 15 and 20 min, to follow the water release kinetics.

The released water was normalized per unit area. All the measurements were performed in triplicate.

Rheological measurements

Rheological analyses were performed on flat gel samples (thickness ≈ 2 mm) after complete swelling. The viscoelastic properties of the hydrogels were studied by means of oscillatory tests performed using a Discovery HR-3 rheometer (TA Instruments) equipped with a parallel

plate geometry of 40 mm diameter and a Peltier temperature control system (temperature was held at 25 °C in all the experiments).

Amplitude sweep tests were carried out in a range of oscillation strain from 0.01% to 15% at constant oscillation frequency (1 Hz). Frequency sweep tests (frequency range 1-100 Hz) were performed within the Linear Viscoelastic Region (LVE), which was previously determined by means of amplitude sweep tests. The results are presented as averages of 3 repeats.

Morphology of the hydrogels

Morphological characterization of the biocomposite hydrogels was carried out by means of Confocal Laser Scanning Microscopy (CLSM) and Scanning Electron Microscopy (SEM). Confocal images were acquired on gel samples swollen in solutions containing Rhodamine 110 chloride (dye content ≥75%, Sigma Aldrich) as fluorescent probe.

The images acquisition was carried out with a Leica TCS SP8 confocal microscope (Leica Microsystems GmbH, Wetzlar, Germany) using an Argon ion laser as excitation source (λ = 488 nm) and a PMT detector (Photomultiplier Tube, selected detection range = 498-540 nm). A water immersion 63X/1.2 W objective (Zeiss) was used. All samples were placed in the sample-holder (Lab-Tek® Chambered Borosilicate Coverglass System, Nalge Nunc International, Rochester, NY, USA) prior to analysis.

SEM imaging was performed using a Field Emission Gun Scanning Electron Microscope ΣIGMA (FEG-SEM, Carl Zeiss Microscopy GmbH, Germany) on freeze-dried samples. Prior to observation, the samples were subjected to gold-metallization by an Agar Scientific Auto

Sputter Coater. SEM analysis was performed with an acceleration potential of 5 kV and a 3.7-4.4 mm working distance.

Chord-length distribution analysis was carried out on SEM images. Each image was iteratively analyzed through the MATLAB® algorithm developed by MacIver28. Images were converted to grayscale, contrast-enhanced and binarized. Then, a set of 10000 lines, randomly oriented, were drawn on each image, and the number of segments defining phase boundaries (changes from the pore- to the gel-phase) were binned according to chord dimension, R(μm), to extract a histogram of frequencies (f(R)), with a binning size of 1 μm. The minimum chord length in pixels was set to 4, which corresponds to about 0.12 μm.

The obtained histograms show an exponential decay if plotted in a semi-log plot (i.e. log f(R) vs R (μm)) that evolves according to [1]:

Equations (S3) and (S4)

$$f\,Pores(R) \propto exp\left(-\frac{R}{\lambda_{pore\ phase}}\right)$$

$$f\ \ Walls(R) \propto exp\left(-\frac{R}{\lambda_{gel\ phase}}\right)$$

where the persistence length, λ, describes the characteristic length scales of the two phases.

Fourier-transform Infrared Spectroscopy (FT-IR)

FT-IR spectra of freeze-dried samples were collected in ATR mode using a Thermo Nicolet Nexus 870 with an MCT detector (Mercury-

Cadmium-Telluride). The spectra were recorded between 650 cm^{-1} and 4000 cm^{-1}, with a spectral resolution of 2 cm^{-1} and 128 scans for each spectrum.

Small Angle X-ray Scattering (SAXS)

SAXS measurements were performed using a HECUS S3-MICRO SWAXS-camera (Hecus XRS, Graz, Austria) equipped with a Kratky collimation system and a position-sensitive detector (PSD 50M), containing 1024 channels (width = 54 μm). Cu Kα radiation of wavelength, λ = 0.1542 nm, was provided by a Cu anode from a 50W microfocus source, with customized FOX-3D single-bounce multilayer point focusing optics (Xenocs, Grenoble, France). The voltage is generated by the GeniX system (Xenocs). The sample-to-detector distance was 281 mm as calibrated by silver behenate (d = 58.38 Å) [2]. The volume between the sample and the detector was kept under vacuum during the measurements to minimize scattering from the air.

Scattering curves were obtained in the Q-range between 0.009-0.54 Å-1. The temperature was kept at 25.0 ± 0.1°C by a Peltier element. A demountable sealed cell for solid was used as the sample holder with Kapton as the window material (optical path =1 mm). Standard measurement conditions were 50 kV, 1 mA. The acquisition time was from 1 to 2 hours depending on the sample. Scattering curves were corrected for the empty cell/water contribution.

The curves were fitted using the SasView software, using a Shape-independent model.

Preparation of painted mock-ups and cleaning tests

Two different series of mock-ups were prepared, i.e., a water-based tempera and a layer of alkyd paint (Windsor & Newton) with pronounced surface roughness and irregularities, painted on commercial primed canvas. After complete drying of the mock-ups, the painted surface was soiled by brushing with an artificial dirt mixture prepared according to the literature [3] and consisting in organic and inorganic particulate dust suspended in nonane. Some of the alkyd paint mock-ups were soiled with a hydrophobic mixture of fatty acids, triglycerides and wax monoesters that mimics human sebum [4].7

Table S1. Particulate soil (Tate soil) composition

Component	Amount[a]
Carbon black	2.0 g
Iron oxide	0.5 g
Silica	1.7 g
Kaolin	20.0 g
Gelatin powder	10.0 g
Soluble starch	10.0 g
Cement	17.5 g
Olive oil	10.0 ml
Mineral oil	20.0 ml

[a] The amounts here reported are relative to 1 L of dispersion in nonane. The particulate soil was prepared according to the literature[3].

Details of the artificial soils' composition are reported in tables S1 and S2. The gels were used as prepared for the removal of the particulate

soil. Prior to the cleaning of sebum soiled surfaces, the gels were loaded overnight with a solution of triammonium citrate (TAC 97%, Merck) and a methoxy-pentadeca(oxyethylene) surfactant (MPD, Nikko, Japan, assay 99%), 7% and 3% w/w respectively, in water.

Cleaning tests were performed by applying the gels directly onto the soiled mock-up surface. The gel sheets were cut in squares (4x4 cm2), gently squeezed with blotting paper to remove surface water excess, and put in contact with the soiled mock-ups. Each cleaning step was 5 minutes long, and the operation was repeated up to 3 times on the same spot, with no additional mechanical action.

For comparison, three benchmark formulations, commonly used by conservators, were also applied on the soiled mock-ups, i.e., a gellan sheet (3% w/w in water), a pHEMA/PVP hydrogel (Nanorestore Gel® HWR), and a PVA-based hydrogel (Nanorestore Gel® Peggy 6).

Table S2. Sebum soil composition

Component	Amount[a]
Squalene	130 mg
Wax monoester (jojoba oil)	250 mg
Triglyceride (triolein)	450 mg
Fatty acid (oleic acid)	170 mg

[a] The reported amounts are referred to a total of 1 g of sebum soil. The artificial sebum soil was prepared according to the literature[4].

Cleaning assessment

Cleaning effectiveness was assessed by photographic and spectroscopic (2D FTIR) imaging. High resolution photos of the treated areas were taken, before and after cleaning, by means of a Canon EOS S60D with

a 100mm macro-objective. The 2D FTIR imaging of the mock-ups was carried out using a Cary 620-670 FTIR microscope, equipped with a Focal Plane Array (FPA) 128 x 128 detector (Agilent Technologies). This set up allows for the detection of analytes inhomogeneously distributed on surfaces, even at low local concentrations [5]. The spectra were collected in reflectance mode directly on the samples, with a spectral resolution of 8 cm^{-1} and 128 scans for each spectrum. The result of each acquisition consisted in a "single tile" map with dimensions of 700 x 700 μm^2, corresponding to 128 x 128 pixels. Each pixel has dimensions of 5.5 x 5.5 μm^2 and provides an independent spectrum. In each 2D map, the intensity of characteristic bands of artificial soil or starch was imaged. The chromatic scale of the maps shows increasing absorbance of the bands as follows: blue<green<yellow<red.

Results and Discussion

SAXS curves fitting

SAXS curves of the samples were fitted according to the following model [6] [7]:

Equation (S5)

$$I_{(q)} = I_L(0)\frac{1}{\left[1+\frac{D^f+1}{3}\left(q^2\xi^2\right)\right]^{\frac{D^f}{2}}} + I_G(0)\,exp\left(-\frac{q^2R^2}{3}\right) + B$$

The fitting equation is the result of the combination of two separate contributions.

The first term on the right side of the equation is a Lorentzian function describing the scattering behavior of a polymer in a semi-dilute regime, i.e., the relaxed polymeric chains of the amorphous portions of the hydrogel network. The term ξ refers to the correlation length, which represents the characteristic distance above which the mass distribution of the scattering cluster is no longer described by a fractal law [8], D^f is the fractal dimension and $I_L(0)$ (Lorentzian parameter) is a scale factor that takes into account the polymer/solvent contrast and the gel's volume fraction.

The second term describes the scattering contribution of the gel's crosslinking points, where R is the gyration radius of the dense domains that form the tie-points in the network, and $I_G(0)$ is the Guinier scale factor.

Table S3. Complete fitting parameters of the SAXS curves for the gel samples.

Sample[a]	$I_G(0)$[b]	$I_L(0)$[c]	ξ (nm)[d]	D^f[e]	R(nm)[f]	B[g]
A	14.992	84.045	3.655	3.098	4.950	0.023
	±0.49	±0.83	±0.13	±0.01	±0.05	±0.01
B	16.816	92.354	4.648	2.944	4.638	0.078
	±0.09	±0.25	±0.07	±0.01	±0.01	±0.01
C	33.199	197.290	4.694	2.958	5.244	0.051
	±0.20	±0.44	±0.06	±0.01	±0.02	±0.01
D	19.716	109.631	4.480	3.135	4.506	0.103
	±0.08	±0.23	±0.05	±0.01	±0.09	±0.01

[a] **A** = PVA gel; **B** = PVA:Starch 2:1; **C** = PVA:Starch 1:1; **D** = PVA:Starch 1:2. [b]. Guinier scale. [c] Lorentz scale. [d] Correlation lenght. [e] Fractal dimension. [f]Gyration radius. [g] Background.

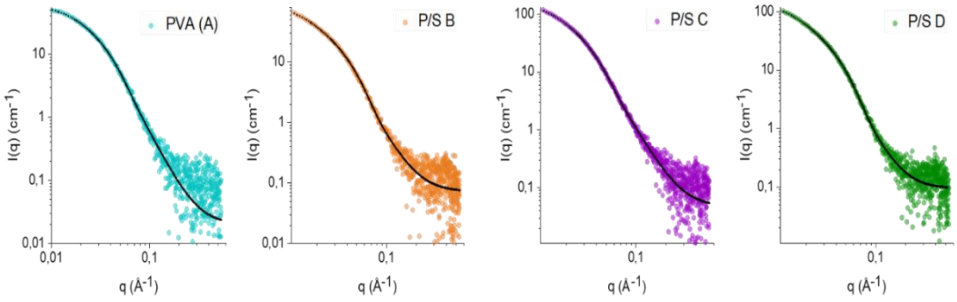

Figure S1. SAXS curves of the samples. (Points = raw data. Black lines = fitted curves);A = PVA gel;P/S B = PVA:starch 2:1; P/S C = PVA:starch 1:1; P/S D = PVA:starch 1:2).

Thermal analysis

DSC measurements allowed the detection of a single melting transition for all the samples (Figure S2). Given the temperature at which it occurred, the thermal event was associated to the melting of PVA crystallites.

No other crystalline domains could be detected during the experiments. Physical entanglements giving rise to amorphous relaxed portions are reasonably co-responsible for the long-range structure of the biocomposite networks.

Changes in the PVA glass transition (T_g) temperature at around 60°C were also detected, confirming the increase of partially disordered structures in the PVA organization due to the presence of starch. Variations in the T_g around 80°C were not taken in account since they are comprised in the fluctuations due to experimental errors (Table S4).

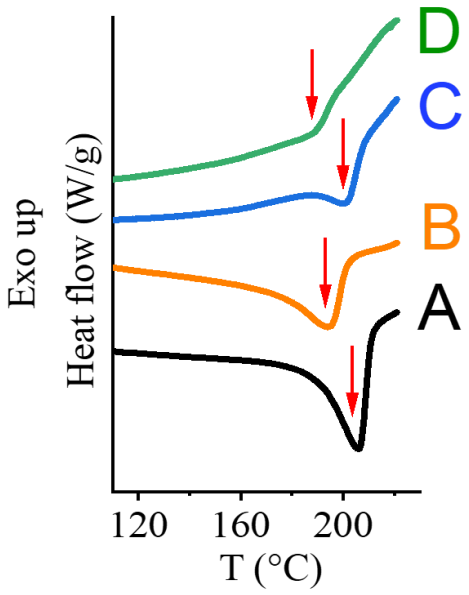

Figure S2. Thermograms detail (Heating ramp 5°C/min, 100-250°C) highlighting the endothermic peaks associated to the melting of PVA crystallites. (**A** = PVA gel; **B** = PVA:starch 2:1; **C** = PVA:starch 1:1; **D** = PVA:starch 1:2).

Table S4. Summary of the glass transition events (T_g) recorded in DSC experiments.

Sample[a]	T_g[b] (°C)	
A	60.04 ±0.24	81.84 ±0.15
B	56.72 ±0.14	83.43 ±1.27
C	56.54 ±0.69	80.23 ±2.84
D	57.69 ±0.06	83.08 ±1.73

[a] **A** = PVA gel; **B** = PVA:Starch 2:1; **C** = PVA:Starch 1:1; **D** = PVA:Starch 1:2. [b] Glass transition temperature.

FT-IR ATR Spectra

FT-IR spectra were collected on freeze-dried samples to avoid signal noise due to water. An additional starch sample prepared with the same concentrations and underwent the same thermal treatment of the investigated samples was prepared and analyzed. All the spectra were collected in ATR mode to avoid xerogels from being exposed to further mechanical stress.

The complete spectra (collected from 3900 to 600 cm^{-1}) are reported in Figures S3-S7. In Figure S8, a closer detail of the 3000-3500 cm^{-1} range is reported, to underline the shifting of the wavenumbers associated to the -OH stretching modes.

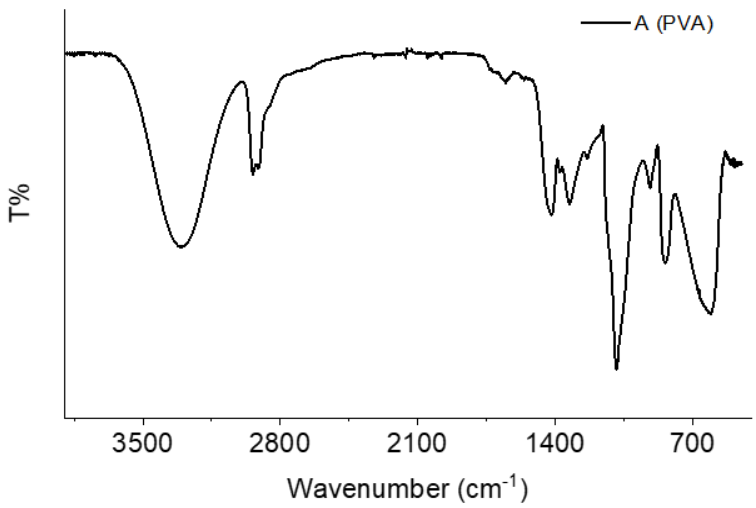

Figure S3. FT-IR ATR Spectrum of freeze-dried PVA gel (sample A).

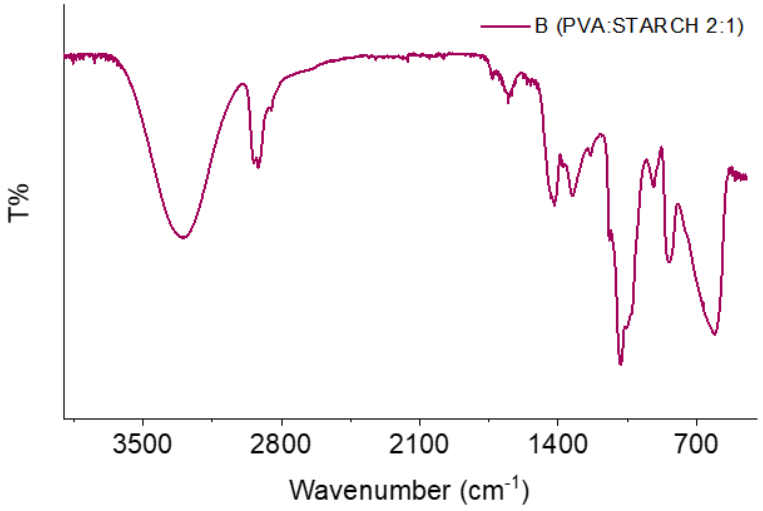

Figure S4. FT-IR ATR Spectrum of freeze-dried gel B (PVA:Starch 2:1).

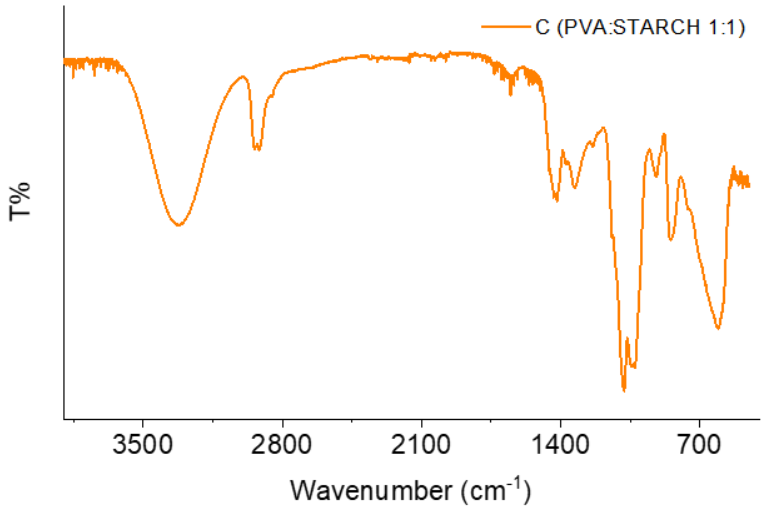

Figure S5. FT-IR ATR Spectrum of freeze-dried gel C (PVA:Starch 1:1).

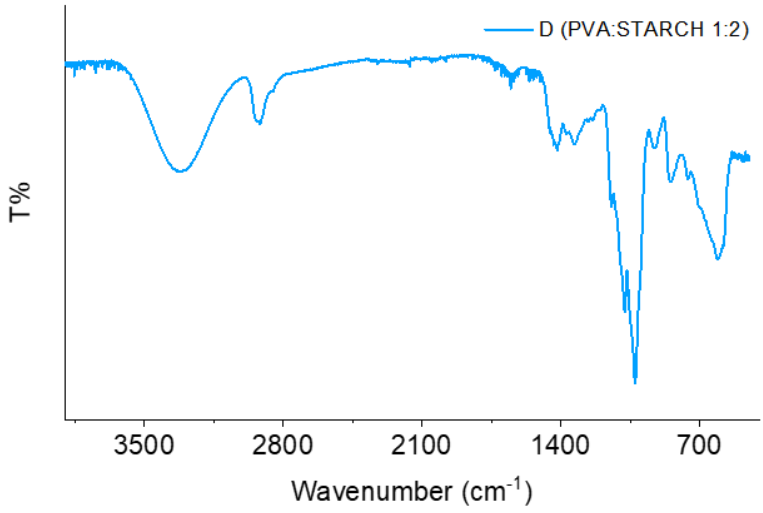

Figure S6. FT-IR ATR Spectrum of freeze-dried gel C (PVA:Starch 1:1).

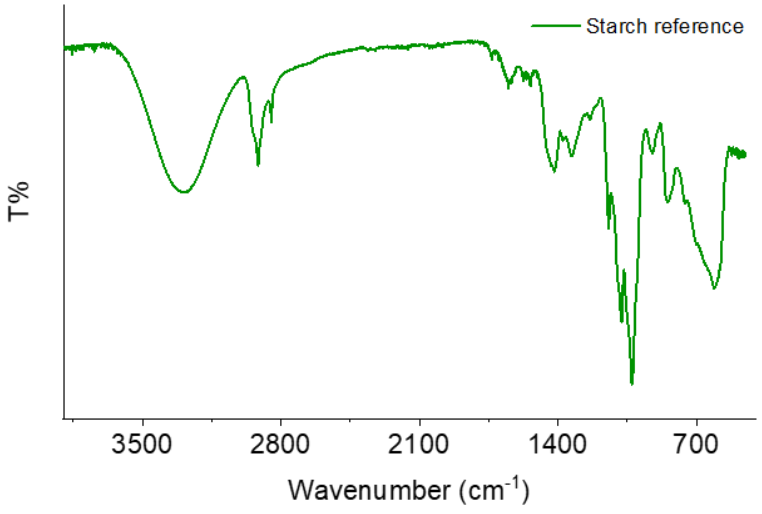

Figure S6. FT-IR ATR Spectrum of freeze-dried gel C (PVA:Starch 1:1).

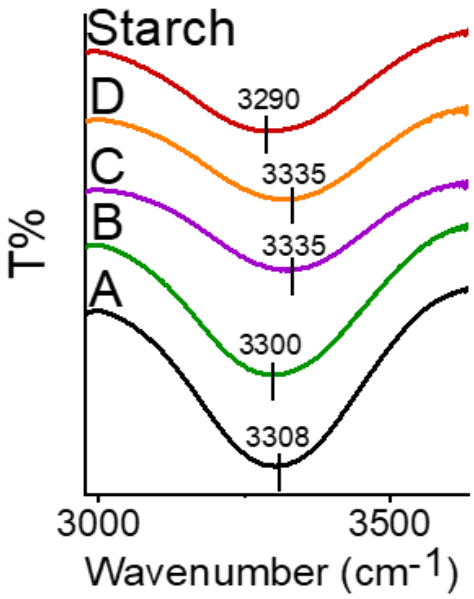

Figure S8. Detail of FT-IR ATR spectra collected on freeze-dried samples (A = PVA gel; B = PVA:starch 2:1; C = PVA:starch 1:1; D = PVA:starch 1:2).

Rheological measurements - amplitude sweep

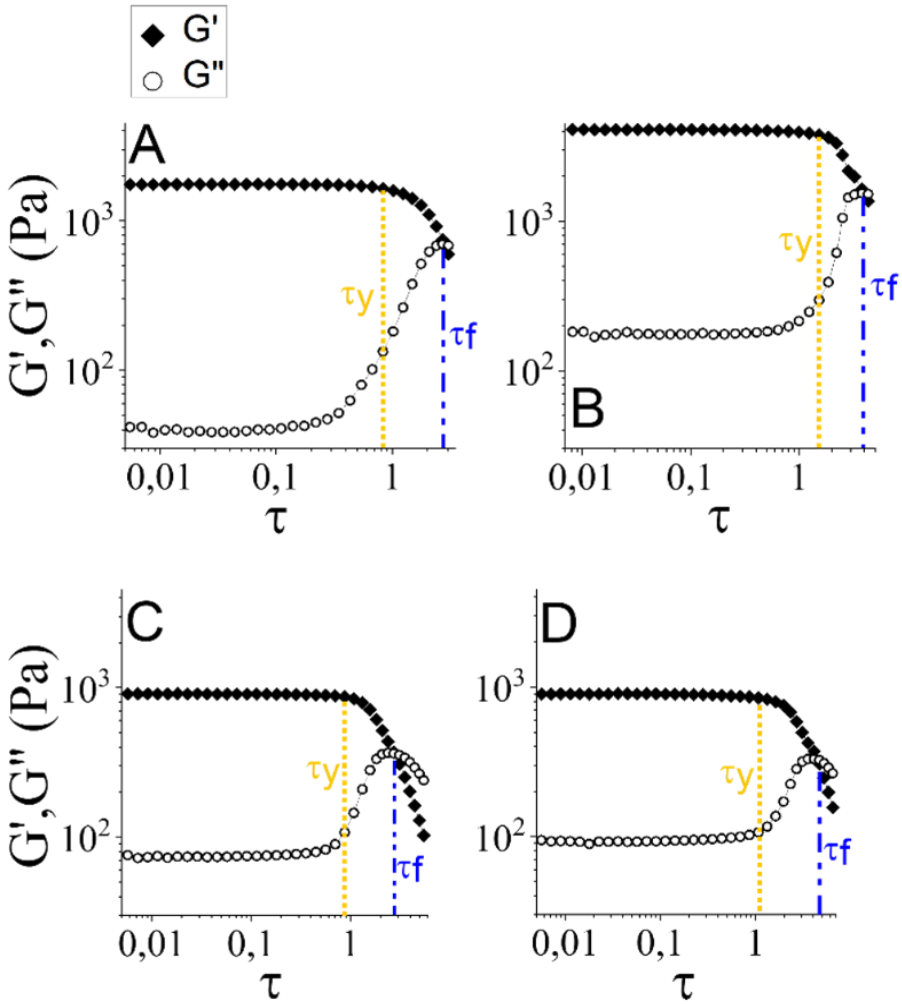

Figure S9. Summary of the results of the rheological analysis performed in amplitude sweep mode. Storage and loss moduli (G' and G") are plotted against applied shear stress (τ, Pa). Yield points (τy) and flow points (τf) are highlighted in yellow and blue, respectively. Error bars not shown for sake of clarity. Errors do not affect significantly τy and τf. (**A** = PVA gel; **B** = PVA:starch 2:1; **C** = PVA:starch 1:1; **D** = PVA:starch 1:2).

Cleaning tests – removal of hydrophobic soil

Cleaning tests were performed to remove artificial sebum from rough alkyd painted mock-ups. For this purpose, PVA/Starch gel D and PG6 Nanorestore® were used. Prior to application, the hydrogels were loaded overnight with a solution of triammonium citrate (TAC) and a methoxy-pentadeca(oxyethylene) surfactant (MPD), respectively 7% and 3% w/w in water. Each gel was applied three times on the same spot; each application lasted 5 minutes.

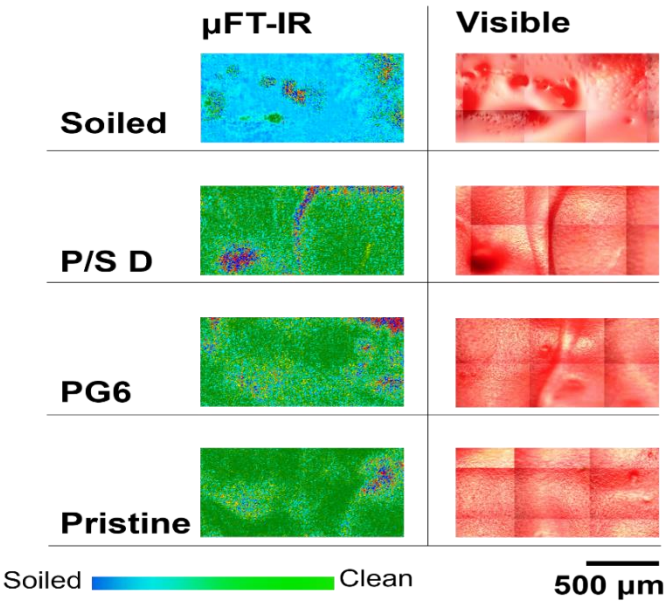

Figure S10. Summary of the results of the cleaning tests performed with P/S D and PG6 gels loaded with a solution of triammonium citrate (TAC) and a methoxy-pentadeca(oxyethylene) surfactant (MPD) on alkyd paint soiled with artificial sebum. From the top: 2D FT-IR microimaging and microphotography of soiled, cleaned and pristine alkyd paint. FT-IR maps in false colors are referred to the intensity of the strong derivative band at 2900 cm^{-1} relative to the stretching modes of aliphatic carbons of the artificial sebum. (**PS/D** = PVA:starch 1:2; **PG6** = PG6 Nanorestore gel®).

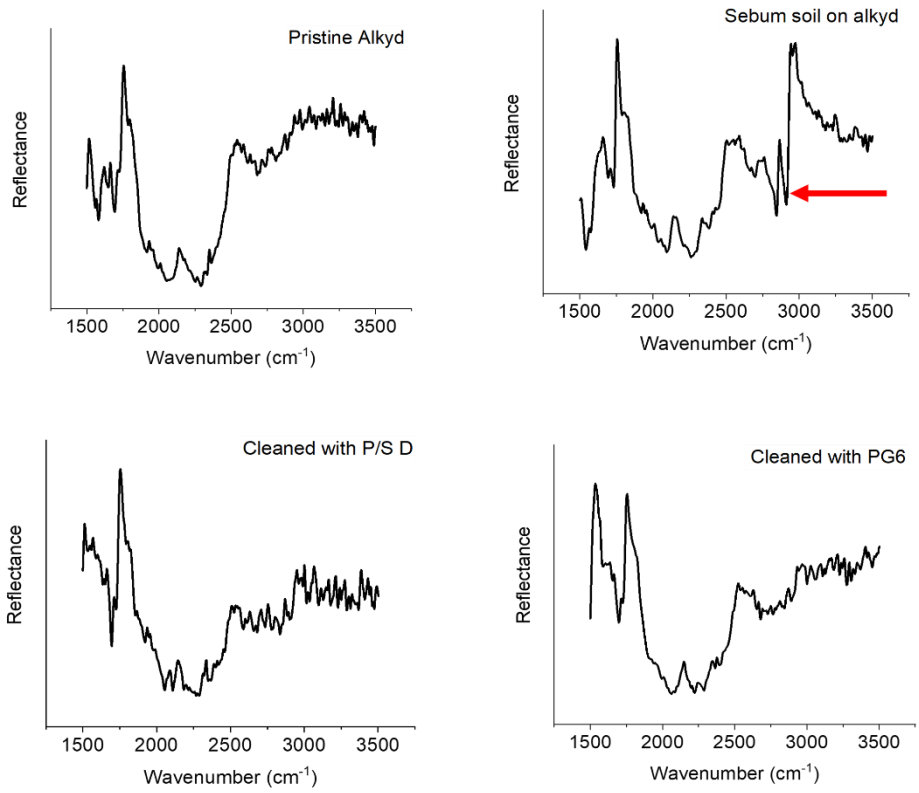

Figure S11. Summary of the results of the cleaning tests performed with P/S D and PG6 gels loaded with a solution of triammonium citrate (TAC) and a methoxy-pentadeca(oxyethylene) surfactant (MPD) on alkyd paint soiled with artificial sebum: FT-IR spectra collected in reflectance mode of pristine, soiled and cleaned alkyd paint. The red arrow shows the strong derivative band at 2900 cm^{-1} relative to the stretching modes of aliphatic carbons of the artificial sebum followed for the 2D FT-IR maps. (**PS/D** = PVA:starch 1:2; **PG6** = PG6 Nanorestore gel®).

Cleaning tests – starch residues

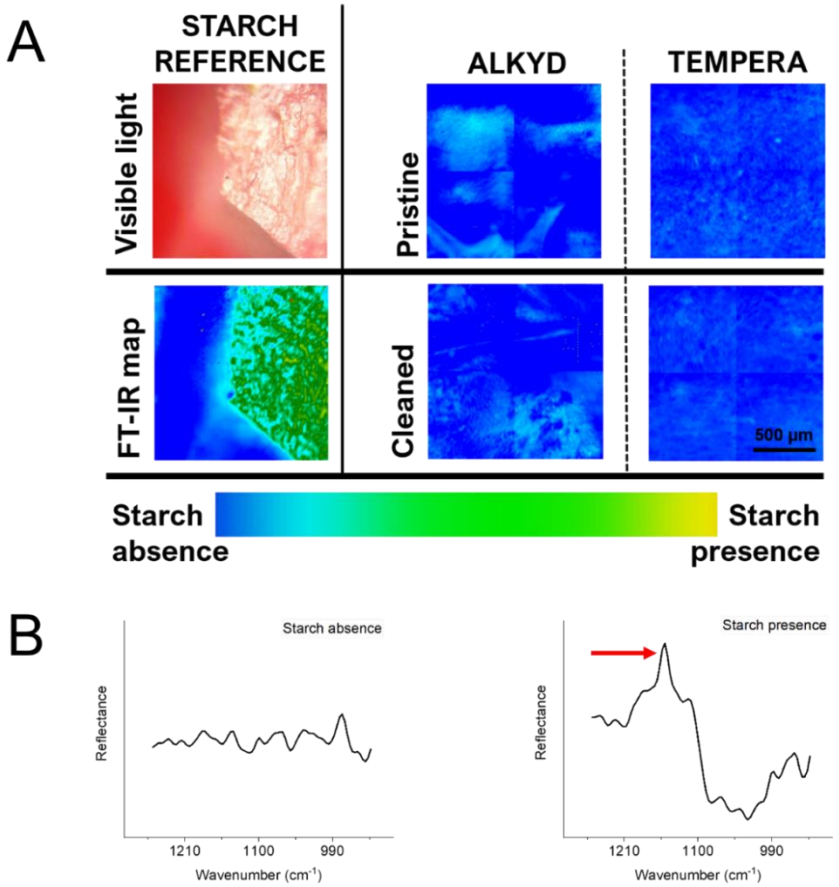

Figure S12. Assessment of the absence of starch residues. For the detection of starch, a P/S D gel (PVA/starch 1:2) was let dry adhered to the painted surface and the spectra collected on the gel were used as reference. **A**: µFTIR maps obtained following the intensity of a starch related band at 1153 cm^{-1}. No differences are observable between the pristine and the cleaned surfaces, confirming the absence of gels' residues on the painted mock-ups. **B**: the band at 1153 cm^{-1}, relative to C-C stretching modes of starch's rings [10], emerged clearly after the subtraction of the paint spectrum from the total one (starch on paint). (Left spectrum: signal residue after paint-paint subtraction; Right spectrum: signal residue after (paint+starch) – paint subtraction.).

The absence of starch residues on the painted mock-ups after the application of the biocomposite gels for cleaning purposes was verified by means of 2D μFT-IR imaging.

Given the partial overlapping of the spectra of starch and of the painted surfaces, spectral subtraction was performed prior to mapping. Shortly, spectra were collected on pristine painted surfaces and on a dry PVA/Starch gel adhered on the same surfaces. Then, to both spectra the ones of the pristine surfaces were subtracted, giving no significative signals in the case of the paint – paint subtraction, while leaving a detectable band at 1153 cm^{-1} for the starch/paint – paint subtraction. The signal at 1153 cm^{-1} is related to the C-C stretching modes of starch's rings [10].

As reported in Figure S12, no residues were observed (detection limit of the FPA detector: 0.02 $pg/\mu m^2$), confirming the safety of the application of PVA/Starch gels on painted artifacts.

References (SI)

[1] P. Levitz, *Cem. Concr. Res.* **2007**, *37* (3), 351–359.

[2] T. N. Blanton, M. Rajeswaran, P. W. Stephens, D. R. Whitcomb, S. T. Misture, J. A. Kaduk, *Powder Diffr.* **2011**, *26* (4), 313–320.

[3] B. Ormsby, A. Soldano, M. H. Keefe, A. Phenix, T. Learner, *AIC Paintings Specialty Group Postprints* **2010**, 23, 77-87.

[4] P. W. Wertz, *Int. J. Cosmet. Sci.* **2009**, *31* (1), 21–25.

[5] R. Mastrangelo et Al., *Proc. Natl. Acad. Sci. USA* **2020**, 117 (13), 7011-7020.

[6] S. Mallam, F. Horkay, A. M. Hecht, A. R. Rennie, E. Geissler, *Macromolecules* **1991**, *24*, 543–548.

[7] M. Shibayama, T. Tanaka, *J. Chem. Phys.* **1998**, *97* (9), 6829.

[8] M. Cattani, M. C. Salvadori, F. S. Teixeira, *arXiv: Atomic and Molecular Clusters*, **2009**, arXive:0907.3131.

[9] A. A. Christy, Z. Xu, P. de B. Harrington, *Chem. Phys. Lipids* **2009**, 158 (1), 22-31.

[10] R. Sachitraa, M. MadhanMohan, S. Vijayachitra, *Int. J. Comp. Appl.* **2003**, *1*, 29.

Part 2.

The Amylose/Amylopectin role

2.1 General Background

Amylose and amylopectin are the main components of natural starch. The two polymers are chemically identical, consisting in a repetition of glucose units linked through glycosidic bonds, but strongly differ in their dimensions and structural organization, both at the molecular and supramolecular scale.

Amylose, the "smaller" of the two (average molecular weights of 10^5-10^6) is a linear α-glucan containing almost exclusively (1→4)-α-linkages, while amylopectin is considerably larger (molecular weight 10^7-10^9) and highly branched, due to the presence of (1→6)-α- linkages connecting its sugar units[13].

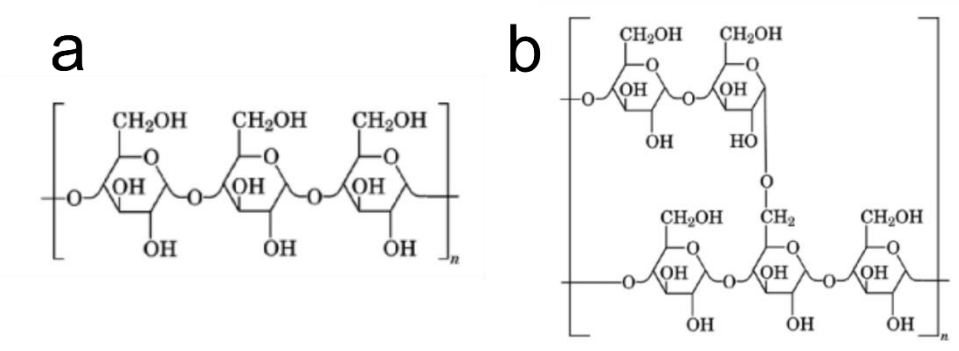

Figure 5. Differences in the organization of the glucose units in amylose (a), and amylopectin (b). Reproduced with permission from "Starch" in Kirk-Othmer Encyclopedia of Chemical Technology, James R. Daniel, Roy L. Whistler, Copyright © 1997 by John Wiley & Sons, Inc. All rights reserved.

The organization of amylose and amylopectin in native starch granules has been long investigated. Microscopy techniques (routinely used for the observation of the typical starch's birefringence cross)[71], thermal analysis[72], and X-ray diffraction[73] have been the most used strategies for understanding the complexity of native starches structure. Despite having been a subject of research for decades, the precise organization of a starch granule is still a matter of debate. However, some general features have been clarified. Roughly, we can describe a starch granule as a concentric structure in which amorphous layers made of linear amylose are alternated with crystalline ones, formed by tightly packed branched amylopectin[74] (figure 6).

Heating the granules in water leads to the loss of this organization, through a process called "starch gelatinization". The gelatinization, therefore, refers to the disruption of the granules and the dissolution of its components in water[75], and it is not to be confused with gelation, which is the "constructive" phenomenon that regards the formation of a new starch gel network[76].

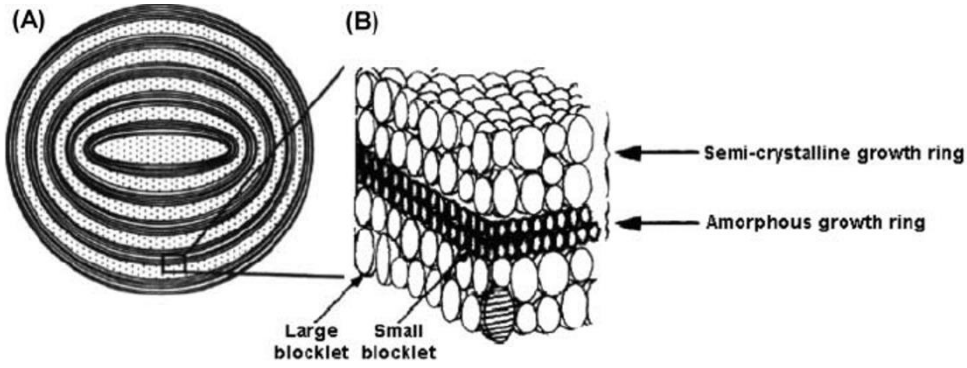

Figure 6. Schematic representation of a starch granule. Smaller amorphous growth rings are formed by linear amylose, while larger crystalline layers are made of tightly packed branched amylopectin. Reproduced with permission from "Application of Ultra High Pressure (UHP) in Starch Chemistry", Hyun-Seok Kim, Byung-Yong Kim & Moo-Yeol Baik, Taylor & Francis 2012.

The gelatinization process has been thoroughly studied in the last decades, and it has been described combining microscopy observations, thermal measurements, X-ray diffraction, and polymer theory[77]. Again, a straightforward in-depth explanation of the process is not fully available, although, all the research works agree on a general picture in which amylose and amylopectin play different roles. When heated in water, as a consequence of their diverse crystalline/amorphous arrangement, amylose and amylopectin show different resistance to dissolution. Hence, water molecules penetrate more easily between amylose chains, causing the swelling of the amorphous portions of the granule's structure. As the process continues, amylose chains can be fully dissolved and leach out the granule, while amylopectin crystals are progressively destabilized by heat and water until the full disruption of these ordered domains occurs, and the granule's organization is completely lost. The conditions at which the full disgregation of the granules is achieved strongly depend on the starch natural source, i.e., the granules dimension and crystallinity. In any case, at the end of the process, the system is represented by a viscous dispersion of amylose and amylopectin in water but, even if the original order is lost, a new one can be achieved through the formation of organized structures, in a process called starch retrogradation.

2.1.1 Amylose and amylopectin in starch retrogradation and gelation

The term retrogradation refers to the changes that occur in gelatinized starch from its initially amorphous state to a more ordered or crystalline organization[78]. The inner tendency of gelatinized starch to undergo this transformation relies on the fact that the system is not in thermodynamic equilibrium. However, this reorganization requires a

lowering of the molecular motion of the starch suspension, hence it is triggered by a decrease in temperature[78].

During retrogradation, amylose and amylopectin rearrange through the formation of inter- and intra-chain hydrogen interactions whose occurrence leads to the formation of crystalline domains. In this process, the differences in the chain ramification of the two polymers play a major role. Indeed, amylose reorders more easily than amylopectin, since its linear structure requires relatively little space for rearrangement.

Consequently, starch retrogradation can be described as a two-step process: a first, faster stage involving the smaller, linear, and more mobile amylose, and a second, slower stage in which the larger amylopectin partially rearranges in ordered structures[79].

During the first stage, which is often referred to as "short-term" retrogradation, amylose chains refold in a helicoidal organization, and these helixes align along a main direction, interacting through hydrogen bonds and forming ordered domains. The second stage is also known as "long-term" retrogradation and consists of a similar, but much slower process involving the helicoidal reorganization of amylopectin outer branches.

The two described steps are tightly connected. Since the amylose content of starch is closely related to its retrogradation degree (i.e., the higher amylose content is, the more easily starch retrogrades), it is generally assumed that short-term retrogradation provides the crystal seeds for long-term retrogradation. A schematic representation of the described two-step retrogradation process is depicted in figure 7.

The term retrogradation is often improperly used as a synonym for gelation (i.e., the formation of a gel network). Indeed, the nomenclature of starch's transformations can be as complicated as the processes themselves, and even though not being the same thing, retrogradation and gelation are strongly connected. Although, it is important to

distinguish them properly, especially for a clearer reading of what will follow in this work.

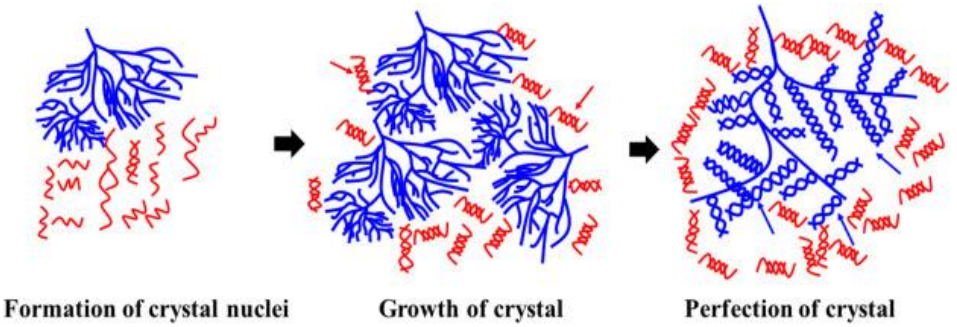

Figure 7. Summary of the sequence of events that lead to "complete retrogradation" of gelatinized starch. Amylose crystallization dominates the first stages of the process, acting as crystalline seeds for the much slower amylopectin reorganization. Reproduced with permission from "A comprehensive review of the factors influencing the formation of retrograded starch", Elsevier 2021.

Several studies have in fact underlined that, even though crystalline reorganization is detected in retrograded starch also at low concentrations, the formation of a three-dimensional network (gelation) requires the presence of sufficiently concentrated long polysaccharidic chains[80].

This behavior is explained by admitting the formation of non-crystalline double-helical junction zones between the polymers. Consequently, if the length of a junction zone is significantly shorter than the total chain length, a single chain can participate in the formation of several separate junction zones to form a cross-linked network[81]. Interestingly, this process appears to be independent of phase-separation mechanisms, which are indeed vital for the nucleation-growth crystallization processes. However, gelation and crystallization can occur either simultaneously or in sequence, and one process will be favored over the other depending on the polymer's length and concentration, and on the retrogradation conditions.

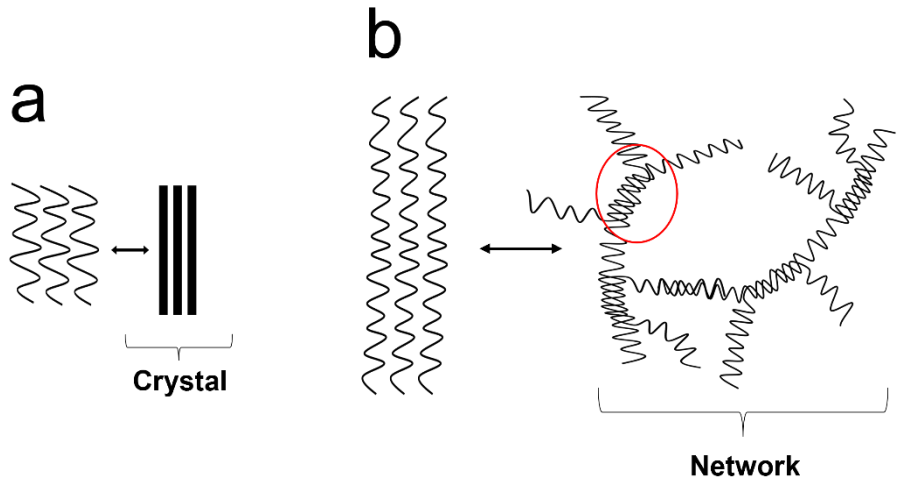

Figure 8. Retrogradation and gelation are two different processes and can occur either separately or together, depending on the system's conditions. Shorter amylose chains tend to rapidly form crystals. The same tendency is observed in dilute solutions. Longer polymer chains or higher concentrations promote the entanglement of the chains and the interaction mediated by non-crystalline single helix-domains, leading to the formation of a three-dimensional network.

2.1.2 Influence of amylose and amylopectin on PVA/starch blends

Blends of PVA and starch have been widely prepared and studied in the last years. Nevertheless, information about interactions between PVA and starch's polymeric components (i.e., amylose, and amylopectin) are few and barely reported. The majority of the knowledge around the subject comes from indirect observations, mostly conducted on cast-dried PVA/starch blend films.

Cascone et Al. prepared P/S films and analyzed their thermal transitions[82]. They reported that the value of PVA melting temperature did not change by varying the starch content in the films (which disagrees with what we have observed in P/S cryogels[83]), while the PVA melting enthalpy value increased by increasing the content of the biopolymer. They interpreted these results as the absence of interaction between PVA, amylose, or amylopectin on a molecular level and attributed it to the tendency of starch's components to re-join each other during solvent evaporation, preventing further interactions with PVA.

They also prepared PVA/amylose films, observing a shifting of PVA melting temperature towards lower values by increasing the amylose content, and interpreted this result as a consequence of possible interactions occurring between the two polymers. Therefore, they concluded that PVA/starch blended films are two-phase systems while significant interactions can occur between PVA and amylose, reasonably due to its molecules being linear.

Yun and Yoon synthesized similar films employing starches with different amylose content to investigate its influence on the PVA/starch blends properties[84]. However, they added sorbitol, tartaric acid, or citric acid in the blends and followed the changes in mechanical properties and biodegradability of the films. Direct PVA/amylose/amylopectin interactions were not taken into account, but a positive correlation between amylose content and tensile strength of the films was found and it was attributed to the occurrence of interactions between the polymer and the additives.

An attempt of elucidating the effect of starch's components on the properties of PVA/starch hydrogels was made by Zhai et Al. in a study regarding the syntheses of grafted hydrogels via irradiation[85]. They synthesized PVA/amylose and PVA/amylopectin gels employing γ-radiation and followed changes in the yield stress and gel fraction of the samples. PVA/amylose hydrogels resulted to have higher gel fractions

and mechanical strength. Moreover, they reported difficulties in obtaining pre-gel homogeneous PVA/amylopectin mixtures, and the gels obtained after irradiation resulted very weak and characterized by low gel fractions. They concluded that the grafting reaction observed in PVA/starch systems was indeed occurring between PVA and amylose.

Surprisingly, no such studies regarding PVA/starch cryogels have been conducted, which is why the experimental work that follows will focus on the investigation of the interactions of PVA with amylose and amylopectin in said materials.

Submitted Paper II

2.2 Phase separation behavior and structural role of amylose and amylopectin in PVA/starch hybrid networks: taking a step back to gain broader perspectives.

2.2.1 Overview

2.2.1.1 Context

Hydrogels based on Poly (vinyl alcohol) (PVA) and native starch obtained via freeze-thawing are eco-friendly versatile materials. They have been prepared and applied by several authors in different fields, going from the cleaning of works of art to the topical treatment of skin wounds. However, their formation mechanism is still a matter of debate, and this lack of information poses a limit in the possibility to predict the composition/structure/properties relationships of these systems. Moreover, native starches are characterized by having different polymeric compositions (i.e., the amylose/amylopectin ratio), which has been reported to strongly affect the properties of the final PVA/starch biocomposite cryogels. Nonetheless, studies on the PVA/amylose/amylopectin interactions in freeze-thawed hydrogels have not been previously reported.

2.2.1.2 Aim

The main scope of this work is to study the influence of starch's polymeric components (i.e., amylose and amylopectin) in PVA/starch hydrogels obtained via freeze-thawing. To better investigate the

dynamic of interaction at play between the involved polymers, as well as their implications on determining the final features of biocomposite networks, we decomposed the real system in its simple components. Analysis was conducted on pre-gel solutions and cryogels containing PVA/amylose, PVA/amylopectin, and PVA/amylose/amylopectin in variable ratios.

2.2.1.3 Findings

Investigation on PVA/amylose, PVA/amylopectin, and PVA/amylose/amylopectin systems with variable PVA/polysaccharide ratios allowed a deeper understanding of the possible evolution of a real PVA/starch cryogel. Thanks to CLSM imaging of pre-gel fluorescently labeled solutions, we determined the absence of miscibility between PVA and amylose, as well as PVA and amylopectin, in the considered temperature range (25- 98°C). In PVA solutions, amylose shows a supramolecular arrangement, reasonably corresponding to single helixes forming liquid crystals with nematic order. Instead, PVA and amylopectin solutions show liquid-liquid phase separation.

In the cryogels, for PVA:polysaccharide ratios of 2:1, the heteropolymeric interactions are strongly unfavored, whereas PVA-PVA interactions are increased, leading to the formation of more compact and crystalline PVA networks. The maximum extent of PVA polysaccharide interactions is likely to occur at a 1:1 ratio. Nevertheless, PVA amylopectin interactions are "destructive", given the inability of amylopectin to form proper networks, while PVA-amylose interactions can be "constructive" and lead to the formation of hybrid tie points in the gel, containing both the polymers in strong association, as suggested by DSC and SAXS measurements. A first attempt of predicting the variation of one simple parameter (the gel fraction, G%) for any possible PVA/amylose/amylopectin mixing ratio was made. A 3D plot was obtained based on the G% values of 23 samples and a preliminary

test on its reliability was conducted: the G% of a sample containing PVA and native starch was calculated, and the amylose/amylopectin ratio was analytically determined. For the corresponding PVA/amylose/amylopectin ratio, the predicted value was about 72%, in perfect agreement with the experimentally derived value of 72.36±0.25%.

Phase separation behavior and structural role of amylose and amylopectin in PVA/starch hybrid networks: taking a step back to gain broader perspectives.

Vanessa Rosciardi, Piero Baglioni

(Submitted Manuscript)

Abstract:

The constant increase in production, use, and disposal of synthetic plastic represent a concerning threat to the sustainability of our ecosystem. A possible strategy to reduce the consumption of synthetic polymers is to blend them with available natural products. A well-established couple for the production of biocomposite plastic materials is represented by PVA and starch. Nevertheless, the interactions between PVA and starch's polymeric components (amylose and amylopectin) are still a matter of debate. In this contribution, we prepared and analysed simple PVA/amylose, PVA/amylopectin, and PVA/amylose/amylopectin systems in order to formulate a wider theoretical framework that describes said interactions and their consequences on the features of PVA/starch-based materials. As an example of the implications that this broader knowledge could have, we provided a prevision of the variation of one simple parameter (the gel fraction) for any possible PVA/amylose/amylopectin mixing ratio and preliminarily tested its validity on a real PVA/starch sample.

Introduction

Plastic pollution has become one of the most dangerous threats to the sustainability of our planet[1]. The advantageous properties of plastics in terms of lightness, strength, and durability have promoted the constant increase of its usage, from its invention up to the present day, reaching the striking amount of nine billion tons produced worldwide in 2017[2].

It has been estimated that more than 75% of said plastic remained unrecycled nor incinerated[2], further contributing to the ubiquitous accumulation of plastic debris in soil and water. Clearly, a problem of such dimensions needs to be faced with multiple synergistic strategies, one of which is drastically diminishing the production of non-biodegradable synthetic polymers substituting them with more eco-sustainable counterparts[3].

Aside from the research and development of new biodegradable polymers, a possible alternative is to directly recur to natural products as sources of materials to be transformed into plastic-like products. However, such bio-based plastics often lack satisfactory mechanical properties[4], [5], but a strategy to overcome this limitation can consist in the chemical modification of the raw biopolymers to confer them features not otherwise displayed[6].

Another approach is represented by merging synthetic polymers with low toxicity and acceptable eco-compatibility with raw biopolymers, to obtain new biocomposite materials displaying substantially higher biodegradability yet optimal mechanical performances[7]. Even though not representing the final solution to the problem of the overproduction of synthetic plastic, this last approach is probably the most immediate, which, in times of emergency, can be a great advantage.

One of the most suitable synthetic polymers to be coupled with bio-derived counterparts is poly (vinyl alcohol) (PVA)[8], given its solubility in water, abundance in hydroxyl functionalities (which is key for the

formation of stabilizing hydrogen interactions with available moieties), low toxicity[9] and good biodegradability[10].

Attempts to formulate biocomposite materials combining PVA and natural products have been made in the last years, employing different biopolymers (e.g., cellulose[11], chitosan[12], gelatin[13], and starch[14]) and different preparation strategies, ranging from the chemical modification and/or crosslinking of the involved chains[15], to the simple blending of the polymers in solution[16]. It is important to notice, however, that the former method usually involves the use of organic solvents and further reactants (e.g., activators and cross-linkers) which is counterproductive if the goal is to "go greener".

Physical blends, on the other side, are usually obtained from an aqueous solution of the polymers, with no other chemicals needed, and can be processed into two main classes of materials: films[17] [18] [19], obtained by cast-drying methods, and cryogels[20] [21]. Regarding films, a well-established couple consists of PVA and starch, often used together in the attempt to obtain biodegradable systems, mostly for packaging purposes[22] [23] [24].

The structure of said materials relies uniquely on the occurrence of weak physical interactions between the components, hence showing poor water resistance[25] that can lead to the partial and uncontrolled dissolution of the films both during usage and after disposal. This process is to be avoided since it can lead to the undesired introduction of PVA in the environment, considering that, even though PVA is reported to be biodegradable, its chains can be effectively broken up only in specific conditions and by a restricted number of microorganisms[26] [27] [28].

On the other hand, PVA-based hydrogels obtained via freeze-thawing display physical interactions that lead to the formation of locally ordered structures characterized by a degree of crystallinity (depending on the

polymer concentration) high enough to mimic the effect of a chemical crosslinking[29].

Consequently, PVA/starch (P/s) cryogels, along with having good mechanical properties, are not solubilized by water at ambient temperatures. Instead, they show thermal-induced instability (with different critical temperatures depending on the system's crystallinity)[30], meaning that they can be redissolved in a controlled manner, allowing the safe recovery and reuse of the polymeric fraction. Moreover, P/s hydrogels can be further processed into different types of materials by simply removing water from the system. For instance, when the liquid fraction is lost upon freeze-drying, the result is a low-density flexible xerogel that can find its application in packaging as an alternative to polystyrene[31] [32], while loss of water through ambient temperature evaporation gives systems that resemble hard plastics (Figure 1).

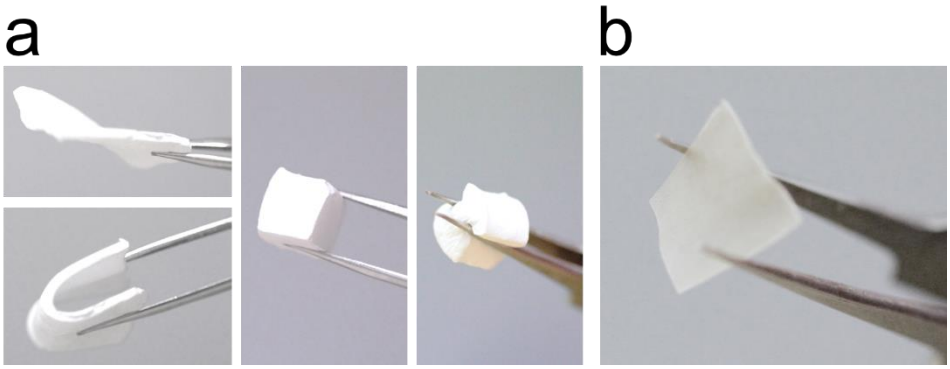

Figure 1. PVA/starch cryogels can be further processed to obtain materials with appealing features. Subtracting water from these systems via freeze-drying processes leads to low-density flexible xerogels that can substitute polystyrene for packaging purposes (a), while dehydration at ambient conditions gives materials that resemble hard plastic (b).

Despite having been prepared and applied by few research groups in different fields[33-35], P/s cryogels have long been lacking a systematic characterization.

An in-depth analysis of said biocomposite materials has been recently provided in one of our previous works[36], highlighting that polymer-polymer interactions strongly depend on the relative amount of each component in the blend and are crucial in determining the final properties of the systems, which are broadly tunable and can therefore meet a considerable number of applicative needs.

Nevertheless, starch as a raw product comes with a high variety of features, especially regarding the composition of its polymeric portion, i.e., the amylose to amylopectin ratio, which covers a broad range from waxy (0-5% amylose content) to highly crystalline (35-70% amylose content) starches[37].

It is therefore clear that the characterization of generic PVA/starch biocomposites is useful only limited to specific contexts, while a wider knowledge of the role of each involved polymer (i.e., PVA, amylose, and amylopectin) could set a theoretical basis for predicting the composition/properties relations of P/s networks. Especially in the perspective of a realistically affordable and scalable production of biocomposite products, a step back into the fundamental interactions between the main involved components is necessary to set a reliable base from which to start developing state-of-the-art materials, drastically reducing the usage of synthetic reagents without compromises in terms of performances.

Said mutual interactions and their consequences have been investigated and the results are proposed in this work. The real PVA-starch system has been ideally decomposed and simplified into bi- and tri- component formulations (tri- and quadri-, counting water) constituted by PVA, amylose, amylopectin, or both, in variable ratios. Direct laser imaging of fluorescently labeled systems, thermal analysis, and X-ray scattering profiles of the samples have been coupled with rheological measurements and gel fraction trends to provide a preliminary theoretical framework, the aim of which is to support future developments of highly performing eco-sustainable materials.

Results and discussion

In this contribution, we prepared and analyzed different samples containing highly hydrolyzed PVA, amylose, and amylopectin in variable ratios in water. Samples were characterized both as pre-gel solutions (sol-samples) and freeze-thawed hydrogels (gel-samples). The sol-samples were obtained after heating the components in water at 98°C under moderate stirring for 2 hours. In all the samples the total polymeric fraction in water was kept constant and equal to 9% (w/w). The composition of the samples and their names are summarized in table 1, while their synthesis route and storage details are available in SI.

Table 1. Summary of the composition of the samples.

Sample name (sol)	Sample name (gel)	PVA content (w/w) %	Amylose content (w/w) %	Amylopectin content (w/w) %
--	PVA gel	100	--	--
A1	Amy1	66.67	33.33	--
A2	Amy2	50	50	--
A3	Amy3	33.33	66.67	--
B1	Pec1	66.67	--	33.33
B2	Pec2	50.00	--	50.00
B3	Pec3	33.33	--	66.67
C1	AP1	66.66	16.67	16.67
C2	AP2	50.00	25.00	25.00
C3	AP3	33.33	33.33	33.33

The percentages of each component are referred to a total amount of polymeric fraction equal to 9% (w/w) in water.

Given the impact that phase separation events in PVA solutions have in determining the structural and mechanical features of the subsequent cryoformed gels[38] [39], we started from the observation of the former,

by means of Confocal Laser Scanning Microscopy (CLSM). The PVA employed for the preparation of the sol-samples was chemically labeled with fluorescein isothiocyanate (FITC). After labeling, PVA was washed and precipitated in ethanol several times, until reaching a constant absorption signal of the PVA-FITC solution, as recorded through UV-Visible experiments.

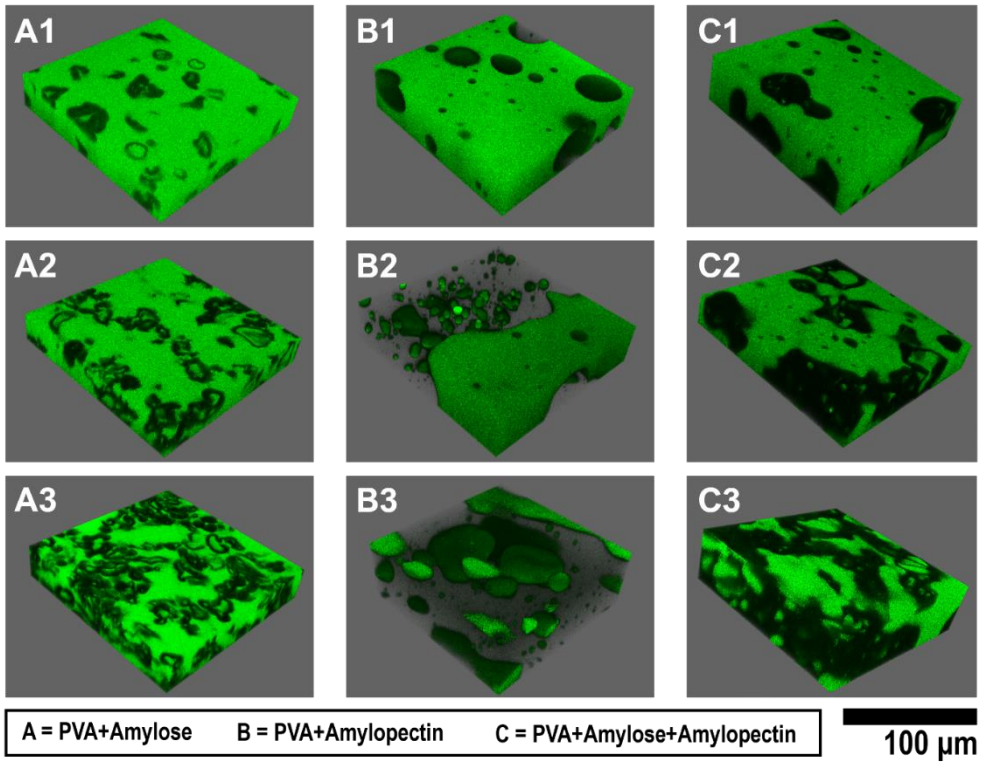

Figure 2. Confocal Laser Scanning Microscopy (CLSM) imaging of sol-samples containing a fluorescently labeled PVA (PVA-FITC). In the images, the green color corresponds to PVA, while the black refers to amylose, amylopectin, or both. The samples are named A, B, or C referring to the composition specified in the legend. The numbers 1, 2, and 3 correspond to a PVA content of 66, 50, and 33%, respectively.

The observed PVA/amylose/amylopectin solutions did therefore not contain any free molecule of the fluorophore. Details of the employed synthetic route and product purification are reported in SI.

The CLSM observations of the sol-samples were carried out in a temperature range of 80 to 25°C. Since no drastic changes were observed, the images reported in Figure 2 and collected at 80°C are to be considered as representative of the entire range mentioned above. In the images, the green color refers to the presence of PVA, while the black corresponds to amylose, amylopectin, or both.

It is immediately noticeable that the 3 compositional series show broad differences in morphology. The sol-samples containing PVA and amylose are characterized by the presence of recognizable structures, with repetitive and peculiar shapes, formed by amylose alone. A detail of these structures is provided in the 2D images reported in Figure 3.

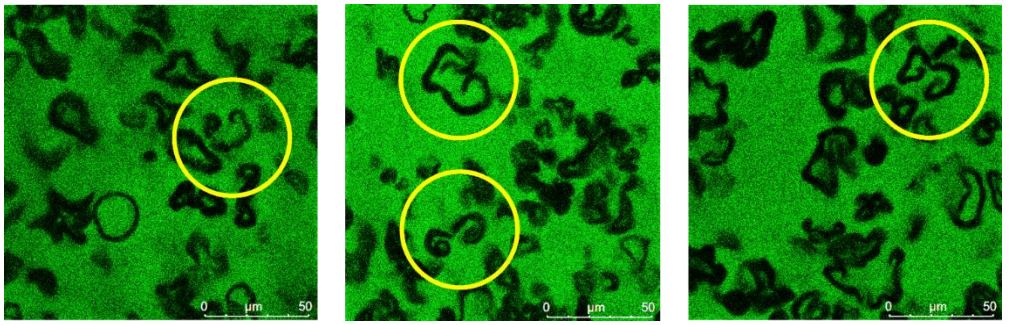

Figure 3. Detail of the PVA/amylose sol-samples, as acquired by means of Confocal Laser Scanning Microscopy (CLSM) imaging. The black portions in the images correspond to pure amylose, which appears to be organized in peculiar and well-distinguishable structures.

Apparently, at the considered temperatures, PVA is a continuous solution in which amylose is not fully dissolved. Indeed, Gidley[40] and Lelay[41] reported that amylose mixtures in water must be heated above 170°C to obtain proper solutions (i.e., transparent systems) and, before

them, a similar observation even led to the famous Reinitzer's discovery of liquid crystals[42].

Creek et al. suggested that, when heated in water at temperatures ranging from 70 to 130°C, amylose loses its crystalline order going from a double-helix organization to a single-helix one. However, the anisotropic nature of the helicoidal structures favors the formation of partially oriented systems, in which amylose is organized in liquid crystals with a nematic arrangement. The liquid crystalline phase is stable up to 170° and transforms in an isotropic solution afterward[43]. The described evolution of an amylose solution is schematically depicted in Figure 4.

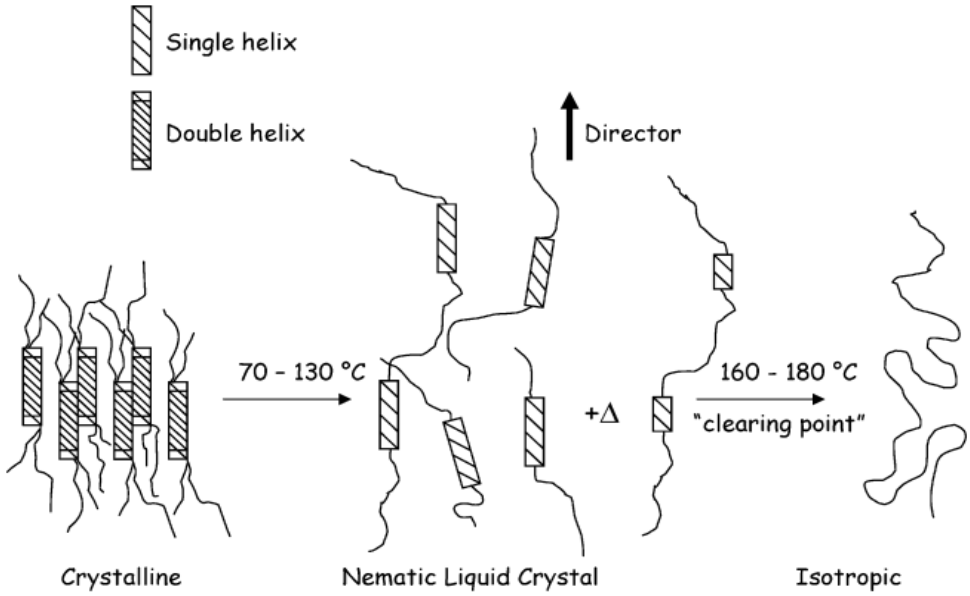

Figure 4. Structural evolution of an amylose solution, depending on the heating temperature. Adapted with permission from Biomacromolecules 2006, 7, 3, 761-770. Copyright 2006 American Chemical Society.

The sol-samples were heated at 98°C and observed from 80°C to 25°C, hence the observed amylose structures reasonably correspond to a liquid crystalline phase, indicating that a primitive supramolecular arrangement is present in the pre-gel systems before the freeze-thawing process. As the amylose concentration increases in the A-series (proceeding from A1 to A3), the appearance of its structures remains practically the same, but an obvious crowding arises, up to the point that in sample A3 (see Figure 2) the amylose domains are in continuous contact forming an extended network.

In the PVA/amylopectin solutions, the situation appears substantially different, and classical liquid-liquid phase separation is observed in the considered sol-samples. In sample B1 (PVA66%/Amylopectin 33%), an amylopectin-rich phase is visible as non-connected globular domains in a continuous PVA solution. Sample B3, with opposite composition, displays also the opposite organization, with PVA blobs in a continuous amylopectin phase.

An intermediate situation is instead observed when PVA and amylopectin are mixed in equal amounts (B2), where both the just depicted morphologies are detected. Although, the average dimension of the blobs in the continuous phases is smaller than the one observed in the other solutions, indicating overall better miscibility of the components in a 1:1 ratio.

In the last series (sol-samples C), PVA was mixed with both amylose and amylopectin in equal amounts. In these solutions, nor amylopectin blobs neither amylose structures were observed. Instead, the polysaccharidic components appeared as organized in more complex network-like structures in which entrapped PVA inclusions could be detected. Again, as in sample A3, when the concentration of amylose and amylopectin was sufficiently high, a continuous polysaccharidic network was formed across the entire observed volume of solution.

These observations naturally pose a question about the real mutual miscibility of PVA and starch, especially when it is added as a raw product and not as amylose and amylopectin separate polymers. Indeed, PVA/starch compatibility represents a widely debated issue. Computational studies, for example, suggested that PVA and starch are totally miscible when in a 1:1 w/w ratio[44], while more empirical observations lead to hypothesize that actual miscibility could occur only between PVA and linear amylose[45], excluding amylopectin's participation.

Our observations suggest that none of these hypotheses are completely true since, regardless of the state of the polymers, single-phase systems were never observed. Nevertheless, this does not mean that interactions between PVA and starch (or its components) are completely hindered, but processing conditions of the solutions are fundamental in favoring (or disfavoring) their occurrence.

Indeed, the freezing process could promote the interactions between PVA and amylose or amylopectin, since the formation of ice crystals leads to further phase separation and generates a progressive increase of the concentration in the polymer-rich phases. As these phases become growingly crowded, mutual interactions are statistically maximized. The phase separation processes observed in the pre-gel solutions, however, can play a major role in determining the overall final properties of the cryogels, which is not necessarily a disadvantage.

Another open question is whether amylose and amylopectin can actively play a structural role in PVA/starch hydrogels. The organization of the solutions as observed via CLSM suggests that amylose networks can be formed, while amylopectin may act as a porogen with little to no involvement in the final network. To further investigate their possible role in cryoformed PVA/starch networks, we tried to obtain pure amylose and pure amylopectin gels via freeze-thawing. While in the first case the result was a rigid white gel, in the second the gelation process

did not occur. (Images available in SI), confirming the ability of amylose to form self-supporting networks after freeze-thawing.

Gel samples with the same composition of the observed solutions were also analyzed by means of CLSM. In this case, the employed PVA was not chemically labeled.

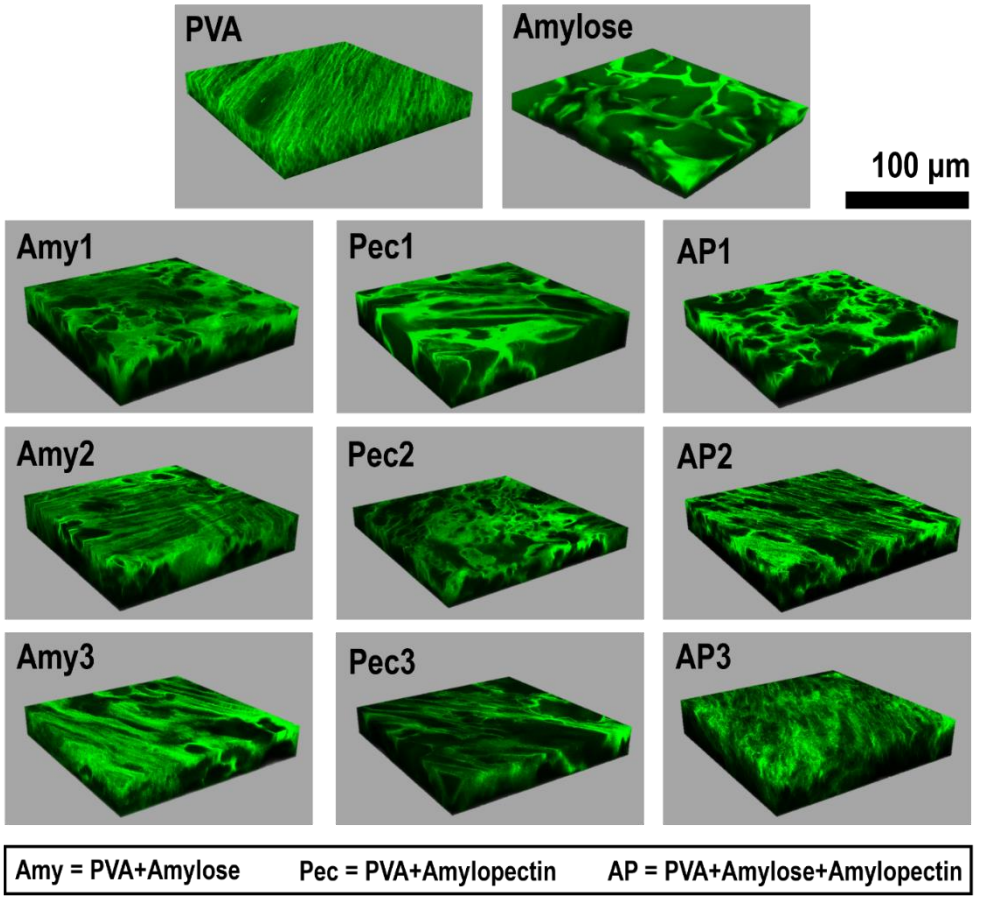

Figure 5. Confocal Laser Scanning Microscopy (CLSM) imaging of gel samples swollen in Rhodamine B solution. In the images, the green color corresponds to the gel network, while the black refers to the pores. The numbers 1, 2, and 3 at the end of the names indicate a PVA content of 66, 50, and 33%, respectively.

Instead, the cryogels were first thoroughly washed in ultrapure water for 2 weeks to allow the unbound polymeric fraction to leave the network, then immersed in a Rhodamine B solution for 24 hours. The hydrophilic character of the Rhodamine B molecule favors its adsorption on the hydrophilic walls of the cryogel, allowing the observation of the gel structure in its entirety. Hence, in figure 5, the green-colored parts correspond to the network with no compositional distinction, while the black portions are void (i.e., pores). Pure PVA and pure amylose cryogels are also reported as references.

As noticeable, the typical PVA oriented structure, characterized by tight elongated pores with elliptical section, is completely lost for any PVA/polysaccharide composite system. Interestingly, in the amylose-containing series (Amy1, 2, and 3), neither the structure observed in the pure amylose gel is detected.

In sample Amy1, irregularly shaped and scarcely interconnected pores interrupt a rather isotropic gel matrix. Observing the corresponding pre-gel solution (A1, figure 2), the gel-matrix can be assumed as formed by pure PVA in which parallel structures are no longer recognizable due to the formation of a more compact network, where chains are pushed together by the increase of concentration in the PVA-rich phase, generated by the amylose separation. Moreover, observing the amylose organization in A1, we can notice that some of its structures are not open but loop on themselves trapping small portions of PVA solution. After freezing and thawing, these irregularly round domains are not included in the gel network and abandon the structure after washing, leaving hollow spaces behind.

Similar pores are visible also in gel sample Amy2 (PVA:amylose 1:1), but the gel structure appears overall less porous, and parallelly oriented domains are easily distinguishable. Although, these domains differ from the ones of pure PVA, since the walls of the elongated pores appear larger as if they were formed by a higher amount of polymers. Moreover, given the scarce presence of amylose-formed pores but the consistent

presence of amylose in the composition (50% of the total polymeric fraction), it is reasonable to assume that it is mostly incorporated in a composite PVA/polysaccharide network.

In gel sample Amy3, the one with the highest amylose content (66% of the total polymeric fraction), anisotropy of the structure is observed, but the gel domains appear more fibrous and "wavy", although maintaining parallelity.

As regards the amylopectin-containing series (Pec1, 2, and 3), the effects of the liquid-liquid phase separation observed in the pre-gel solutions are evident. As expected, broader porosities are visible in the samples with opposite compositions (Pec1 and Pec3), where PVA/amylopectin separation was more pronounced.

Although, if in sample Pec1(PVA66%, amylopectin 33%), the gel structure is compact and well-formed, in Pec3 (PVA33%, amylopectin 66%) the network is inconsistent and its domains are barely connected, consequently to the inability of amylopectin to directly participate in the gel formation. Indeed, amylopectin is reasonably mostly lost after washing the gels, behaving, as already hypothesized, as a porogen. Similar to sample Amy1, the compact network in sample Pec1 is most likely formed by PVA alone, with chains in tight interaction pushed together by the amylopectin phase separation.

For the amylose/amylopectin series, (AP1, 2, and 3), the identification of the gelation dynamics is not straightforward. As observed for the other series, the sample with the highest PVA content (66%, AP1), is the most porous. This observation suggests that regardless of the nature of the added polysaccharide, at the considered mixing ratio the PVA-PVA interactions are strongly favored, at the expense of the PVA-polysaccharide ones, and the polymeric fraction excluded from the network formation is lost upon washing.

Proceeding along the series (i.e., increasing the polysaccharidic content), large pores progressively disappear leading to more homogeneous

structures, possibly formed by all three polymers. Nevertheless, the gel networks are seemingly loose and rather fibrous, features that, as it is going to be discussed, have an obvious impact on the elastic response of the samples.

The effects of the hypothesized phase-separation events have been investigated by means of rheological measurements in frequency sweep mode (the Linear Viscoelastic Region was previously determined through amplitude sweep tests, details of the experiments are reported in SI). All the samples were, rheologically speaking, classifiable as "chemical-like" gels (i.e., "strong" gels), since the elastic moduli (G') were considerably higher than the viscous ones (G") over the entire span of investigated frequencies (see SI). This information alone already suggests that a considerable number of entanglements and strong interactions are occurring between the chains in the gels, despite the purely physical method through which they were obtained. Figure 6 illustrates the elastic behavior of the polysaccharides-containing samples, with respect to a gel of pure PVA as reference.

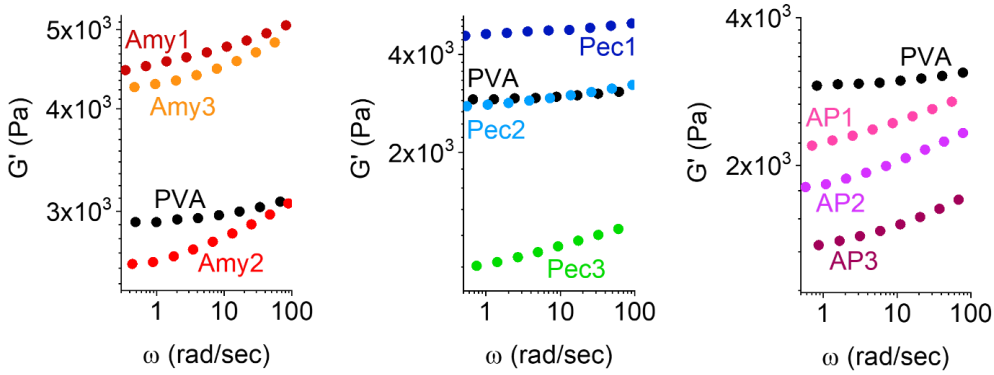

Figure 6. Summary of the elastic behavior of the samples, as measured by means of rheological experiments in frequency sweep mode. Error bars are not reported for sake of clarity and do not affect the "hierarchy" of the responses of the sample. (Amy = PVA+Amylose; Pec = PVA+Amylopectin; AP = PVA+Amylose+Amylopectin; the numbers 1, 2, and 3 refer to a PVA content of 66, 50, and 33%, respectively).

Three samples are characterized by G' values higher than the freeze-thawed PVA gel: Amy1, Amy3, and Pec1. Among them, in the samples containing 66% of PVA (Amy1 and Pec1), the increment of the elastic modulus is to be interpreted as a consequence of the aforementioned phase-separation processes. In the considered proportions, PVA and amylose or amylopectin interact neither in solution nor in the cryogel, the PVA-PVA interactions are enhanced, and the polysaccharidic components are lost upon washing. Compared to a pure PVA, the resulting cryogels have a more compact network with a consequently higher elastic response. The hypothesis of an increase in PVA-PVA interactions is strongly supported by the increase in PVA crystallinity in these systems when compared to a PVA gel, as detected by means of DSC. Indeed, as reported in table 2, the enthalpy variation associated with the melting of PVA crystals (occurring between 200 and 220°C) goes from about 37 $J*g^{-1}$ in the pure PVA gel to about 43 and 47 $J*g^{-1}$ in Amy1 and Pec1, respectively. The crystallinity of PVA was here calculated as a percentage in respect to the melting enthalpy of a 100% crystalline sample (138.60 $J*g^{-1}$)[46].

In the case of sample Amy3 (PVA:amylose 1:2), considering its composition, and the morphology of the pre-gel solution and the cryogel, the increment in G' can be interpreted as a strengthening of the structure either due to a constructive interaction of the polymers or to the formation of two different networks made of PVA and amylose, respectively. Nevertheless, DSC data support the second hypothesis better, since PVA crystallinity in Amy3 was found to be the same as a pure PVA gel (25.49 ± 1.10% vs. 26.54 ±0.87%), suggesting that no amylose-PVA interactions are occurring, since if they were, they would hinder the formation of PVA crystalline domains[47] [48]. Moreover, given the high amount of amylose in this formulation, together with the morphology of the corresponding pre-gel solution, it is reasonable to expect that the main network in the sample is made of amylose itself.

On the contrary, extended amylose-PVA interactions are likely to be present in Amy2, where the crystallinity of PVA was found to be about 35% lower than in the pure PVA sample, and the lowest amongst all the samples.

Table 2. Summary of the thermal events associated with the melting of PVA crystals, as detected by Differential Scanning Calorimetry (DSC).

Sample name	T_m (°C)	ΔH_m (J*g^{-1})	X_c%
PVA	207.42 ± 2.08	36.79 ± 1.47	26.54 ± 1.10
Amy1	216.85 ± 2.98	43.07 ± 2.64	31.08 ± 1.90
Amy2	202.33 ± 0.53	23.86 ± 0.92	17.21 ± 0.66
Amy3	206.86 ± 1.64	35.33 ± 1.21	25.49 ± 0.87
Pec1	218.43 ± 0.56	46.83 ± 2.61	33.79 ± 1.88
Pec2	201.34 ± 0.28	29.11 ± 3.32	21.01 ± 2.40
Pec3	206.52 ± 3.08	48.07 ± 7.52	34.68 ± 5.43
AP1	218.97 ± 1.74	49.30 ± 3.83	35.57 ± 2.76
AP2	182.75 ± 5.37	36.03 ± 4.08	25.99 ± 2.94
AP3	220.52 ± 9.29	30.46 ± 3.53	21.98 ± 2.55

T_m=Melting temperature measured at peak; **ΔH_m**=Melting enthalpy, weighed in respect to PVA content; **X_c%**=Crystalline fraction **Amy**=PVA/amylose; **Pec**=PVA/amylopectin; **AP**=PVA/amylose/amylopectin; Numbers **1**, **2**, and **3** refer to a PVA content of 66, 50, and 33%, respectively.

Interestingly, all the samples containing both amylose and amylopectin together are characterized by a lowering in the elastic modulus compared to the pure PVA gel, even though having higher (AP1) or same (AP2, AP3) crystallinity of the latter. For AP1, this can be justified by the lower gel content in respect to PVA (71.18% vs. 79.17%,

complete dataset available in SI) corresponding to a less packed structure, while for AP2 and AP3, the reason can also be related to the overall structural system's organization. Indeed, the trend of the G'/G" crossover point along the AP series (figure 7, data obtained by means of rheological measurements in amplitude sweep mode, full data available in SI) highlights an increase of "stretchability" in the samples that follows the incremented amylose/amylopectin content.

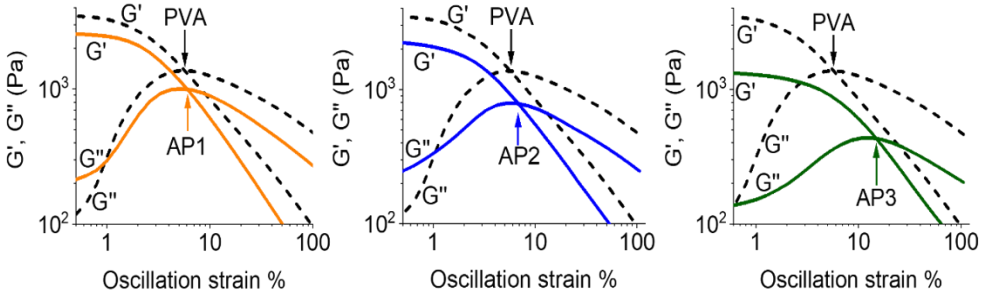

Figure 7. Detail of the rheology experiments in amplitude sweep mode, highlighting the progressive increase of the strain value of the G'/G" crossover point in AP samples. (AP=PVA/amylose/amylopectin; the numbers 1, 2, and 3 refer to a PVA content of 66, 50, and 33, respectively).

Since this feature in PVA/starch cryogels was previously attributed to starch domains acting as plasticizers[36], we can assume that in these samples domains containing only polysaccharides or only PVA are alternated and loosely bound to each other. Nevertheless, the gel fractions of AP2 and AP3 resulted to be the lowest amongst all the samples (63.91% and 60.09%, respectively), indicating that considerable portions of the gels have abandoned the structure upon washing.

Further insight into the samples' structure was provided by Small Angle X-ray Scattering (SAXS) measurements. SAXS data were collected in a q range from 0.004 to 0.6 $Å^{-1}$ and fitted according to a model specifically

developed for hydrogels presenting both loose amorphous domains and densely packed regions. The fitting equation corresponds to[49] [50]:

Equation (1)

$$I_{(q)} = I_L(0)\frac{1}{\left[1+\frac{D^f+1}{3}\left(q^2\xi^2\right)\right]^{\frac{D^f}{2}}} + I_G(0)\,exp\left(-\frac{q^2R^2}{3}\right) + B$$

The right side of the equation is composed of two terms since in these systems the intensity of the scattering vector is the result of the sum of two separate contributions. The first term is a Lorentzian function describing the scattering behavior of a polymer in a semi-dilute regime, i.e., the relaxed polymeric chains of the amorphous portions of the hydrogel network. The term ξ refers to the correlation length, which represents the characteristic distance above which the mass distribution of the scattering cluster is no longer described by a fractal law[51], D^f is the fractal dimension and $I_L(0)$ (Lorentzian parameter) is a scale factor that accounts for the polymer/solvent contrast and the gel's volume fraction. The second term describes the scattering contribution of the gel's crosslinking points, where R is the gyration radius of the dense domains that form the tie-points in the network, and $I_G(0)$ is the Guinier scale factor. A summary of the obtained data is reported in table 3 (experimental settings and complete scattering curves available in SI).

Since the radius of gyration in our cryogels is to be intended as referred to the dimensions of the tie-points in the network, and in freeze-thawed PVA-based systems the tie-points are formed by the crystallites of PVA itself, it is interesting to confront R_g values with the PVA melting temperatures measured in DSC experiments. Indeed, the melting temperature of the crystals is directly related to their dimensions. Small crystals are in fact less stable due to the dominance of the surface energy on the cohesion energy between the molecules, which shifts the

breakdown of the lattice to lower temperatures[52]. This behavior is mathematically represented by Thomson-Gibbs equation (equation 2),

Equation (2)

$$T_{fus}^{\infty} - T_{fus}^{r} \cdot T_{fus}^{\infty} = 2\sigma q_{fus} \rho r$$

where T_{fus}^{∞} and T_{fus}^{r} are the melting temperatures of a crystal with infinite dimensions and of a spherical 'aggregate' of radius r, σ is the specific free energy of the crystal-melt phase boundary, q_{fus} is the specific heat of fusion and ϱ is the density of solid.

Interestingly, in every series of samples (i.e., Amy, Pec, and AP) the minimum values of PVA melting temperatures (T_m) were registered for intermediate compositions (Amy2, Pec2, and AP2, PVA:polysaccharides 1:1), corresponding to smaller crystals. A similar trend was found for the R_g values detected in SAXS experiments, but only in Pec and AP series. In the amylose-containing samples (Amy), instead, the trend is exactly the opposite, with sample Amy2 showing the highest R_g value. Moreover, said value is the highest amongst all the analyzed samples, including the pure PVA and pure amylose references. This result is in perfect agreement with the previously proposed theory about the existence of cooperative PVA-amylose interactions in the sample. The biggest R_g and the smallest PVA crystals can be indeed interpreted as relative to hybrid tie-points in which PVA and amylose are densely packed in a mixed crystalline-amorphous structure forming a properly hybrid biocomposite network.

It is also worth noticing that, in the same series, Amy3 is characterized by a gyration radius of the same size as the pure amylose cryogel, suggesting that, as previously hypothesized, in this sample no significant

amylose-PVA interactions occur and the main network in the composite gel is formed by amylose itself.

Table 3. SAXS curves fitting parameters (partial dataset).

Sample	R_g (nm)	ξ (nm)	D^f
PVA	4.70 ± 0.06	4.94 ± 0.03	3.12 ± 0.01
Amy1	4.81 ± 0.08	7.22 ± 0.04	2.68 ± 0.01
Amy2	5.54 ± 0.02	7.96 ± 0.02	2.99 ± 0.01
Amy3	5.00 ± 0.02	10.04 ± 0.04	2.42 ± 0.01
Pec1	4.84 ± 0.05	6.14 ± 0.04	2.57 ± 0.01
Pec2	4.40 ± 0.03	7.94 ± 0.04	2.56 ± 0.01
Pec3	4.75± 0.04	8.55 ± 0.03	2.49 ± 0.01
AP1	4.65 ± 0.03	6.26 ± 0.03	2.89 ± 0.01
AP2	4.51 ± 0.02	10.93 ± 0.05	2.36 ± 0.01
AP3	5.09 ± 0.02	7.74 ± 0.03	2.57 ± 0.01
Amylose	4.97 ± 0.03	27.35± 0.18	2.15 ± 0.01

R_g=Gyration radius; **ξ**= Correlation length; **D^f**=Fractal dimension; **Amy**=PVA/amylose; **Pec**=PVA/amylopectin; **AP**=PVA/amylose/amylopectin; Numbers **1**, **2**, and **3** refer to a PVA content of 66, 50, and 33%, respectively.

The smallest gyration radius was found for sample Pec2 (≈4.4 nm). In this case, also considering the crystalline fraction characterizing this sample (the lowest in the Pec series) is evident that, in a 1:1 PVA:amylopectin ratio, the phase-separation is less pronounced but interactions between the polymers occur in a non-cooperative way since PVA crystallization is hindered while no hybrid tie-points seem to be formed.

Regardless of the crystallinity, the R_g dimension or the composition, for all the polysaccharide-containing samples the correlation lengths (ξ) were found to be considerably larger than in the pure PVA gel, indicating that, also when strong interactions are not occurring, the large amylose and amylopectin chains remain physically entangled in the network acting as spacers between the PVA amorphous chains. In freeze-thawed PVA-based hydrogels, in fact, ξ is to be considered as the mean distance between the polymeric chains in a liquid-like environment (i.e., in the loose amorphous portions of the cryogel).

Before concluding with the last observations, it is worth resuming the main information obtained from the data discussed up to this point:

-In the 25°-98°C temperature range, no miscibility is observed between PVA and amylose or amylopectin.

-A 9% (w/w) amylose solution is able to form self-supporting networks after freeze-thawing. No structuring was observed for amylopectin.

-Amylopectin mostly act as a porogen.

-In a 2:1 (w/w) PVA:polysaccharide ratio, heteropolymeric interactions are unfavoured and PVA strongly segregates. PVA-PVA interactions are enhanced resulting in an overall incremented crystallinity.

-Heteropolymeric interactions are statistically maximized at a PVA:polysaccharide ratio of 1:1 (w/w). Amylose participates constructively with PVA in the formation of hybrid tie-points in the gel networks. Amylopectin hinders PVA crystallization and do not form hybrid structures.

Finally, a first attempt of predicting the trend of a simple parameter (i.e., the gel fraction, G%) of systems with any possible PVA/amylose/amylopectin ratio (valid for freeze-thawed gels obtained from 9% w/w solutions) is proposed.

The gel fraction (or gel content, G%), corresponds to the polymeric fraction that is stably retained in the network and does not dissolve in

water. Hence, its prediction can have remarkable implications in projecting reliable materials without renouncing the eco-compatibility aspect.

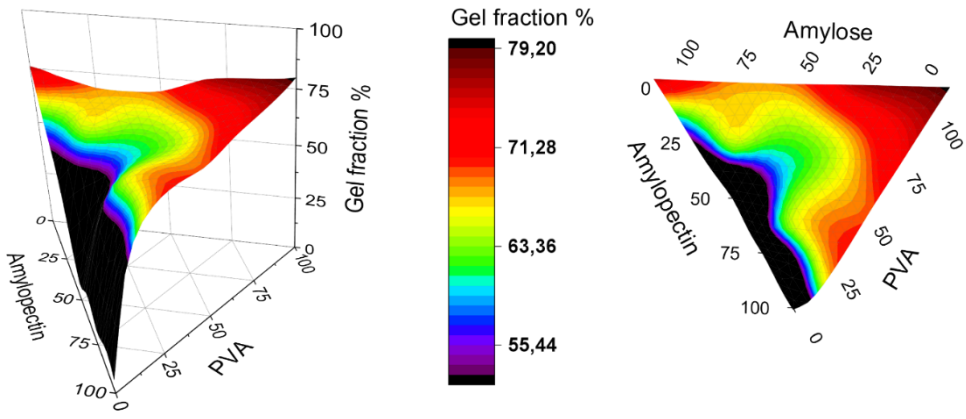

Figure 8. Prediction of the gel fraction (G%) in PVA/amylose/amylopectin cryogels (valid for freeze-thawed gels obtained from 9% w/w solutions). The black color in the plots and in the legend corresponds to the absence of gel formation (here intended as the formation of a strong chemical-like network).

In order to formulate a prediction with statistical meaning, 12 additional cryogels with variable PVA/amylose/amylopectin ratios were prepared and stored following the same procedure applied to the other samples (composition of the additional samples available in SI).

For all the samples (a total of 23) gel fraction (G%) values were calculated as the ratio between the weight of dry unwashed gels and of the dry gels after washing (detailed procedure in SI). The resulting values were plotted in a 3D ternary graph and are reported in figure 8. Interestingly, trends in G% were not the only obtained information, but also the limit compositions at which a gel can be formed were found. The black portion of the 3D plot refers in fact to the absence of gel

formation (with the term "gel" we here refer to a strong, chemical-like cryogel), while the colored parts refer to the different G% values, as specified in the legend bar. The coordinates comprised in the orange-red portions of the plot correspond to the PVA/amylose/amylopectin ratios that lead to the formation of stronger, more compact, and highly interconnected networks, while the ones in the green-blue portions correspond to polymer ratios that lead to the formation of less dense structures.

This information can have an important impact on deciding which type of raw starch to use, depending on the desired features of the biocomposite material to develop. For example, in the case of freeze-dried cryogels (i.e., xerogels) that could be used as packaging materials instead of expanded polystyrene, a lower density can be an advantage, hence starches with an amylose content of around 20% should be used, mixed with PVA in 4:1 w/w ratio (green area in the graph). On the contrary, if dried at ambient temperature to obtain plastic-like materials, formulations belonging to the red-orange part of the graph should be pursued.

To test the validity of our prevision, a cryogel containing PVA and commercial rice starch was prepared and stored in the same conditions as the other samples, and its G% was calculated. Then, the amylose content of the employed starch was determined by means of UV-Visible spectrophotometry after alkaline treatment and reaction with iodine solution, following a protocol specifically optimized for rice starches by Avaro et al[53] (experimental procedure in SI). The composition of the gel was therefore calculated and corresponded to a PVA/amylose/amylopectin content of 66.67%, 5.67%, and 27.66%, respectively. The G% for this sample resulted to be 72,36 ± 0.25%, in perfect agreement with what was expected, based on our prevision (see figure 9).

This result suggests that, despite the variety of starches compositions, mostly depending on their botanical origin, some macroscopical

features of their blends with PVA can be predicted on the simple basis of their amylose/amylopectin content.

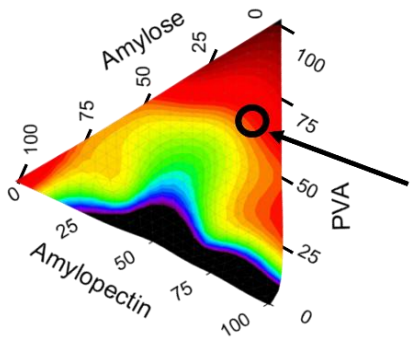

PVA	66,66%
Amylose	5,67%
Amylopectin	27,66%
G% (predicted)	≈72%
G% (calculated)	72,36±0,25%

Figure 9. Position of the experimentally obtained G% value for a PVA/rice starch cryogel on the "G% prevision plot". The amylose/amylopectin content of the employed starch was previously determined by means of UV-Visible spectrophotometry, following a protocol developed by Avaro et. Al. The experimental value (G%(calculated)) is in perfect agreement with the expected one (G%(predicted)).

The evaluation of the gel fraction for 23 samples, not only provided a good prediction of the G% values of real starch-containing samples but confirmed the structural role of amylose over amylopectin. Observing the plots in figure 10, in fact, it is clear that above a certain amylopectin content, the G% of the system drops, indicating a partial structural collapse. The G% curve relative to PVA/amylose samples shows instead a minimum value which we think corresponds to the maximum heteropolymeric interactions occurring in that range of mixing ratio. This statement may sound counterintuitive, but it is to be considered that, even if the interactions are maximized, they are still occurring between two polymers with different spatial organizations and substantially diverse steric encumbrance, which can lead to less compact, weaker structures (i.e., lower G%).

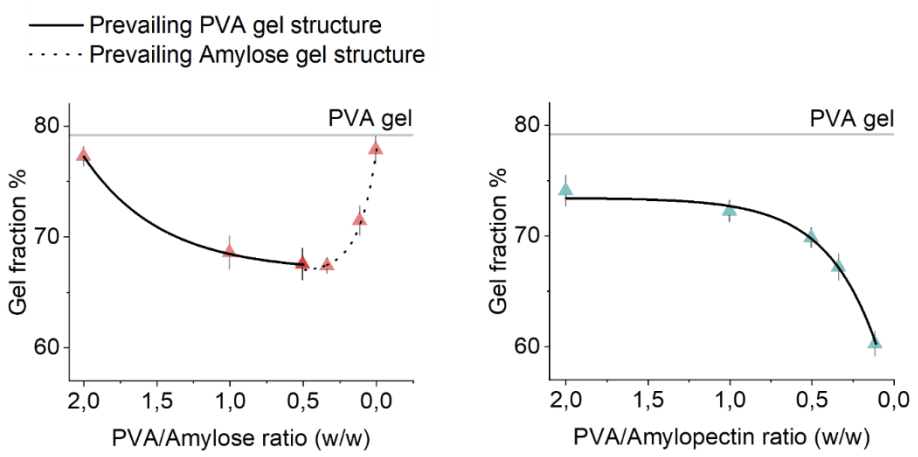

Figure 10. Gel fraction (G%) trends for binary mixtures of PVA/amylose (left) and PVA/amylopectin (right). PVA/amylose blends show a drop in G% from 1 to 0.4 w/w ratio, followed by an increase for higher amylose content, confirming the ability of amylose to form self-supporting networks. PVA/amylopectin systems show a drop in G% for w/w from 1 to "0", which corresponds to a structural collapse, due to amylopectin's inability to form networks.

Conclusion

Starch is a mixture of two polysaccharides (amylose and amylopectin), and its interactions in blends with PVA can be complex to predict. To better investigate the dynamic of interaction at play between PVA, amylose, and amylopectin, as well as their implications on determining the final features of biocomposite PVA/starch networks, a good approach is to decompose the real system in its simple components. Investigation on PVA/amylose, PVA/amylopectin, and PVA/amylose/amylopectin systems with variable PVA/polysaccharide ratios allowed a deeper understanding of the possible evolution of a real PVA/starch cryogel.

Thanks to CLSM imaging of pre-gel fluorescently labeled solutions, we determined the absence of miscibility between PVA and amylose, as well as PVA and amylopectin, in the considered temperature range (25-98°C). In PVA solutions, amylose shows a supramolecular arrangement, as already hypothesized by Creek et Al.[43], reasonably corresponding to single helixes with liquid-crystalline nematic order. Instead, PVA and amylopectin solutions show a rather classical liquid-liquid phase separation.

In the cryogels, for PVA:polysaccharide ratios of 2:1, the heteropolymeric interactions are strongly unfavoured, whereas PVA-PVA interactions are increased leading to the formation of more compact and crystalline PVA networks. The maximum extent of PVA-poysaccharide interactions is likely to occur at a PVA/polysaccharide ratio of 1:1. Nevertheless, PVA/amylopectin interactions are "destructive", given the inability of amylopectin to form proper networks (i.e., amylopectin hinders PVA crystallite formation but does not actively participate in the construction of a network), while PVA/amylose interactions can be "constructive" and lead to the formation of hybrid tie points in the gel containing both the polymers in strong association, as suggested by DSC and SAXS measurements.

A first attempt of predicting the variation of one simple parameter (the gel fraction, G%) for any possible PVA/amylose/amylopectin mixing ratio was made. A 3D plot was obtained based on the G% values relative to 23 different samples and a preliminary test on its reliability was conducted: G% value of a sample prepared with PVA and raw rice starch was calculated and the amylose/amylopectin ratio in the starch was determined. For the corresponding PVA/amylose/amylopectin ratio, the predicted G% value was about 72%, in perfect agreement with the experimentally derived value of 72.36 ±0.25%.

The results reported in this work represent the basis for the construction of a theoretical framework that, far from being complete, can still

substantially help in projecting and developing high-quality biobased materials, with a significant positive impact on the ecosystem.

Author Contributions

Vanessa Rosciardi: conceptualization, experimental analysis, data curation, writing of the original draft. **Piero Baglioni**: conceptualization, project administration, supervision, validation.

References for Paper II

[1] S. B. Borrelle et Al., *Science* **2020**, *369*, 1515–1518.

[2] R. Geyer in *Plastic Waste and Recycling* **2020**, (Eds. T. M. Letcher), Elsevier, pp. 13-32.

[3] M. Shen et Al. *Environ. Pollut.* **2020**, *263*, 114469.

[4] M. Asrofi, S. M. Sapuan, R. A. Ilyas, M. Ramesh, *Mater. Today: Proc.* **2021**, *46*, 1626–1630.

[5] M. Jiménez-Rosado, E. Bouroudian, V. Perez-Puyana, A. Guerrero, A. Romero, *J. Clean. Product.* **2020**, *262*, 121517.

[6] H. Tian, Z. Tang, X. Zhuang, X. Chen, X. Jing, *Prog. Polym. Sci.* **2012**, *37*, 237–280.

[7] S. T. Sam, M. A. Nuradibah, K. M. Chin, N. Hani in *Natural Polymers: Industry Techniques and Applications* **2016**, (Eds. Ololade Olatunji), Springer, pp. 163–184.

[8] Z. W. Abdullah, Y. Dong, I. J. Davies, S. Barbhuiya, *Polym. Plast. Technol. Eng* **2017**, *56*, 1307– 1344.

[9] C. C. DeMerlis, D. R. Schoneker, *Food Chem. Toxicol.* **2003**, *41*, 319–326.

[10] E. Chiellini, A. Corti, S. D'Antone, R. Solaro, *Macromol. Symposia* **1999**, *144*, 127–139.

[11] M. I. Voronova, O. v. Surov, S. S. Guseinov, V. P. Barannikov, A. G. Zakharov, *Carbohyd. Polym.* **2015**, *130*, 440–447.

[12] A. A. Menazea, A. M. Ismail, N. S. Awwad, H. A. Ibrahium, *J. Mater. Res. Tech.* **2020**, *9*, 9598–9606.

[13] M. Atlan et Al., *Sci. Rep.* **2018**, *8*, 1–12.

[14] A. Hassan, M. B. K. Niazi, A. Hussain, S. Farrukh, T. Ahmad, *J. Polym. Environ.* **2017**, *26*, 235–243.

[15] A. K. Sonker, K. Rathore, A. K. Teotia, A. Kumar, V. Verma, *J. Appl. Polym. Sci.* **2019**, *136*, 47393.

[16] B. Liu, H. Xu, H. Zhao, W. Liu, L. Zhao, Y. Li, *Carbohydr. Polym.* **2017**, *157*, 842–849.

[17] A. I. Cano, M. Cháfer, A. Chiralt, C. González-Martínez, *J. Food Eng.* **2015**, *167*, 59–64.

[18] H. Ismail, N. F. Zaaba, *Polym. Plast. Technol. Eng.* **2011**, *50*, 1214–1219.

[19] M. C. Popescu, B. I. Dogaru, M. Goanta, D. Timpu, *Int. J. Biolog. Macromol.* **2018**, *116*, 385–393.

[20] N. E. Vrana, P. A. Cahill, G. B. McGuinness, *J. Biomed. Mater. Res. Part A* **2010**, *94A*, 1080–1090.

[21] H. Zhang, F. Zhang, J. Wu, *React. Funct. Polym.* **2013**, *73*, 923–928.

[22] P. Mustafa et Al., *J. Food Saf.* **2020**, *40*, e12725.

[23] R. Tanwar, V. Gupta, P. Kumar, A. Kumar, S. Singh, K. K. Gaikwad, *Int. J. Biol. Macromol.* **2021**, *185*, 451–461.

[24] A. Ounkaew et Al., *J. Polym. Environ.* **2018**, *26*, 3762–3772.

[25] X. Tang, S. Alavi, *Carbohydr. Polym.* **2011**, *85*, 7–16.

[26] J. Chen, Y. Zhang, G. C. Du, Z. Z. Hua, Y. Zhu, *Enzyme Microb. Technol.* **2007**, *40*, 1686–1691.

[27] Y. Tokiwa, G. Kawabata, A. Jarerat, *Biotechnol. Lett.* **2001**, *23*, 1937–1941.

[28] F. Kawai, X. Hu, *Appl. Microbiol. Biotechnol.* **2009**, *84*, 227–237.

[29] C. M. Hassan, N. A. Peppas, *Adv. Polym. Sci.* **2000**, *153*, 37– 65.

[30] V. I. Lozinskii, L. v. Domotenko, Y. S. Vainerman, S. v. Rogozhin, *Polym. Sci. U.S.S.R.* **1989**, *31*, 1983–1988.

[31] V. Baudron, P. Gurikov, I. Smirnova, S. Whitehouse, *Gels* **2019**, *5*, 12.

[32] L. Zuo, Y. Zhang, L. Zhang, Y.-E. Miao, W. Fan, T. Liu, *Materials* **2015**, *8*, 6806–6848.

[33] A. M. N. Santos et Al., *Materials* **2019**, *12*, 559.

[34] S. Ceylan, D. Göktürk, D. Demir, M. D. Özdemir, N. Bölgen, *Int. J. Polym. Mater. Biomater.* **2018**, *67*, 855-864.

[35] L. P. Bagri, J. Bajpai, A. K. Bajpai, *J. Macromol. Sci., Part A* **2009,** *46*, 1060-1068

[36] V. Rosciardi, D. Chelazzi, P. Baglioni **2021**. *" Green " Biocomposite Poly (vinyl alcohol)/ starch cryogels as new advanced tools for the Cleaning of Artifacts* [Manuscript submitted for publication].

[37] P. Suwannaporn, S. Pitiphunpong, S. Champangern, *Starch/Staerke* **2007**, *59*, 171–177.

[38] C. M. Hassan, N. A. Peppas, *Adv. Polym. Sci.* **2000**, *153*, 37– 65.

[39] R. Mastrangelo et Al., *Proc. Natl. Acad. Sci. USA* **2020**, *117* 7011-7020.

[40] M. J. Gidley, *Int. J. Biol. Macromol* **1989**, *22*, 1103–1110.

[41] P. le Lay, G. Delmas, *Carbohydr. Polym.* **1998**, *37*, 49–60.

[42] U. Finkenzeller, *Adv. Mater.* **1991**, *3*, 518–519.

[43] J. A. Creek, G. R. Ziegler, J. Runt, *Biomacromolecules* **2006**, *7*, 761–770.

[44] L. T. Sin, W. A. W. A. Rahman, A. R. Rahmat, A. A. Samad, *Polymer* **2010**, *51*, 1206–1211.

[45] E. A. Kamoun, X. Chen, M. S. Mohy Eldin, E. R. S. Kenawy, *Arab. J. Chem.* **2015**, *8*, 1–14.

[46] N. A. Peppas, E. W. Merrill, *J. Appl. Polym. Sci.* **1976**, *20*, 1457–1465.

[47] M. G. Cascone, N. Barbani, C. C. P.Giusti, G. Ciardelli, L. Lazzeri, *J. Biomater. Sci* **2012**, *12*, 267–281.

[48] P. Zhou, Y. Luo, Z. Lv, X. Sun, Y. Tian, X. Zhang, *Int. J. Biol. Macromol.* **2021**, *183*, 1903–1910.

[49] S. Mallam et Al., *Macromolecules* **1991**, *24*, 543–548.

[50] M. Shibayama, T. Tanaka, C. C. Han, *J. Chem. Phys.* **1998**, *97*, 6829.

[51] M. Cattani, M. C. Salvadori, F. S. Teixeira, *arXiv: Atomic and Molecular Clusters*, **2009**, arXive:0907.3131.

[52] G. W. H. Höhne, *Polymer* **2002**, *43*, 4689–4698.

[53] M. R. A. Avaro, Z. Pan, T. Yoshida, Y. Wada, *Plant Prod. Sci.* **2015**, *14*, 164–168.

Supporting Information for Paper II

Supporting Information for:

Phase separation behavior and structural role of amylose and amylopectin in PVA/starch hybrid networks: taking a step back to gain broader perspectives.

Vanessa Rosciardi, Piero Baglioni

Experimental Procedures

Samples preparation and storage

Hydrogels were prepared via freeze-thawing starting from aqueous solutions of PVA (99% hydrolyzed, 146000-186000 Mw, Sigma Aldrich), amylose (Biosynth/Carbosynth), and amylopectin (Biosynth/Carbosynth). All the reagents were used as received without further purification. All the pre-gel solutions contained a total amount of reagents fixed to 9 g/100 mL, with variable PVA/amylose/amylopectin w/w ratios.

The preparation process can be resumed as follows: reagents were added in the specified proportions to water (purified by a Millipore system with resistivity > 18 MΩ/cm) in round-bottomed flasks; the suspensions were then kept at 98°C for 3 hours under vigorous stirring, to obtain homogeneous viscous solutions. The solutions were poured in two types of molds (polystyrene molds to obtain "flat" hydrogels, 14 x 7 x 0.2 cm^3, and silicone molds to obtain "cubic" hydrogels, 1 x 1 x 1 cm^3) and let cool to ambient temperature. Afterward, the solutions were

kept at -20°C then thawed at 25°C. The freezing and thawing process was then repeated once, under the same conditions.

The obtained hydrogels were stored in water for 2 weeks, to allow the polymeric fraction that was not stably involved in the newly formed three-dimensional network to leave the structure. All the hydrogels were stored at room temperature, and the storage water was changed daily.

Pre-gel solutions containing the fluorescently labeled PVA were obtained with the same procedures as described above and transferred directly from a 98°C oil bath to the Confocal Laser Scanning Microscope (CLSM) sample holder, and immediately observed.

Synthetic route for PVA labeling

The PVA used for the preparation of solutions to be observed by means of CLSM was chemically labeled with fluorescein isothiocyanate (FITC, dye≥95%, Merck). The reaction was conducted through direct interaction between the two substrates in anhydrous dimethyl sulfoxide (DMSO, purity 99,9%, Merck), in the presence of triethylamine (Et_3N, purity 99%, Merck) as the activator, exploiting the coupling of the -OH moieties of PVA with the isothiocyanate groups on FITC. Briefly, 1.5 g of PVA (27 mmol -OH) were dissolved in DMSO at 70°C under N_2 atmosphere; 30 mg of FITC (0.077 mmol) and 17 mg of Et_3N (0.17 mmol) were added and the solution was left under stirring for two days at 25°C.

The synthetic pathway is schematically depicted in Figure S1.

The solution was then added dropwise to a mixture of acetone and ethanol (1:3 volume ratio) in order to precipitate the labeled PVA. The recovered polymer was centrifuged to separate it from the solvents,

redissolved in water at 98°C and reprecipitated in ethanol. Centrifugation, redissolution, and reprecipitation were repeated until reaching a constant FITC/PVA ratio in the product, as evaluated by means of UV/Vis spectroscopy.

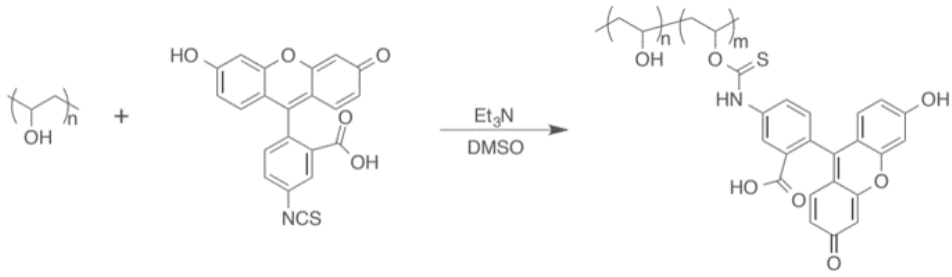

Figure S1. Schematic representation of the synthetic route followed for the chemical labeling of PVA with Fluorescein Isothiocyanate (FITC).

Confocal Laser Scanning Microscopy (CLSM)

The images acquisition of both cryogels and pre-gel solutions was carried out with a Leica TCS SP8 confocal microscope (Leica Microsystems GmbH, Wetzlar, Germany) using an Argon ion laser as excitation source (λ = 488 nm) and a PMT detector (Photomultiplier Tube, selected detection range = 498-540 nm). A water immersion 63X/1.2 W objective (Zeiss) was used. All samples were placed in the sample-holder (Lab-Tek® Chambered Borosilicate Coverglass System, Nalge Nunc International, Rochester, NY, USA) prior to analysis. The pre-gel solutions containing fluorescent PVA-FITC were observed as prepared, while the hydrogels were soaked in a Rhodamine B solution for 24 hours prior to observation.

Rheological measurements

Rheological analyses were performed on flat gel samples (thickness ≈ 2 mm) after complete swelling. The viscoelastic properties of the hydrogels were studied by means of oscillatory tests performed using a Discovery HR-3 rheometer (TA Instruments) equipped with a parallel plate geometry of 40 mm diameter and a Peltier temperature control system (temperature was held at 25 °C in all the experiments).

Amplitude sweep tests were carried out in a range of oscillation strains from 0.01% to 15% at constant oscillation frequency (1 Hz). Frequency sweep tests (frequency range 1-100 Hz) were performed within the Linear Viscoelastic Region (LVE), which was previously determined by means of amplitude sweep tests. The results are presented as averages of 3 repeats.

Gel fraction

Cubic gel samples (pre-swelling volume = 1mL) were used to estimate the gel fraction (G%). G% expresses polymers' amount stably linked to the three-dimensional gel network, and was calculated as the ratio between the weight of the xerogel (obtained by freeze-drying the hydrogel after equilibration in water), W_d, and the weight of the initial polymer content of the same sample (considering 1 mL of the pre-gel solutions, whose concentration is known), W_0:

Equation (S1)

$$G(\%) = \frac{W_d}{W_0} \cdot 100$$

Thermal analysis

Differential Scanning Calorimetry (DSC) measurements were performed by means of a DSC Q1000 (TA Instruments) apparatus. The measurements were performed on freeze-dried samples placed in hermetically sealed steel pans. The experimental set-up was chosen to detect melting events of crystalline domains eventually present in the samples. The heating ramp was set from 25 to 250°C, with a heating rate of 5°C/min. In all the samples a single first-order transition was detected, corresponding to the melting of PVA crystallites. The crystallinity degree (X%) of PVA in the samples was calculated as as tratio between the detected specific enthalpy of fusion of the samples and the specific enthalpy of fusion of a perfectly crystalline PVA (138.60 $J*g^{-1}$). All the DSC results are presented as the average of 3 repeats.

Small-Angle X-ray Scattering (SAXS)

SAXS measurements were performed on a Xeuss 3.0 HR (Xenocs) instrument, featuring a GeniX 3D Cu High Flux Very Long Focus (HFVL) Complete X-ray generator equipped with a high brightness X-ray tube (30W/40μm) and a FOX 3D single reflection multilayer optic. The signal was collected with a Detris Eiger 2R 1M hybrid photon counting detector (pixel dimension of 75x75 μm^2). 2D SAXS images were collected and circularly averaged through the XSACT software, to be expressed as Intensity vs. Q (where the modulus of the scattering vector is defined as $Q=(4\pi/\lambda)\sin\theta$, being 2θ the scattering angle). Glassy carbon was used to convert the intensity in absolute scale by considering the thickness of each sample. SAXS data were collected at two sample-

to-detector distances: 450 mm and 1800 mm. The two data sets were corrected by subtracting the scattering intensities of both water and empty cell (normalizing for the time of measurement and the relative transmission factors) and combined in a single curve through the XSACT software, covering a final Q-range between 0.004 and 0.6 $Å^{-1}$. SAXS curves were finally fitted through the SasView software, using a Shape-independent model.

Determination of amylose content in rice starch

Quantification of the amylose content in the rice starch used for the preparation of the PVA/starch cryogel was conducted following a protocol developed by Avaro et. Al (2011). Briefly, 100mg of rice starch were dried in an oven at 135°C for 1 hour and then put in a flask to which 1 mL of 95% ethanol and 9 mL of NaOH 1M were added. The flask was kept in an oil bath at 100°C for 10 min. The solution was allowed to cool to ambient temperature and ultrapure water was added up to reaching a 100 mL total volume; 5 mL of this solution were then transferred to a 100 mL volumetric flask and 1 mL of a solution of acetic acid 1N was added to adjust the pH. A 0.2% iodine solution was previously prepared (0.2g I_2, 2g KI in 100 mL) and 2mL of it were added to the flask, together with ultrapure water up to reaching a 100 mL total volume. The absorbance of the final solution was measured by means of a Cary 3500 UV-Vis (Agilent) spectrophotometer integrated with a Peltier temperature control system (set at 25°C). Absorbance values were recorded at λ=620 nm. Samples were prepared and analyzed in triplicate. The obtained absorbance values were used to calculate the amylose percent content in the samples, following the equation:

$$Amylose\ content\ (\%) = (5.83539 + 1.47157 * \ln(Abs602))^2.$$

Results and discussion

Freeze-thawed amylose gel formation

To test the ability of amylose and amylopectin to form self-supporting gel networks via freeze-thawing, a 100% amylose and a 100% amylopectin cryogels were tried to be obtained following the same procedure applied for the other gel samples, as illustrated in the experimental section. After 2 freeze-thawing cycles, cryoformed amylose gels were obtained, while amylopectin solutions did not show any changes, as illustrated in figure S1.

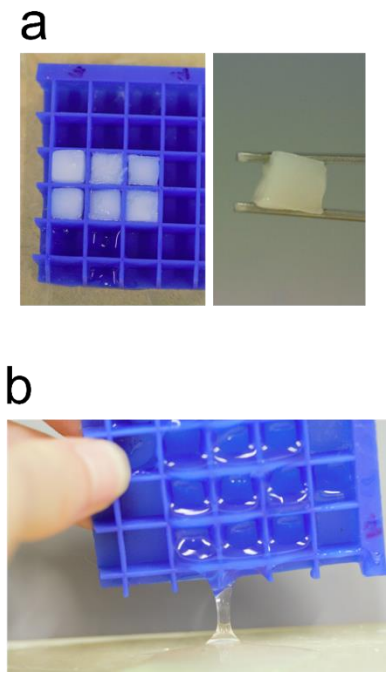

Figure S1. Formation of a cryogel after subjecting a 9% w/w solution of amylose to two freeze-thawing cycles (a). No gelation was observed for a 9% solution of amylopectin subjected to the same process (b).

Rheological characterization, amplitude sweep tests

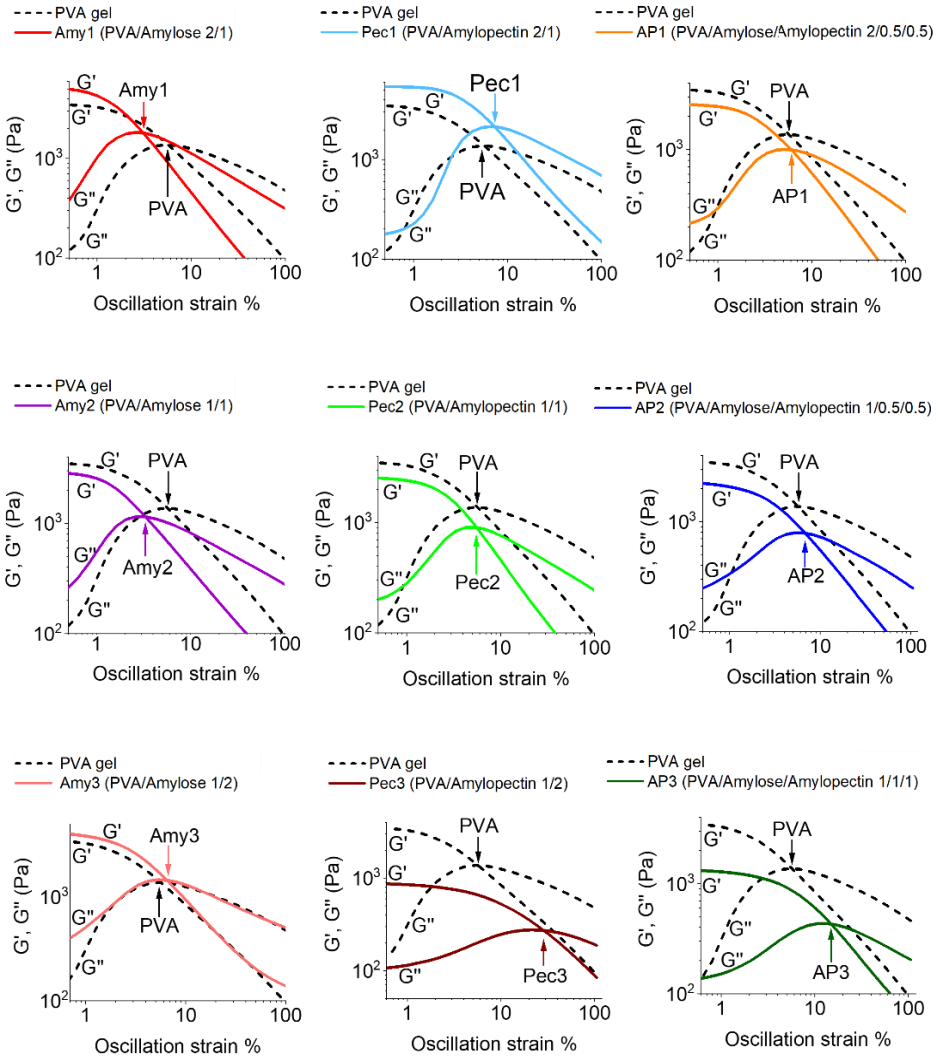

Figure S2. Summary of the rheological characterization of the samples conducted in amplitude sweep mode. Details of the plots are provided to highlight the G'/G" crossover points.

Small-Angle X-Ray Scattering measurements

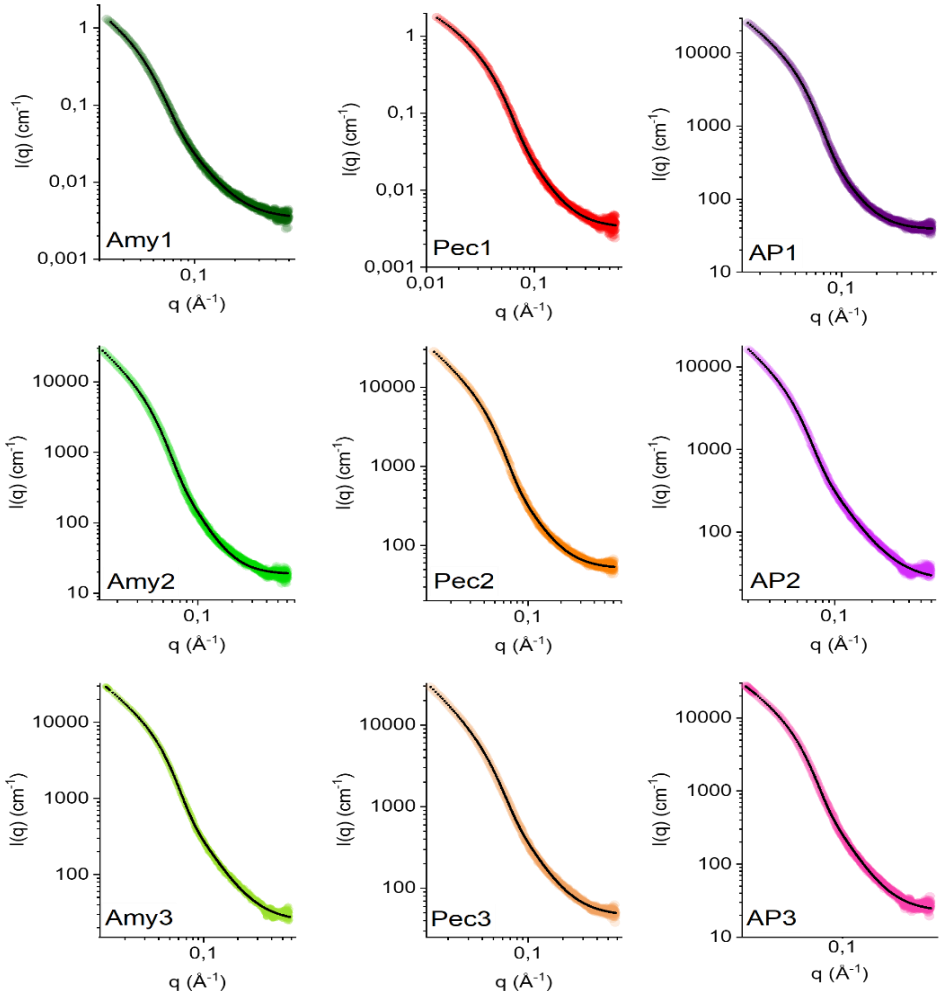

Fig. S3. Complete scattering curves of the samples as collected by means of SAXS experiments. **Amy**=PVA/amylose; **Pec**=PVA/amylopectin; **AP**=PVA/amylose/amylopectin; Numbers **1**, **2**, and **3** refer to a PVA content of 66, 50, and 33%, respectively.

Differential Scanning Calorimetry

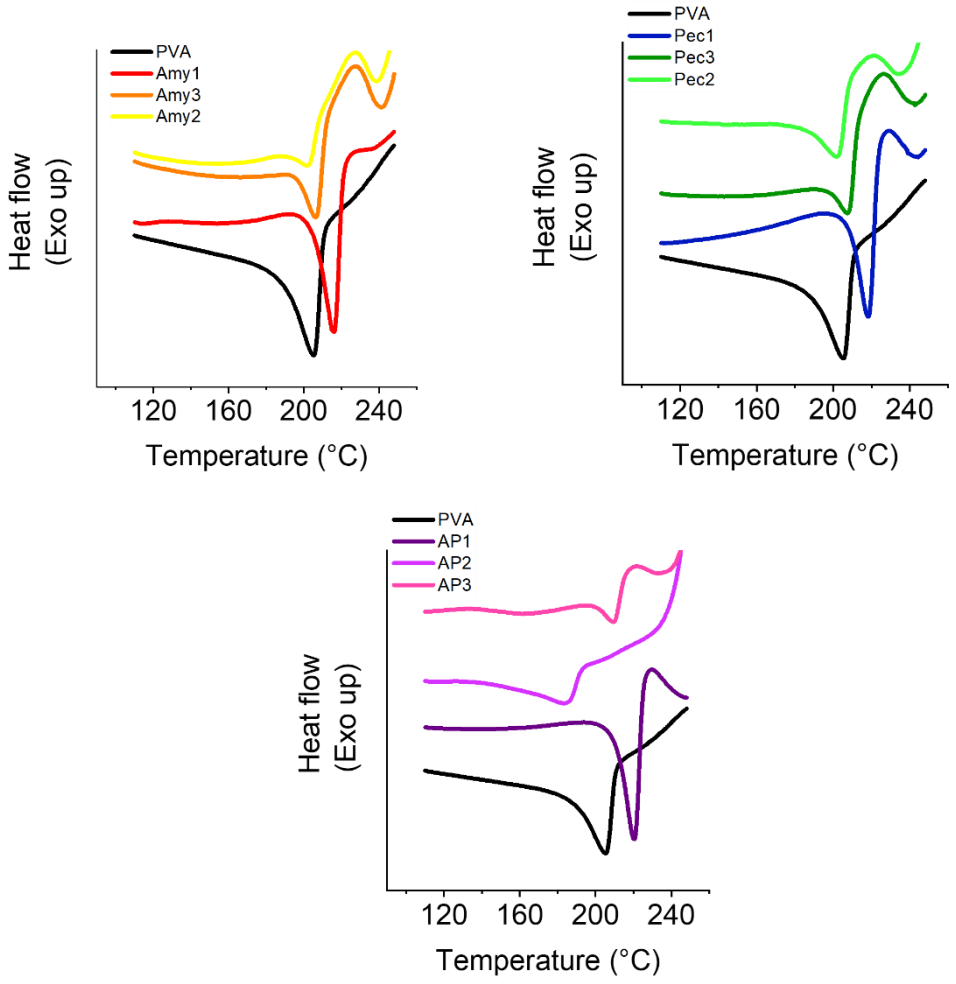

Figure S4. Summary of the first order transitions relative to the melting of PVA crystals, as detected through DSC measurements. **Amy**=PVA/amylose; **Pec**=PVA/amylopectin; **AP**=PVA/amylose/amylopectin; Numbers **1**, **2**, and **3** refer to a PVA content of 66, 50, and 33%, respectively.

Gel fraction (G%)

Gel fractions were calculated for the main set of samples and for 12 additional hydrogels as reported in the experimental section. The composition of all the samples and the corresponding gel contents are summarized in Table S1.

Table S1. Summary of the Gel fractions (G%) for the main set of samples and 12 additional gels.

PVA (w%)	**Amylose (w%)**	**Amylopectin (w%)**	**G%**
100	0	0	79.17±0.48
66.66	33.33	0	77.25±0.63
66.66	0	33.33	74.01±0.86
66.66	16	16.67	71.18±0.74
50	50	0	68.55±0.34
50	0	50	67.85±1.18
50	25	25	63.9±0.62
25	75	0	67.35±0.44
25	50	25	61.22±1.35
0	50	50	0
0	25	75	0
25	75	0	67,96±0.42
25	0	75	67.14±1.12

PVA (w%)	Amylose (w%)	Amylopectin (w%)	G%
25	25	50	63.57±1.33
10	90	0	71.43±0.34
10	0	90	59.2±1.26
10	30	60	64.9±0.82
10	60	30	66.33±0.41
0	100	0	77.85±0.22
0	0	100	0
33.33	66.66	0	67.5±0.35
33.33	0	66.66	69.8±1.12
33.33	33.33	33.33	60.09±1.33

A prediction of G% values for any PVA/amylose/amylopectin ratio (considering a fixed amount of polymers in water equal to 9% w/w) was obtained by plotting the experimental values in a three-dimensional ternary graph: in the graph, the 3 coplanar axes represent the compositional coordinates of the samples, and the one perpendicular to their plane is referred to the corresponding G% values. The obtained 3-D plot was implemented by means of a "smoothing" function applying a total point increase equal to 50. The data treatment was performed with the OriginLab Software.

Conclusion

Cultural Heritage and Material Science are usually considered as remarkably distant fields. Nonetheless, the conservation of our artistic patrimony strongly relies on the use of highly sophisticated products like nanostructured systems and colloidal materials. As a consequence, the distance separating Cultural Heritage from Material Science has progressively reduced in the last few years, promoting the flourishing of the research of new state-of-the-art technologies for the conservation of works of art.

Moreover, this research can have a highly positive side-effect, since materials developed for conservation purposes have to display common features of non-toxicity and tunability that confer to the produced systems the quality of being easily transferrable in other applicative fields.

In other words, the usefulness of the efforts made to formulate and characterize products to be applied to Cultural Heritage does not stop existing beyond this apparently limited field and the knowledge that derives from it can set strong bases for developing materials destined for other purposes.

The main scope of this work was to develop and characterize hydrogels to be mainly applied as cleaning tools on painted artworks, controlling the properties that boost soil removal and dirt pick-up from surfaces displaying different features and problematics. Many hydrogels based on synthetic polymers have been developed in the last years for the same purpose, but little to no attention was dedicated to their environmental impact.

Indeed, in the choice of the starting materials used to obtain hydrogels with the desired features, we decided to take into account the eco-compatibility issue, another transversal topic that is becoming growingly influential in the designing and production of any kind of material, independently from their destination of use.

For this reason, we started from a biodegradable synthetic polymer, PVA, blended it with a natural product, starch, to synthesize hydrogels via a green freeze-thawing route.

We characterized the effects of the freeze-thawing process on the gelation of PVA and native starch blends, tuning the starch content from 33 to 66% (w/w), and studying the gels' structures and structure-related properties.

The obtained hydrogels showed a highly porous organization due to phase separation events occurring as a consequence of mixing different polymers in solution (i.e. PVA and starch's polymeric components, amylose and amylopectin). Such spongy porous arrangements have been previously reported to be key for dirt removal from painted surfaces and our systems have indeed proved effective when applied on artificially soiled painted mock-ups.

Therefore, not only does the partial substitution of PVA with starch diminish the use of the synthetic polymer, with a straightforward advantage in terms of eco-sustainability, but mixing the different components together leads to the formation of a structure that promotes the hydrogels' cleaning effectiveness.

The features of the synthesized PVA/starch hydrogels resulted to be broadly tunable in terms of viscoelastic behavior and water release, controllable by simply varying the PVA:starch mixing ratio. Nevertheless, all the considered formulations resulted in the formation of strong gels (i.e., chemical-like gels), despite the predominantly physical nature of the preparation method. As much as a good porosity

ensures an efficient cleaning, a good cohesion of the gel grants a safe and residue-free application.

Both the aspects have been confirmed through the application of two chosen hydrogels on two different artificially soiled painted surfaces: a poorly bound and water-sensitive tempera, and a highly irregular rough alkyd painting. The excellent outcome of the cleaning operations was assessed by means of micro-FTIR imaging, which also revealed the total absence of any gel residues.

Remarkably, the PVA/starch gels have proven to be as effective as their state-of-the-art commercially available synthetic counterparts, confirming the possibility to formulate greener products for the conservation of Cultural Heritage without compromises in terms of performances and safety.

The results presented in this work candidate the PVA/starch hydrogels as innovative tools in art conservation, where sustainable methodologies based on "green" chemistry are growingly demanded. In addition, given their biocompatibility and environmentally friendly character, these systems are easily transferable to transversal fields where "green" and biocompatible confining networks are needed, such as drug delivery, tissue engineering, topical treatments, cosmetics, and many others.

However, to be able to finely tune the features of the PVA/starch systems in order to formulate materials that can respond to different applicative needs, a deeper insight into their formation mechanism is necessary.

Moreover, starch contains two different polymers (amylose and amylopectin), and their behavior in solutions with PVA is still largely unexplored. The arising of different equilibria, depending on the relative amount of the three polymers in the system (i.e., on the amylose/amylopectin ratio of the employed starch) translates into the possibility to obtain, without varying the components nor the synthesis technique, a broad variety of different hydrogels.

To better investigate the dynamic of interaction at play between PVA and starch components (i.e., amylose and amylopectin), as well as their implications on determining the final features of biocomposite PVA/starch networks, we decomposed the real system in its simple components.

Investigation on PVA/amylose, PVA/amylopectin, and PVA/amylose/amylopectin systems with variable PVA/polysaccharide ratios allowed a deeper understanding of the possible evolution of a real PVA/starch cryogel.

Thanks to CLSM imaging of pre-gel solutions containing fluorescently labeled polymers, we determined the absence of miscibility between PVA and amylose, as well as PVA and amylopectin, in the considered temperature range (25-98°C). The effective miscibility of PVA and starch (or its components) is still a very debated issue and, to our knowledge, has not been investigated by direct CLSM imaging by other authors.

In PVA solutions, characteristic domains formed by amylose in a supramolecular arrangement were observed, reasonably corresponding to single helixes forming liquid crystals with nematic order. Instead, PVA and amylopectin solutions show liquid-liquid phase separation.

Comparing the morphology of PVA/amylopectin solutions and cryogels, the porogen role of amylopectin arises, suggesting that also in PVA/starch networks the observed spongy organization is ascribable to phase separation events specifically regarding amylopectin, rather than amylose. The latter plays instead an active structural role, which was confirmed in this study by preparing self-supporting strong cryogels containing only amylose, while cryogels formed by amylopectin could not be obtained.

The structural characterization performed on the PVA/amylose/amylopectin cryogels allowed us to obtain important information: for PVA:polysaccharide ratios of 2:1, the heteropolymeric

interactions are strongly unfavoured, whereas PVA-PVA interactions are increased, leading to the formation of more compact and crystalline PVA networks characterized by remarkably high elastic responses. The maximum extent of PVA polysaccharide interactions is likely to occur at a 1:1 ratio. Nevertheless, PVA amylopectin interactions are "destructive", given the inability of amylopectin to form proper networks, while PVA-amylose interactions can be "constructive" and lead to the formation of hybrid tie points in the gel, containing both the polymers in strong association, as suggested by DSC and SAXS measurements.

These observations are particularly relevant since they partially clarify the specific contribution of amylose and amylopectin in PVA/starch systems and can therefore help in projecting biocomposite materials with appropriate features by choosing to employ starches characterized by appropriate amylose/amylopectin ratios.

Indeed, PVA/starch hydrogels obtained via freeze-thawing are appealing materials since they display physical interactions that lead to the formation of locally ordered structures characterized by a degree of crystallinity (depending on the polymer concentration) high enough to mimic the effect of a chemical crosslinking.

Consequently, PVA/starch cryogels, along with having good mechanical properties, are not solubilized by water at ambient temperatures. Instead, they show thermal-induced instability, meaning that they can be redissolved in a controlled manner, allowing the safe recovery and reuse of the polymeric fraction.

To conclude, we have started with the development of a "green" hydrogel to be used as a cleaning tool on painted artistic surfaces and finished with studying the physical chemistry behind the interactions between PVA and starch's polymers, obtaining results that can substantially help in projecting and developing high-quality biobased materials, with a significant positive impact on the ecosystem.

This work highlights once more the fundamental importance of a multidisciplinary approach in scientific research, where merging different knowledge, approaches, techniques, and points of view allows to reach unexpectedly useful results.

References for main text

[1] Merriam-Webster's Collegiate Dictionary (11th ed.) **2020**, Merriam-Webster Inc.

[2] C. Gonzalez-Perez, C. Parcero-Oubiña in *Revive the Past: Proceeding of the 39th Conference on Computer Applications and Quantitative Methods in Archaeology* **2011**.

[3] C. Holtorf, *World Archaeol.* **2018**, *50*, 639–650.

[4] J. H. Stoner in *Conservation of Easel Paintings,* (Eds. J. H. Stoner, R. Rushfield), Routledge **2020**, pp. 376–384.

[5] P. Baglioni, E. Carretti, D. Chelazzi, *Nat. Nanotechnol.* ***2015****, 10*, 287–290.

[6] D. Chelazzi, R. Bordes, R. Giorgi, K. Holmberg, P. Baglioni, *Curr. Opin. Colloid Interface Sci.* **2020**, *45*, 108–123.

[7] R. Mastrangelo et Al., *Proc. Natl. Acad. Sci. U.S.A.* **2020**, *117,* 7011-7020.

[8] J. A. L. Domingues, N. Bonelli, R. Giorgi, E. Fratini, F. Gorel, P. Baglioni, *Langmuir* **2013**, *29*, 2746–2755.

[9] N. Bonelli, G. Poggi, D. Chelazzi, R. Giorgi, P. Baglioni, *J. Colloid Interface Sci.* **2019**, *536*, 339-348.

[10] E. Chiellini, A. Corti, S. D'Antone, R. Solaro, *Prog. Polym. Sci.* **2003**, *28*, 963-1014.

[11] C. M. Hassan, N. A. Peppas, *Adv. Polym. Sci.* **2000**, *153*, 37–65.

[12] K. Y. Huang, C. T. Wang, W. L. Chou, C. M. Shu, *Int. J. Photoenergy* **2015**.

[13] R. F. Tester, J. Karkalas, X. Qi, *J. Cereal Sci.* **2004**, *39*, 151-165,

[14] B. Priya, V. K. Gupta, D. Pathania, A. S. Singha, *Carbohydr. Polym.* **2014**, *109*, 171–179.

[15] C. A. Gómez-Aldapa et Al., Mater. *Chem. Phys.* **2020**, *239*, 122027.

[16] R. Jayasekara, I. Harding, I. Bowater, G. B. Y. Christie, G. T. Lonergan, Polym. Test. **2004**, *23*, 17–27.

[17] S. Ceylan, D. Göktürk, D. Demir, M. Damla Özdemir, N. Bölgen, Intern. J. Polym. **2018**, *67*, 855-864.

[18] L. P. Bagri, J. Bajpai, A. K. Bajpai, *J. Macromol. Sci.*: Part A **2009**, *46*, 1060-1068.

[19] A. Bartoletti et Al., *Herit. Sci.* **2020**, *8*, 41.

[20] L. P. Buemi et Al., *Herit. Sci.* **2020**, *8*, 77.

[21] R. K. Tubbs, *J. Polym. Sci. Part A-1: Polym. Chem.* **1966**, *4*, 623–629.

[22] I. Pocsan, S. Serban, G. Hubca, M. Dimonie, H. Iovu, *Eur. Polym. J.* **1997**, *33*, 1805–1807.

[23] N. A. Peppas in *Hydrogels in Medicine and Pharmacy: Fundamentals,* (Eds. N. A. Peppas)*,* CRC Press **2019**, pp. 6-8.

[24] B. Wang, M. Kodama, S. Mukataka, E. Kokufuta, *Polym. Gels Netw.* **1998**, *6*, 71–81.

[25] C. M. Hassan, N. A. Peppas, *Macromolecules* **2000**, *33*, 2472–2479

[26] E. Otsuka et Al., *Soft Matter* **2012**, *8*, 8129–8136.

[27] S. Ghoshal, P. Denner, S. Stapf, C. Mattea, *Macromolecules* **2012**, *45*, 1913–1923.

[28] N. A. Peppas, *Makromol. Chem.* **1975**, *176*, 3433–3440.

[29] F. Yokoyama, I. Masada, K. Shimamura, T. Ikawa, K. Monobe, *Colloid Polym. Sci.* **1986**, *264*, 595–601.

[30] T. Kanaya et Al., *Macromolecules* **1995**, *28*, 3168–3174.

[31] T. Kanaya, M. Ohkura, K. Kaji, M. Furusaka, M. Misawa, *Macromolecules* **1994**, *27*, 5609–5615.

[32] N. A. Peppas, N. K. Mongia, *Eur. J. Pharm. Biopharm.* **1997**, *43*, 51–58.

[33] M. T. Khorasani, A. Joorabloo, H. Adeli, Z. Mansoori-Moghadam, A. Moghaddam, *Carbohydr. Polym.* **2019**, *207*, 542–554.

[34] K. H. Hong, *Polym. Bull.* **2016**, *74*, 2861–2872.

[35] H. L. Lin, Y. F. Liu, T. L. Yu, W. H. Liu, S. P. Rwei, *Polymer* **2005**, *46*, 5541–5549.

[36] B. Sreedhar, M. Sairam, D. K. Chattopadhyay, P. A. S. Rathnam, D. V. M. Rao, *J. Appl. Polym. Sci.* **2005**, *96*, 1313–1322.

[37] L. V. Angelova, P. Terech, I. Natali, L. Dei, E. Carretti, R. G. Weiss, *Langmuir* **2011**, *27*, 11671–11682.

[38] J. Li, X. Cao, Y. Liu, Q. Chen, *J. Rheol.* **2020**, 64, 991.

[39] E. Carretti et Al., *J. Cult. Herit.* **2010**, *11*, 373–380.

[40] A. Phenix in *Conservation of Easel Paintings,* (Eds. J. H. Stoner, R. Rushfield), Routledge **2020**, pp. 549–573.

[41] I. Natali, E. Carretti, L. Angelova, P. Baglioni, R. G. Weiss, L. Dei, *Langmuir* **2011**, *27*, 13226–13235.

[42] T. Guaragnone, A. Casini, D. Chelazzi, R. Giorgi, *Appl. Mater. Today* **2020**, *19*, 100549.

[43] N. Jain, V. K. Singh, S. Chauhan, *J. Mech. Behav.* Mater. **2017**, *26*, 213–222.

[44] A. K. Sonker, K. Rathore, R. K. Nagarale, V. Verma, *J. Polym. Environ.* **2017**, *26*, 1782–1794.

[45] G. Paradossi, R. Lisi, M. Paci, V. Crescenzi, *J. Polym. Sci., Part A: Polym. Chem.* **1996**, *34*, 3417–3425.

[46] C. Mazzuca et Al., *Colloids Surf. B* **2020**, *188*, 110777.

[47] G. Paradossi, F. Cavalieri, E. Chiessi, C. Spagnoli, M. K. Cowman, *J. Mater. Sci.: Mater. Med.* **2003**, *14*, 687–691.

[48] A. Papancea, A. J. M. Valente, S. Patachia, *J. Appl. Polym. Sci.* **2010**, *115*, 1445–1453.

[49] A. Buléon, P. Colonna, V. Planchot, S. Ball, *Int. J. Biol. Macromol.* **1998**, *23*, 85-112.

[50] R. Jayasekara, I. Harding, I. Bowater, G. B. Y. Christie, G. T. Lonergan, *Polymer Testing* **2004**, *23*, 17–27.

[51] X. Tang, S. Alavi, *Carbohydr. Polym.* **2011**, *85*, 7–16.

[52] A. M. Nafchi, M. Moradpour, M. Saeidi, A. K. Alias, *Starch - Stärke* **2013**, *65*, 61–72.

[53] Z. Liu, Y. Feng, X. Yi, *J. Appl. Polym. Sci.* **1999,** *74*, 2667-2673.

[54] H. R. Park, S. H. Chough, Y. H. Yun, S. D. Yoon, *J. Polym. Environ.* **2005**, *13*, 375–382.

[55] R. Shi et Al., *Carbohydr. Polym.* **2008**, *74*, 763–770.

[56] X. Y. Zhou, Y. F. Cui, D. M. Jia, D. Xie, *Polym. Plast. Technol. Eng.* **2009**, *48*, 489–495.

[57] S. Y. Yang, C. I. Liu, J. Y. Wu, J. C. Kuo, C. Y. Huang, *Macromolecular Symposia* **2008**, *272*, 150–155.

[58] J. W. Lawton, *Carbohydr. Polym.* **1996**, *29*, 203–208.

[59] B. Ramaraj, *J. Appl. Polym. Sci.* **2007**, *103*, 909–916.

[60] L. Chen, S. H. Imam, S. H. Gordon, R. Greene, *J. Environ. Polym. Degrad.* **1997**, *5*, 111–117.

[61] A. Hassan, M. B. K. Niazi, A. Hussain, S. Farrukh, T. Ahmad, *J. Polym. Environ.* **2017**, *26*, 235–243.

[62] F. O. Onofre, Y. J. Wang, *Int. J. Pharm.* **2010**, *385*, 104–112.

[63] F. O. Onofre, Y.-J. Wang, *J. Appl. Polym. Sci.* **2010**, *117*, 1558–1565.

[64] L. Passauer, F. Liebner, K. Fischer, *Starch - Stärke* **2009**, *61*, 621–627.

[65] S. Wattanachant, K. Muhammad, D. Mat Hashim, R. A. Rahman, *Food Chemistry* **2003**, *80*, 463–471.

[66] K. Thakur, A. Rajhans, B. Kandasubramanian, *Environ. Sci. Pollut. Res.* **2019**, *26*, 32013–32028.

[67] A. M. N. Santos et Al., *Materials* **2019**, *12*, 559.

[68] L. P. Bagri, J. Bajpai, A. K. Bajpai, Bull. Mater. Sci. **2011**, *34*, 1739–1748.

[69] L. P. Bagri, R. K. Saini, A. Kumar Bajpai, R. Choubey, *Polym. Eng. Sci.* **2019**, *59*, 254-263.

[70] L. T. Sin, W. A. Rahman, A. R. Rahmat, A. A. Samad, *Polymer* **2010**, *51*, 1206–1211.

[71] H. Xiao et Al., *J. Food Compost. Anal* **2020**, *92*, 103576.

[72] F. J. Warren, M. J. Gidley, B. M. Flanagan, *Carbohydr. Polym.* **2016**, *139*, 35–42.

[73] D. R. Kreger, *Biochimica et Biophysica Acta* **1950**, *6*, 406–425.

[74] H. S. Kim, B. Y. Kim, M. Y. Baik, *Crit. Rev. Food Sci. Nutr.* **2011**, *52*, 123–141.

[75] M. Schirmer, M. Jekle, T. Becker, *Starch - Stärke* **2015**, *67*, 30–41.

[76] S. G. Ring, *Starch - Stärke* **1985**, *37*, 80–83.

[77] J. W. Donovan, *Biopolymers* **1979**, *18*, 263–275.

[78] S. Wang, C. Li, L. Copeland, Q. Niu, S. Wang, *Compr. Rev. Food Sci. Food Saf.* **2015**, *14*, 568-585.

[79] M. A. Ottenhof, I. A. Farhat, *Biotechnol. Genet. Eng. Rev.* **2004**, *21*, 215–228.

[80] M. J. Gidley, *Int. J. Biol. Macromol.* **1989**, *22*, 1103–1110.

[81] M. J. Gidley, P. Bulpin, *Chem. Phys. Lett.* **1989**, *22*, 1532.

[82] M. G. Cascone, N. Barbani, C. C. P.Giusti, G. Ciardelli, L. Lazzeri, *J. Biomater. Sci. Polym. Ed.* **2001,** *12*, 267-281.

[83] V. Rosciardi, D. Chelazzi, P. Baglioni **2021**. *" Green " Biocomposite Poly (vinyl alcohol)/ starch cryogels as new advanced tools for the Cleaning of Artifacts* [Manuscript submitted for publication].

[84] Y. H. Yun, S. D. Yoon, *Polym. Bull.* **2009**, *64*, 553–568.

[85] M. Zhai, F. Yoshii, T. Kume, K. Hashim, *Carbohydr. Polym.* **2002**, *50*, 295-303.

Appendix A:

Small-Angle X-ray Scattering (SAXS): theoretical aspects

Small-Angle Scattering (SAS) techniques are a powerful tool to investigate nanostructured fluids and materials, being able to resolve inhomogeneities with dimensions ranging from one to hundreds of nanometers[1]. The main advantage of a SAS experiment consists in not requiring any manipulation of the samples, avoiding procedures like freeze-drying, metalation, or sectioning which can easily cause the occurrence of artifacts as in the case of Electron Microscopy. However, the result of a SAS experiment is not an image in the real space, but a statistically relevant averaging of the sample's structure represented in the reciprocal space.

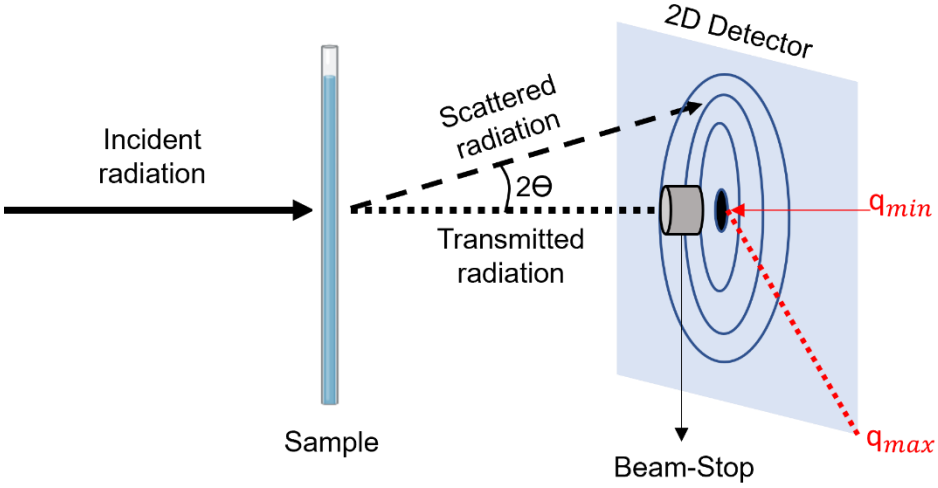

Figure 1A. Schematic representation of a Small Angle Scattering experiment.

In a scattering experiment, a beam of radiation (photons or neutrons) with a given wavelength is collimated on the sample, and its interaction with the investigated system will obviously depend on the nature of the radiation itself. The three probes mainly used in scattering experiments are visible light, X-rays, and neutrons.

When employing X-rays, inhomogeneities in the electronic density of the analyzed system are highlighted, since the interaction between the radiation and the sample occurs at the electronic level.

Independently from the employed source, part of the incident radiation is transmitted through the sample, part is absorbed by it and part will be scattered. The scattered radiation is collected and revealed by means of a position-sensitive detector.

The transmitted radiation is instead either blocked by a beam stop before reaching the detector or considered as the reference for determining the origin of the scattering experiment (i.e. where the scattering angle 2θ is zero). If the scattering is isotropic, which is the case for classical fluids, the bi-dimensional position-dependent signal collected by the detector can be reduced, by means of a radial averaging, to a mono-dimensional curve, i.e., the scattering curve.

When an X-ray beam hits the sample, every atom in the system becomes a scattering center producing a spherical wave. The intensity registered by the detector is the result of the destructive and constructive interferences occurring between the spherical waves emitted by the sample and therefore contains structural information of the system.

The scattering intensity (I(q)) is therefore the dependent variable in a SAXS experiment. It contains information on the dimension and shape of the scattering centers in the sample and on the interaction occurring between them. The scattering intensity can be expressed as[2]:

Equation (1)

$$I(q) = KN_p V_p^2 (\Delta\rho)^2 P(q) S(q) + B$$

where K is a parameter that depends on the instrument and its variables (incident flux, detector efficiency, etc.), N_p is the numerical density of the scattering particles, V_p is the volume of a single particle, $\Delta\varrho$ is the contrast of the experiment (i.e., it quantifies the difference of interaction between the probe with the sample and of the probe with the continuous phase), P(q) is the form factor, S(q) is the structure factor, q is the scattering vector and B is a linear background that depends on the instrumental noise and the non-coherent scattering coming from the sample.

The scattering vector (q)

The scattering vector, usually indicated with the letter q, is defined as the difference between the wavevector of the scattered radiation (k_s) and the wavevector of the incident radiation (k_i). Considering the elastic approximation, we can write:

Equation (2)

$$|k_s| = |k_i| = 2\pi/\lambda$$

and through simple geometrical considerations we can demonstrate that:

Equation (3)

$$|q| = |k_s - k_i| = \left(\frac{4\pi n}{\lambda}\right) sin\theta$$

where n is the refractive index of the sample (which can be approximated to 1 for X-rays) and λ is the wavelength of the employed radiation. This definition of q has two advantages: firstly, differently from 2θ, it does not depend on the λ of the chosen probe and secondly, it has the dimension of a reciprocal length (usually expressed as $Å^{-1}$ or nm^{-1}).

Rewriting λ as 2dsin θ (Bragg equation), we can express Equation 3 as:

Equation (4)

$$q = 2\pi/d$$

where d is the characteristic distance sampled by the chosen scattering vector. In other words, we can consider the scattering experiment as a microscope that works in the reciprocal space and uses a "Fourier transform lens". This "lens" selects the periodicity $2\pi/q$ in the sample along the q direction, i.e. filters the Fourier components with $\lambda=2\pi/q$[3].

From Equations 3 and 4 we can calculate the range of q that can be covered by a given experiment, once the wavelength of the incident radiation and the angles sampled by the detector are known.

The definition of the q range also leads to the definition of the maximum and minimum dimensions that are accessible by the scattering experiment. For example, with a laboratory SAXS instrument, using the X emission of copper (Cu Kα =1.542 Å), with a sample-detector distance of 30 cm, the covered q range is 0.01-0.5 $Å^{-1}$, corresponding to a range of accessible dimensions in the real space of 1-60 nm.

In a scattering experiment, the resolution is defined as $\Delta R=\pi/q_{max}$ and corresponds to the minimum discriminable dimension (with q_{max} being the maximum accessible value of q).

Considering the mentioned laboratory SAXS instrument, it is easy to calculate that for $q_{max}=0.5$ $Å^{-1}$, ΔR is about 6 Å.

The small angle scattering experiments are therefore low-resolution techniques, contrarily to wide-angle diffraction techniques where interatomic distance can be sampled.

Indeed, we must abandon the concept of atomic detail and imagine an average situation. To obtain information from molecules (or molecular clusters) with dimensions lower than ΔR, we have to define a density of interaction, also called scattering length density (ϱ)[2].

Equation (5)

$$\rho = \frac{\sum_i^n b_i}{V} = \frac{\delta N_A}{M} \sum_i^n b_i$$

Where b_i is the scattering length of the i-th atom, V is the molecular volume, δ is the bulk density of the considered molecule, M is its molecular weight, and Na is the Avogadro constant. The scattering length b_i is therefore a characteristic length of the i-th atom through which the probe-sample interaction can be quantified. For X-rays, this length is proportional to the number of electrons in the considered atom and can be easily calculated as $b_i=Z_ib_e$, where Zi is the atomic number of the i-th atom and b_e is the scattering length of an isolated electron, which is known to be $2.85x10^{-13}$ cm.

Form factor and polydispersity

The form factor P(q), also defined as the intraparticle structure factor, is a function that describes how the scattering intensity is modulated by the effects of interference resulting from the scattering from atoms that constitute the same type of inhomogeneity. In other words, P(q) depends on how the atoms of an inhomogeneity (a nanoparticle, a

polymeric aggregate, etc.) are distributed around a shared center of mass, i.e. on the shape of the inhomogeneity. Given a known simple shape, it is usually possible to derive the analytical expression of P(q). A summary of simple geometrical arrangement and their P(q) is reported in Table1[4].

However, the analytical forms of P(q) as expressed in Table 1 are strictly valid only for monodisperse systems (i.e., systems characterized by one characteristic dimension), which is an ideal scenario rarely encountered in real samples, where the polydispersity inevitably arises from the synthetic pathways through which the sample are obtained.

Table 1. Form factors for simple geometrical arrangements[4].

Shape	P(q)
Sphere with radius=R	$P(q) = \left[\frac{3\sin(qR) - qRcos(qR)}{(qR)^3}\right]^2$
Cylinder of negligible section and length=L (Sif is the integral sine function)	$P(q) = \frac{2}{qL}\left[Sif(qL) - \frac{1-\cos(qL)}{(qL)}\right]$
Disc with negligible thickness and radius = R ($J_1(x)$ is the first order Bessel function)	$P(q) = \frac{2}{(qR)^2}\left[1 - \frac{J_1(2qR)}{qR}\right]$
Gaussian chain formed by N segments with length = L (Debye function)	$P(q) = \frac{2(e^{-x}+x-1)}{x^2}, \quad x = \frac{q^2Nl^2}{6}$

In these cases, we need to recur to distribution functions like the Gaussian, the log-normal, the bimodal, and the Schulz-Zimm distribution. The form factor for polydisperse systems can be then obtained from the convolution of the appropriate distribution function and the P(q) of the correspondent monodisperse system[5]:

Equation (7)

$$\langle P(q)\rangle = \int_0^\infty D(R)V^2(R)P(q,R)dR$$

Where D(R) is the dimensional distribution characterizing the systems and the other symbols have the same meaning that we have already explained in the previous equations.

Structure factor

The structure factor S(q), also called interparticle structure factor, is a function that describes the interference effects due to the scattered radiation coming from different inhomogeneities (scattering objects) in the sample (i.e., coming from the different centers of mass). It is generically described as[6]:

Equation (8)

$$S(q) = 1 + \frac{4\pi N_p}{qV}\int_0^\infty [g(r)-1]rsin(qr)dr$$

Where g(r) is the pair correlation function of the mass centers and V is the sampled volume. Consequently, the higher the concentration of the system (and the stronger the potential of interaction), the more this term becomes important. With a small angle scattering experiment is thus

possible to extrapolate information about the local order imposed by interactions occurring between the objects composing the sample, but also about the nature of the interactions themselves. For instance, a SAXS curve of a sample containing monodispersed spheres is substantially different in the case of rigid, charged, or adhesive particles. In the first case, the contribution of S(q) will strongly diminish by simply diluting the system, while in the second case this effect will not disappear after dilution and the introduction of ions in the continuous phase will be necessary to modulate the repulsive effects between the spheres.

In general, unless the main purpose of the experiment is to study the interaction potential of the particles in the sample, it is preferrable to work in conditions near to infinite dilution., in order to make the P(q) contribution negligible and simplify the scattering equation(Equation 1), that in this case will depend only on the shape of the analyzed objects. However, a good scattering intensity strongly depends on the sample concentration, and a compromise is required in order to avoid excessively long experiments.

Guinier and Porod's approximations

As just mentioned, the scattering equation (Equation 1) can be simplified in condition of infinite dilution, where S(q)=1 and the only structural term to be considered is P(q). In this condition, and for q values smaller than the reciprocal of the maximum characteristic dimension of the sample, P(q) shows an asymptotic behavior independent from the shape of the scattering objects[7].

The q range in which this assumption is valid is called the Guinier region. In this case the spatial resolution ($2\pi/q$) is not high enough to

determine the local structure but information on the average dimension of the objects can be obtained. It is mathematically demonstrated that in the Guinier region P(q) achieves a gaussian functional form[8]:

Equation (9)

$$I(q) = (\Delta\rho)^2 V^2 P(q) = (\Delta\rho)^2 V_p^2 \exp\left(-\frac{R_G^2 q^2}{3}\right)$$

Where R_G is the gyration radius of the scattering particle and Vp is its volume. It is important to remember that this approximation is valid only if the inequality $q<1/R_G$ is respected.

To extrapolate the Rg value it is useful to recur the linearized form of Equation 9:

Equation (10)

$$lnI(q) = c - \frac{R_G^2 q^2}{3}$$

Plotting lnI(q) vs q^2 in the so-called Guinier representation, we obtain a straight line with slope $=-R_G^2/3$. Once Rg is determined, it is necessary to verify if the inequality $q_{max}R_G<1$ is verified, where q_{max} is the maximum q value considered for the linear fitting. Otherwise, the q range considered for the linear fitting will be narrowed until convergence is reached.

Finally, if the Guinier approximation is not applicable in any range, we will either know that the characteristic dimension of the investigated system is too big to be sampled by our experiment, or that the structural factor is not negligible.

Given the "shape-independent" nature of the Guinier approximation, we must bear in mind that the same value of R_G can refer to broadly different shapes. However, the functional form of R_G can be calculated

assuming an hypothetical expected shape (and in this case preliminary experiments conducted with complementary techniques are highly useful) and analytically resolving the integrals in the equation:

Equation (11)

$$R_G^2 = \frac{\int \rho(r) r^2 \, dV}{\int \rho(r) dV}$$

Some examples for R_G for simple geometries are reported in Table 2.

Table 2. Gyration radius (R_G) for simple geometrical arrangements[4].

Shape	R_G
Sphere with radius=R	$R_G = \sqrt{\frac{3}{5}} R$
Cylinder of negligible section and length=L	$R_G = \frac{L}{\sqrt{12}}$
Disc with negligible thickness and radius = R	$R_G = \frac{R}{\sqrt{2}}$
Gaussian chain formed by N segments with length = L	$R_G = \sqrt{\frac{N}{6}} L$

The Guinier approximation is therefore a simple yet powerful tool for SAS data analysis, since it allows to obtain the average representative dimension characterizing the investigated system independently from any assumption related to the objects' shape (it is indeed known "shape

independent model"). Following R_G variations in function of external variables as temperature, pH, or incoming radiation, it is possible to observe important structural transitions in the investigated sample[9].

On the extreme opposite of Guinier's region, i.e., for q values significantly higher than the reciprocal of the investigated objects' dimension, the spatial resolution becomes so high that we can only observe the interphase between the scattering objects and the continuous phase in which they are located. This q range is called the Porod's region[10]. Here, the dependency of I(q) from q varies in function of the scale at which the surface of the objects is observed. As a consequence, the fractality of the objects can be investigated.

Plotting the scattering data as $Log_{10}(I(q))$ vs I(q), a straight line with slope=p is obtained:

Equation (13)

$$Log_{10}(I(q) - B) = -p * Log_{10}(q)$$

where a Is a constant dependent on the sample's nature, B is the background and p is the Porod exponent. As a rule of thumb, for a mono-dimensional rigid object p=1, while for a planar geometry p=2. Values comprised between 2 and 3 are typically encountered in gels, three-dimensional networks and systems with a nanometric interconnected porosity.

When polymeric chains are considered, p is related to the reciprocal of the excluded volume. A value of p=2 is obtained for gaussian chains in dilute regime, p=5/3 indicates a completely swollen coil, and p=3 refers to a fully collapsed polymeric chain.

If $3<p<4$, the sampled fractal is a surface fractal with fractal dimension $D_s=6-p$ and in this interval the roughness of the surface is as higher as much p is lower. In the ideal case of a neat, smooth interface, p=4 and the Porod's equation is valid[10]:

Equation (13)

$$I(q) = (\Delta\rho)^2 V_p^2 P(q) = 2\pi(\Delta\rho)^2 \left(\frac{S_V}{q^4}\right)$$

where S_V is the surface per volume unit of the particle. The portion of the scattering curve characterized by high q values, (Porod's region, $q>2\pi/d_{min}$, with d_{min} corresponding to the smaller inhomogeneity in the sample), therefore allows to extrapolate the surface area per volume of the sample. Usually, S_v is obtained through a $q^4I(q)$ vs q plot (Porod representation): the resulting curve will show a plateau corresponding to $2\pi(\Delta\varrho)^2 S_v$.

All the information regarding the shape of the sample is therefore comprised between the Guinier's and the Porod's region.

Another useful approximation is the so-called Kratky representation, obtained by plotting $q^2I(q)$ vs q. The Kratky plot allows the quick extrapolation of information about the compactness of the studied system[11]. In the case of a sphere, for example (nanoparticle, globular protein or polymer in dendritic conformation), the curve shows a maximum and then goes to zero for high q values (as predicted by the relationship between I(q) and q^{-4} typical of the Porod's region). For a system in which the objects are only partially globular, we can observe a peak at low q values (relative to the globular shape) followed by a plateau at higher q values (typical of a random coil). Finally, in the case of a polymer in a good solvent (or a protein in its denaturized state), the Kratky plot gives a curve that grows asymptotically until reaching a plateau that is proportional to R_G^{-2}. This happens since a polymer swollen chain cain be approximated to the Debye function, where for high q values the function is dependent from q^{-2}.

Curve modelling

The modelling of a complete scattering curve can be a long process, especially in the absence of information coming from complementary techniques. Usually, the first operation is to recur to the Porod and Guinier approximation and then to opt for one of the two following approaches: the direct approach and the indirect one.

In the direct approach we chose a plausible form (and eventually a plausible structure factor) and we variate the dimensional parameters (and the interaction potential) until the experimental curve overlaps as much as possible the theoretical one[12]. The convergence is obtained through a non-linear minimization method.

In the indirect approach, the scattering curve is reported in the real space through a Fourier transform[13]:

Equation (14)

$$p(r) = \frac{1}{2\pi^2}\int_0^\infty I(q)(qr)\sin(qr)\,dq$$

where p(r) is the pair distance distribution function, i.e., the probability that a certain distance exists, considering all the couples of the scattering objects in the system. Once p(r) is known, we proceed to find the theoretical three-dimensional distribution of the scattering centers that is closer to the experimental distribution.

Scattering from a hydrogel

Hydrogels can be considered as semi-dilute solutions of neutral polymers in a good solvent. The scattering function for a polymeric solution in semi-dilute regime can be described by a Lorentzian function[14]:

Equation (15)

$$I_{Lor}(q) = \frac{I_{Lor}(0)}{1 + \xi^2 q^2}$$

Where ξ is the average mesh size of the three-dimensional gel network and $I_{Lor}(0)$ is a scale factor that depends on the polymer/solvent contrast and on the volume fraction of the gel. Even though this function (also called Ornstein-Zernicke term[15]) well describes the scattering from an ideal gel, it is less accurate when applied to real systems, especially considering chemical gels with a high content of crosslinking units that introduce denser scattering regions in the regular mesh.

In these cases, the equation is corrected by the addition of a second term that takes accounts for the excess of scattered radiation coming from the more compact portions of the sample (e.g., where the concentration of crosslinker is particularly high). This scattering excess is described by the Debye-Bueche function[16]:

Equation (16)

$$I_{ex}(q) = \frac{I_{ex}(0)}{(1 + a^2 q^2)^2}$$

where a is the representative dimension of the denser inhomogeneities and I_{ex} is a scale factor that depends on the contrast of the experiment and on the concentration of the sample.

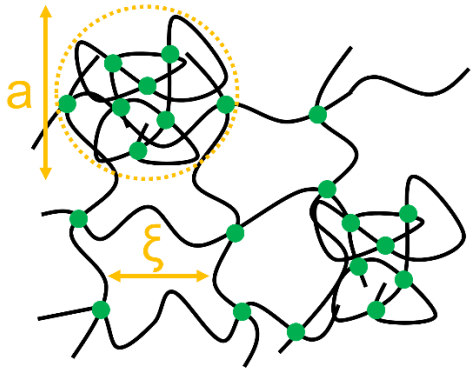

Figure 2A. Schematic representation of a gel's structure. The two characteristic dimensions (ξ and a, referred to the mesh of the network and to the solid inhomogeneities, respectively) are highlighted in yellow.

The complete scattering function for a hydrogel can be therefore considered as the sum of two contributions, one accounting for the network, and the other for the inhomogeneities[17]:

Equation (17)

$$I_{Gel}(q) = I_{Lor}(q) + I_{ex}(q) + B$$

where B is the instrumental background, not dependent from q.

References for Appendix A

[1] M. J. Hollamby, *Phys. Chem. Chem. Phys.* **2013**, *15*, 10566–10579.

[2] O. Glatter in *Scattering Methods and their Application in Colloid and Interface Science*, Elsevier **2018**, pp. 19-32.

[3] J. Teixeira in *Structure and Dynamics of Strongly Interacting Colloids and Supramolecular Aggregates in Solution,* (Eds. S. H. Chen, J. S. Huang, P. Tartaglia) Springer Netherlands **1992**, pp. 635-658.

[4] R.-J. Roe in *Methods of X-ray and Neutron Scattering in Polymer Science*, Oxford University Press New York **2000**.

[5] T. Narayanan in *Applications of Synchrotron Light to Scattering Diffraction in Materials and Life Sciences*, (Eds. T. A. Ezquerra, M. C. Garcia-Gutierrez, A. Nogales, M. Gomez, Springer Berlin Heidelberg **2009**, *776*, 133-156.

[6] J. B. Hayter, J. Penfold, *Molecular Physics* **1981**, *42*, 109–118.

[7] A. Guinier, G. Fournet, *Small Angle Scattering X-Rays*, Wiley **1955**.

[8] R. F. Ravi Saraf, *J. Polym. Sci., Polym. Phys. Ed* **1976**, *66*, 248.

[9] S. Doniach, *Chemical Reviews* **2001**, *101*, 1763–1778.

[10] S. Ciccariello, J. Goodisman, H. Brumberger, *J. Appl. Crystallogr.* **1988**, *21*, 117–128.

[11] A. G. Kikhney, D. I. Svergun, *FEBS Letters* **2015**, *589*, 2570–2577.

[12] S. Hansen, *J. Appl. Cryst.* **2008**, *41*, 436–445.

[13] E. Walenta, *Acta Polymerica* **1985**, *36*, 296–296.

[14] J. S. Higgins, H. C. Benoit in *Polymers and neutron scattering*, Clarendon Press **1994**.

[15] U. Genz, R. Klein, *Journal de Physique* **1989**, *50*, 439–447.

[16] P. Debye, A. M. Bueche, *J. Appl. Phys.* **2004**, *20*, 518.

[17] M. Shibayama, *Soft Matter* **2012**, *8*, 8030–8038.